Analyses for the Production and Dosimetry of Adding Uranium-232 as a Tracer to the Uranium Fuel Cycle

A Dissertation Presented for the
Doctor of Philosophy
Degree
The University of Tennessee, Knoxville

Joshua H. Rhodes
December 2021

Copyright © 2021 by Joshua H. Rhodes
All rights reserved.

ACKNOWLEDGEMENTS

I would like to thank my advisor, Dr. G. Ivan Maldonado for his advice, guidance, and the opportunities he has provided for me. He has been incredibly generous and helpful and I am grateful for the opportunities he has offered me. I would also like to thank Dr. Brandon Grogan for providing the opportunity to work on an exciting and innovative project. He provided the primary opportunity and project under which most of this work was performed. His information and guidance have been crucial to performing the work for this dissertation. I would like to thank Dr. Nicholas Luciano for his advice and understanding on this project and on tools used in this project. I would like to thank Dr Lawrence Heilbronn for his advice and understanding and insight that helped further this work. A portion of this work was performed under the guidance of Dr. Steve Herring of CSNR and Brad Kirkwood, formerly of INL, whom I would like to thank for their guidance, as well as for allowing me to include the work performed for them to be included in this dissertation.

ABSTRACT

This dissertation is an examination of the use of uranium-232 as a tracer in nuclear fuel. Decay daughters from ^{232}U, particularly thallium-208, produce high energy gamma rays that, when added to uranium, may increase detectability in case of theft or diversion, but are also hazardous in high quantities. Previous studies of the ^{232}U decay chain are examined. This work will go into a dosimetry study to determine how hazardous varying levels of ^{232}U are, and how to efficiently produce ^{232}U in sufficient quantities.

A dosimetry study was performed to determine the dose hazards due to the addition of ^{232}U to uranium. This dosimetry study determined that the concentration of ^{232}U to add to uranium is approximately 10 to 100 parts per trillion. A production scoping study was performed to determine the preferred target materials for producing ^{232}U via neutron irradiations. Calculations performed using SCALE 6.2 ORIGEN determined that ^{231}Pa and ^{230}Th are the optimum target materials, and that reactor irradiations are preferred. ORIGEN Calculations using flux spectra from the High Flux Isotope Reactor determined that for ^{231}Pa targets the optimum irradiation time is 2 HFIR cycles, yielding 0.35 grams of ^{232}U per gram ^{231}Pa. Thorium-230 irradiations yielded 0.15 grams ^{232}U per gram ^{230}Th after five cycles. Neutronics analyses examined the neutron spectra in targets modeled in MCNP, and determined that self-shielding is a concern that may reduce yield, especially in ^{230}Th, lowering the yield to 0.1 grams after five cycles. Cost analyses were performed to examine the cost-effectiveness for different targets and ^{230}Th enrichments.

A study of ^{238}Pu contaminated with ^{236}Pu produced at the Advanced Test Reactor was also conducted based on work from the CSNR. It examined strategies for mitigating against ^{236}Pu contamination by chemical removal of ^{232}U. Only material irradiated close to the center of the ATR needed this extra processing, and only a few micrograms of ^{232}U is recoverable. However, these small quantities may still have a use for small stockpiles or testing purposes.

TABLE OF CONTENTS

Chapter 1. Introduction and Background 1

1.1. Motivations 1

1.1.1. Problems with the use of a tracer: Isotope Choice, Radiological Hazards, and Isotope Sources. 1

1.2. Properties of Uranium-232 2

1.2.1. The ^{232}U Decay Chain and Gamma Emissions. 2

1.3. Objectives and Scope 4

1.3.1. Dosimetry 4

1.3.2. Production 5

Chapter 2. Literature Review of Previous studies of Uranium-232 6

2.1. Uranium-232 in the Thorium Fuel Cycle 6

2.1.1. Radiation Hazards from the Contamination of ^{233}U with ^{232}U 7

2.1.2. Radiation and Decay Heat causing Degradation of Weapons Components 7

2.1.3. Proliferation Resistance of the Thorium Fuel Cycle in Conjunction with Molten Salt Reactors 8

2.2. Protection of ^{235}U Enriched Uranium with ^{232}U 8

2.2.1. Proliferation Resistance of ^{235}U via Excessive Dose and Decay Heating .. 9

2.2.2. Sourcing ^{232}U from Reprocessed Uranium to Protect LWR Fuel 9

2.2.3. Previous Examinations on Producing ^{232}U from ^{230}Th and ^{231}Pa 10

2.3. Literature Review Summary 11

2.4. Originality of Work Compared to Previous Studies. 11

Chapter 3. Radioactive Decay Chains, Isotope Production, and Computational techniques Utilized 13

3.1. Radioactive Decay of ^{232}U and ^{208}Tl 13

3.1.1. Alpha and Beta Decay 13

3.1.2. Gamma Decay 15

3.2. The Bateman Equation 15

3.3. SCALE 6.2 ORIGEN Overview 17

3.4. Chapter Conclusions 18

Chapter 4. Examining the dose Rate Increase due to the Addition of Uranium-232 to the Uranium Fuel Cycle 19

4.1. Chapter Abstract 19

4.2. Chapter Introduction 20

4.3. Dosimetry Modeling and Methodology 21

4.4. SCALE 6.2 ORIGEN Gamma Source Terms 21

4.5. MCNP Model Geometry and Materials 24

4.5.1. 55-gallon Drum of Yellowcake 24

4.5.2. Uranium Hexafluoride Cylinders 24

4.5.3. Pressurized Water Reactor Fuel Assembly 25

4.6. Dosimetry Tallies 25

4.7. Model Results 29

4.7.1. 55-gallon Drum 29

4.7.2. 30B Cylinder 32

4.7.3. 48Y Cylinder 32

4.7.4. Fuel Assembly 32

4.8. Effects of Varying ^{232}U Concentration 35

4.9. Material Aging and Decay 38

4.10. Chapter Conclusions 39

Chapter 5. Exploration of Uranium-232 Production Pathways and Target Materials 40

5.1. Chapter Abstract 40

5.2. Chapter Introduction 41

5.3. Potential Source Materials 41

5.3.1. Protactinium-231 41

5.3.2. Thorium-230 44

5.3.3. Neptunium-237 44

5.3.4. Thorium-232 44

5.3.5. Uranium-233 48

5.4. Initial Examination of Reactions and Physics 48

5.5. HFIR Irradiation ORIGEN Simulations 51

5.5.1. The High Flux Isotope Reactor (HFIR) 51

5.6. Results 53

5.6.1. Hydraulic Tube ORIGEN Calculations 53

5.6.2. ISVXF ORIGEN Calculations 57

5.7. Chapter Conclusions 59

Chapter 6. Examination of HFIR Target Neutronics and Self-Shielding for Uranium-232 Production Targets 61

6.1. Chapter Abstract 61

6.2. Chapter Introduction 61

6.3. HFIR Target MCNP Model 62

6.3.1. Flux Trap Target Positions 62
6.3.2. HFIR Target Composition 62
6.3.3. Neutron Flux Tallies Utilized. 65
6.4. Flux Tally Results 65
6.4.1. Protactinium-231 Results 65
6.4.2. Thorium-230 Results 68
6.5. ORIGEN Results 73
6.5.1. Protactinium-231 73
6.5.2. Thorium-230 76
6.5.3. Thorium-230 Depletion 80
6.6. Chapter Conclusions 84
Chapter 7. Analysis of Anticipated Costs of producing ^{232}U 86
7.1. Chapter Abstract 86
7.2. Chapter Introduction 86
7.3. Proposed Production Pathway Steps and Associated Costs 86
7.3.1. Raw Material Extraction. 88
7.3.2. Thorium-230 Enrichment 88
7.3.3. Target Fabrication 89
7.3.4. Irradiation 89
7.3.5. Product Recovery 91
7.3.6. Procedure for Analysis 91
7.4. Cost Analysis Results for Once-Through Production Cycles 92
7.4.1. Protactinium Once-Through 92

7.4.2. Thorium-230 Once-Through 92

7.5. Protactinium Recycling Costs Results 93

7.5.1. Unutilized Protactinium from a Protactinium Target 93

7.5.2. Weighted Average Cost of Once-through Thorium with Protactinium Recovery 94

7.6. Discussion of Analyses 94

7.7. Cost Analysis Conclusions 96

Chapter 8. Mitigation of Plutonium-236 Contamination in Plutonium-238 Produced in in the Advanced Test Reactor via Recovery of Uranium-232 99

8.1. Chapter Abstract 99

8.2. Chapter Introduction 100

8.2.1. Problems with Using ^{237}Np for ^{232}U Production 100

8.2.2. History of ^{238}Pu Production. 100

8.2.3. Study Motivations. 101

8.3. Simulated Processing Procedure, Methodology, and Variables. 103

8.3.1. Processing Procedure Steps 103

8.3.2. Computational Methodology 103

8.3.3. Parameters Examined 104

8.4. Modeling Objectives 105

8.5. ORIGEN Results and Observations on ^{208}Tl Mitigation 107

8.5.1. Effects of ^{236}Pu Concentration 107

8.5.2. Effects of Material Aging and Decay Time Before Second Processing . 107

8.5.3. Effects of Increased Removal of Uranium and Thorium 111

8.5.4. Analysis of Parameters for ^{208}Tl Mitigation 111

8.5.5. Analysis of ^{232}U Growth and Recovery in ^{238}Pu..... 114

8.6. Chapter Conclusions 116

Chapter 9. Conclusions and Future Work..... 119

References..... 120

Appendices..... 126

Appendix A: Models and Data for ^{232}U Dosimetry..... 127

Appendix B: Example ORIGEN Models for Chapter 5 HFIR HT and VXF..... 153

Appendix C: ORIGEN Models for Chapter 6 Self-Shielded Production Results 174

Appendix D: Example ORIGEN Models for Chapter 7 ^{236}Pu Mitigation..... 194

Vita..... 200

LIST OF TABLES

Table 4.1. Prominent Gamma Energies and Intensities of the ^{232}U Decay Chain 22

Table 4.2. List of ^{232}U Concentrations Examined..... 23

Table 5.1. Source materials for initial ^{232}U production scoping study. 50

Table 5.2. Scoping study ^{232}U yield. Units are grams of ^{232}U per gram of source material. Yields greater than 10^{-4} are highlighted in green. Uranium-233 thermal irradiations, consume more ^{232}U than produced. 50

Table 5.3. Ratio of 233U to 232U. Highlighted are ratios less than 10. 50

Table 6.1. Thorium-230 Enrichments Examined..... 64

Table 6.2. Total flux tallied in the HFIR target for each ^{230}Th enrichment. 72

Table 6.3. Mass of ^{232}U, ^{233}U, and ^{231}Pa per gram of Pa Target material. 75

Table 6.4. Uranium-232 mass (g) per Gram of Source Material for Six HFIR Cycles 79

Table 6.5 Isotope Buildup Mass (g) per Gram of Th-230 Source Material for Four HFIR Cycles..... 81

Table 7.1. EMIS Enrichment Feeds, Products, and Costs. 90

Table 8.1. Uranium-232 Recovered from processes that met the ^{208}Tl criteria 118

LIST OF FIGURES

Figure 1.1. The ^{232}U Decay Chain 3

Figure 3.1 Gamma decay level scheme for ^{208}Tl [14]. 16

Figure 4.1. MCNP geometry of a 55-gal drum. Yellow represents U_3O_8. Blue is structural material. The wall thickness is 6 mm (0.24 in). 26

Figure 4.2. 30B cylinder. The UF_6 (green) is assumed to have accumulated on the cylinder wall (blue). The wall is 13 mm (0.5 in) thick. 27

Figure 4.3. 48Y cylinder. The UF_6 (green) is assumed to have accumulated on the cylinder wall (blue). The wall is 16 mm (5/8 in) thick. 27

Figure 4.4. Westinghouse 17 × 17 fuel assembly and single fuel pin. Green is UO_2 fuel, red is the helium plenum, and blue is zirconium alloy cladding. 28

Figure 4.5. Ring detectors for the 30B cylinder model (top view). 30

Figure 4.6. Radial Dose Rate at 30 cm vs. U-232 Concentration for a 55-gallon Drum of U_3O_8. 31

Figure 4.7. Radial Dose Rate at 30 cm vs. U-232 Concentration for a 30B Cylinder with natural uranium. 33

Figure 4.8. Radial Dose Rate at 30 cm vs. U-232 Concentration for a 30B Cylinder with 5 percent LEU. 33

Figure 4.9. Radial Dose Rate at 30 cm vs. U-232 Concentration for a 48Y Cylinder with natural uranium. 34

Figure 4.10. Side Dose Rate at 30 cm vs. U-232 Concentration for a 17x17 PWR fuel assembly with 5 percent enriched uranium. 36

Figure 4.11. Dose rate vs. ^{232}U concentration for each model at a 30 cm distance after 1 year of aging. 36

Figure 4.12. Dose rate vs. ^{232}U concentration for the 55-gal drum of U_3O_8, when baseline uranium dose is subtracted. This is for 10 years of decay at 90 cm. 37

Figure 5.1. Uranium-232 and ^{233}U production pathways. Desired ^{232}U pathways are in green, and the undesired ^{233}U pathways are in red. 42

Figure 5.2.Plots of the (n,γ) (red) and (n,2n) (blue) cross-sections for ^{231}Pa [2]. Plotted using JANIS 4.0. 43

Figure 5.3. Plots of the (n,γ) (red) and (n,2n) (blue) cross-sections for ^{230}Th [2]. Plotted using JANIS 4.0. 45

Figure 5.4. Plots of the (n,γ) (red) and (n,2n) (blue) cross-sections for ^{237}Np [2]. Plotted using JANIS 4.0. 46

Figure 5.5. Plots of the (n,γ) (red) and (n,2n) (blue) cross-sections for ^{232}Th [2]. Plotted using JANIS 4.0. 47

Figure 5.6. Plots of the (n,γ) (red) and (n,2n) (blue) cross-sections for ^{233}U [2]. Plotted using JANIS 4.0. 49

Figure 5.7. HFIR Core Diagram. This diagram has been modified to highlight in blue the ISVXF positions considered. One of pneumatic facilities, in green, is also in one of these facilities..... 52

Figure 5.8. Flux per unit Lethargy Spectra for the Hydraulic Tube and Inner Small Vertical Experimental Facilities from the MCNP cycle 400 model. 54

Figure 5.9. Irradiation of one gram of Protactinium-231 in the HFIR hydraulic facility for six cycles. 55

Figure 5.10. Irradiation of one gram of Thorium-230 in HFIR hydraulic facility for six cycles..... 56

Figure 5.11. Irradiation of one gram of 10:90 ^{230}Th:^{232}Th in HFIR hydraulic facility for six cycles. 56

Figure 5.12. Protactinium-231 irradiation in an Inner Small Vertical Experimental Facility for eight cycles. 58

Figure 5.13. Thorium-230 irradiation in an ISVXF for eight cycles. 58

Figure 5.14. 10:90 ^{230}Th:^{232}Th Irradiation in an ISVXF for eight cycles. 60

Figure 6.1. Cross-Section of the HFIR core from the Cycle 400 MCNP model. 63

Figure 6.2. Cross-Section of the HFIR flux trap from the Cycle 400 MCNP model. 64

Figure 6.3. Cross-section of the HFIR target geometry. Orange is the oxide-aluminum target material, lime green is an aluminum liner, and the teal is the cladding and outer coolant shroud. 66

Figure 6.4. 238-group neutron spectra in flux per unit lethargy for various depths in a ^{231}Pa target. 66

Figure 6.5. 238-group neutron spectra for the outer layer of a ^{231}Pa target. 67

Figure 6.6. 238-group neutron spectra for the center of a ^{231}Pa target. 67

Figure 6.7. 238-group neutron spectra for various depths in a pure ^{232}Th target. 69

Figure 6.8. 238-group neutron spectra for various depths in a 40 percent ^{230}Th target. 69

Figure 6.9. 238-group neutron spectra for various depths in a 100 percent ^{230}Th target. 70

Figure 6.10. 238-group neutron spectra for the outer layer of a 100 percent ^{230}Th target. 70

Figure 6.11. 238-group neutron spectra for the center of a 100 percent ^{230}Th target. 71

Figure 6.12. 238-group neutron spectra between ¾ radius and ½ radius of a 100 percent ^{230}Th target. 71

Figure 6.13. ORIGEN results for a ^{231}Pa HFIR target irradiated for six HFIR cycles. 74

Figure 6.14. Protactinium-231 ORIGEN data for hydraulic tube data and MCNP flux data. 74

Figure 6.15. ORIGEN results for a 100 percent ^{230}Th target. 77

Figure 6.16. Comparison of 100 percent Thorium-230 ORIGEN data for hydraulic tube data and MCNP flux data. 77

Figure 6.17. ORIGEN results for a 10 percent ^{230}Th target. 78

Figure 6.18. Comparison of 10 percent Thorium-230 ORIGEN data for hydraulic tube data and MCNP flux data. 78

Figure 6.19. Uranium-232 Buildup for each ^{230}Th Enrichment. 79

Figure 6.20. Remaining ^{230}Th mass (g) per Gram of Source Material for Six HFIR Cycles 82

Figure 6.21. Thorium-228 mass (g) per Gram of Source Material for Six HFIR Cycles. 83

Figure 6.22. Thorium-229 mass (g) per Gram of Source Material for Six HFIR Cycles. 83

Figure 6.23. Remaining Elemental Thorium – Sum of all thorium isotopes. 85

Figure 6.24. Remaining ^{230}Th Fraction in Elemental Thorium. 85

Figure 7.1. Proposed ^{230}Th Target cycle 87

Figure 7.2. Proposed ^{231}Pa Target cycle. 87

Figure 7.3. Costs per gram of ^{232}U for Each Production Process Examined. 95

Figure 7.4. Costs per gram of ^{232}U focused on the region of lowest cost per gram of ^{232}U. The Pa recycling case with $200,000 extraction costs is indicated. 97

Figure 7.5. Costs per gram of ^{232}U centered on the weighted average of thorium irradiation with protactinium recovery. The case of averaged 80 percent enriched thorium from 3 percent feed with Pa recovery is indicated. 97

Figure 8.1. Cross-section of the Advanced Test Reactor 102

Figure 8.2. Baseline case with 2 ppm of ^{236}Pu with a single 0.97 removal reprocessing after 150 days. 106

Figure 8.3. Activity vs. Time for relevant isotopes for 1 ppm ^{236}Pu for an aging time of 5 years and a removal fraction of 0.99. 108

Figure 8.4. Activity vs. Time for relevant isotopes for 12 ppm ^{236}Pu for an aging time of 5 years and a removal fraction of 0.99. 108

Figure 8.5. Thallium-208 Activity for each tested ^{236}Pu concentration for 5 years of decay and a removal fraction of 0.99 109

Figure 8.6. Activity vs. Time for relevant isotopes for 4 ppm ^{236}Pu for an aging time of 1 year a removal fraction of 0.99. 109

Figure 8.7. Activity vs. Time for relevant isotopes for 4 ppm ^{236}Pu for an aging time of 8 years and a removal fraction of 0.99. 110

Figure 8.8. Activity vs. Time for relevant isotopes for 12 ppm ^{236}Pu for an aging time of 5 years and removal fraction of 0.97. 112

Figure 8.9. Activity vs. Time for relevant isotopes for 12 ppm ^{236}Pu for an aging time of 5 years and removal fraction of 0.9999. 112

Figure 8.10. Comparison of ^{208}Tl activity from a ^{236}Pu concentration of 12 ppm with 5 years of aging for each removal fraction. 113

Figure 8.11. Aging time vs. ^{23}Pu concentration for each ^{232}U removal fraction. 113

Figure 8.12. Uranium-232 Mass vs. time for 4 ppm ^{236}Pu for 5 Years – 0.97 Removal, 4 Years – 0.99 Removal, and 3 Years – 0.9999 Removal 115

Figure 8.13. Uranium-232 Mass vs. time for 6 ppm ^{236}Pu for 8 Years – 0.97 Removal, 6 Years – 0.99 Removal, and 5 Years – 0.9999 Removal 115

CHAPTER 1.
INTRODUCTION AND BACKGROUND

Enriched uranium is the primary fuel for most nuclear reactors all over the world. In the United States, fresh enriched uranium is the sole source of fuel for nuclear reactors. In nations that conduct reprocessing, enriched uranium is still vital for the operation of nuclear power plants. With international development in nuclear power in recent years, meeting the demand for fuel requires the mining and shipment of uranium all over the world. The mining and shipment of uranium in several nations leads to the potential for diversion and nuclear proliferation by rogue nations and non-state actors.

1.1. Motivations

The low energy gamma emissions of enriched uranium are easily shielded, making the detection of uranium in case of diversion difficult. One way of increasing the detectability of uranium is to add a tracer isotope to uranium that has high energy gamma emissions that are more capable of penetrating shielding materials. However, several questions are raised in considering the choice of isotope to add.

1.1.1. Problems with the use of a tracer: Isotope Choice, Radiological Hazards, and Isotope Sources.

Adding an isotope with high energy emissions to uranium will inherently increase the dose to individuals near any such material, including authorized radiation workers at appropriate facilities. Therefore, the dose rate due to different quantities of additive in uranium must be determined. Several parts of the front end of the fuel cycle will have to be examined. This will provide information on where the tracer emissions become dominant over the baseline uranium emissions, as well as how the dose rate due to the additive changes with concentration. These together will determine what quantity of tracer can be added while minimizing the additional dose.

A source of tracer must also be determined. Based on the appropriate quantity of tracer determined in the dosimetry study, the annual demand for the tracer can be calculated and

a production scheme can be determined. If the tracer isotope chosen is not naturally occurring, then the feasibility of production by target irradiation must be determined. This study will have to determine target material and reaction pathways that produce the chosen tracer isotope. Sources of target material must also be determined. The reaction pathways must be studied to determine product yield, which determines the what the best production pathway is, and what facility to use. Based on the irradiation capabilities of facility chosen and the preferred target material, the product yield can be calculated as well as the ability to meet demand.

For this dissertation, the isotope Uranium-232 will be considered. Uranium-232 has properties that make this isotope preferable for use as a tracer in enriched uranium. High-energy gamma emissions are due to the decay daughter Thallium-208 [1]. The effects of ^{232}U on the uranium fuel cycle will be considered, as well of determining the optimal production scheme for ^{232}U.

1.2. Properties of Uranium-232

Uranium-232 has several properties that make it ideal for use as a tracer in enriched uranium. Since ^{232}U is an isotope of uranium, it cannot be chemically separated from other uranium isotopes. It is also affected by enrichment processes such centrifuge enrichment. This allows for ^{232}U concentration to be correlated to ^{235}U enrichment if ^{232}U is added prior to the enrichment process. The main property of ^{232}U of interest, however, is the high energy gamma ray emissions. These high energy gammas are not from ^{232}U directly, but from the ^{232}U decay chain.

1.2.1. The ^{232}U Decay Chain and Gamma Emissions.

The ^{232}U decay chain is the source of the high energy gamma rays that make ^{232}U the preferred tracer isotope. Uranium-232 has a half-life of 69.8 years, and the decay chain terminates at ^{208}Pb [1]. Most of the daughter isotopes are short-lived, with the longest-lived daughter, ^{228}Th, having a half-life of 1.91 years [1]. A diagram of the ^{232}U decay chain is provided in Figure 1.1.

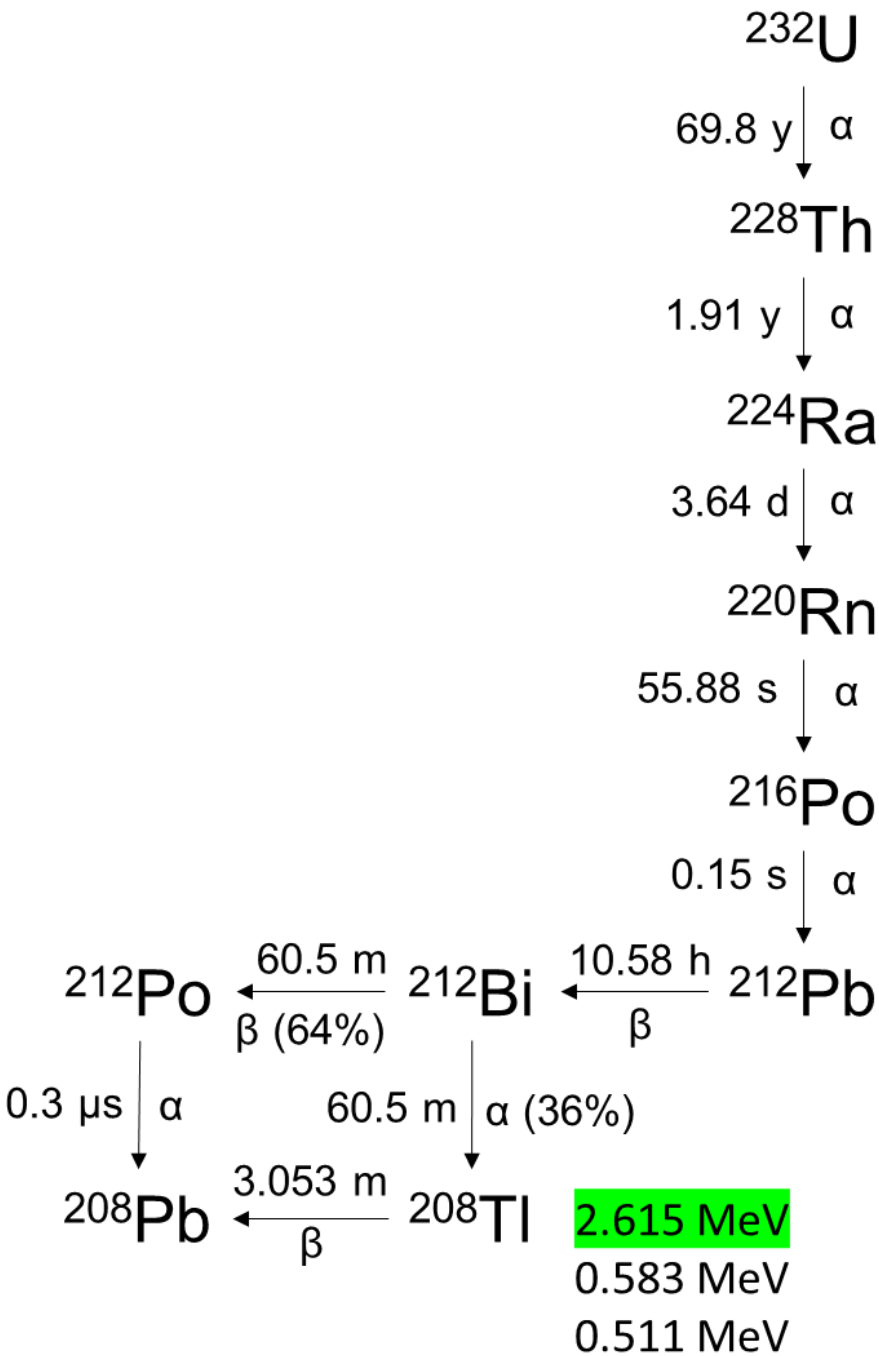

Figure 1.1. The ^{232}U Decay Chain

From the decay daughters of ^{232}U, the most notable is the isotope ^{208}Tl. This particular isotope has a short half-life of 3.053 minutes, emitting gammas with an energy of 2.615 MeV [1]. It is these gamma rays that would be used for detection if ^{232}U is used as a tracer, as the higher energy and intensity is more capable of penetrating shielding, and therefore more difficult to conceal.

1.3. Objectives and Scope

This initiative for using ^{232}U as a tracer examines the dosimetry aspects of using ^{232}U, and the mechanisms and procedures for producing ^{232}U. Several factors of both the dosimetry aspects and production scheme must be examined.

1.3.1. Dosimetry

As noted previously, the higher energy 2.615 MeV gamma rays of ^{208}Tl are more capable of penetrating shielding. This makes this particular gamma ray of interest as a tracer, but also potentially hazardous. However, this is only one of the many gamma rays emitted by the ^{232}U decay chain. Several other gammas of varying energies are also emitted, which may pose a hazard to workers. The higher activity of ^{232}U causes these gammas to be emitted alongside the 2.615 MeV gamma with higher intensities than gamma rays from the decay of the longer-lived uranium isotopes. If ^{232}U is added in sufficient quantities to uranium compounds, the ambient dose rates a worker may be exposed to could be excessive. However, it is not known what concentration of ^{232}U should be added, or how the concentration of ^{232}U affects the ambient dose rates emitted from uranium.

As uranium is processed from ore, enriched, and made into fuel, the uranium is converted into different chemical compounds, such as UF_6 and UO_2. These compounds have different methods of storage, whether as a drum of yellowcake, or as a fuel assembly awaiting loading into a reactor core. The impact of ^{232}U must be determined for each uranium compound and storage system. This can be determined by modeling each compound and storage system with varying concentrations of ^{232}U. Such modeling will determine how ambient dose rates are affected by varying ^{232}U concentrations, and may determine how much ^{232}U should be added.

1.3.2. Production

The concentration that causes a minimum dose rate increase provides information on how much ^{232}U needs to be produced. However, a production scheme needs to be determined. This study will examine producing ^{232}U via neutron irradiation. The source material needs to be determined, as well as reaction pathways for producing ^{232}U. These pathways determine the preferred type of facility. These include facilities such as the high energy neutrons of an accelerator, or the fast and thermal energies of a reactor. Once the preferred target material and neutron spectra are determined, a more specific examination can be performed by modeling a target irradiation with the specific neutron flux of a facility. Target neutronics will also be examined. However, the specifics of target design, target fabrication, and product recovery are beyond the scope. The scope of this study also does not include to specific processes for target material sourcing.

CHAPTER 2.
LITERATURE REVIEW OF PREVIOUS STUDIES OF URANIUM-232

Uranium-232 has had previous occurrences and applications that are worthy of note, and provide context to this current work. While this study aims to use a minimal quantity of ^{232}U as a tracer in ^{235}U based material, previous applications involve the occurrence of ^{232}U in the thorium fuel cycle, or for use as a spiking additive at higher concentrations. Uranium-232 is also a decay daughter of ^{236}Pu, which is a biproduct of ^{238}Pu production. While not fully comprehensive, this chapter examines several previous studies involving ^{232}U.

2.1. Uranium-232 in the Thorium Fuel Cycle

One major occurrence of ^{232}U is in the thorium fuel cycle. Uranium-232 builds up in thorium blanket material as a biproduct of ^{233}U breeding. The pathway of reactions that produce ^{233}U from ^{232}Th is shown in Equation 2.1. Uranium-232 can form as a result of (n,2n) reactions in the ^{232}Th fertile material. This reaction requires fast neutrons with a threshold energy of about 6.6 MeV [2]. These reactions are shown in Equations 2.2, 2.3, and 2.4.

$$^{232}_{90}\mathrm{Th} + ^{1}_{0}\mathrm{n} \xrightarrow[(\mathrm{n},\gamma)]{} ^{233}_{90}\mathrm{Th} \xrightarrow[\beta^-]{} ^{233}_{91}\mathrm{Pa} \xrightarrow[\beta^-]{} ^{233}_{92}\mathrm{U} \tag{2.1}$$

$$^{232}_{90}\mathrm{Th} + ^{1}_{0}\mathrm{n} \xrightarrow[(\mathrm{n},\gamma)]{} ^{233}_{90}\mathrm{Th} \xrightarrow[\beta^-]{} ^{233}_{91}\mathrm{Pa} \xrightarrow[\beta^-]{} ^{233}_{92}\mathrm{U} \xrightarrow[(\mathrm{n},2\mathrm{n})]{} ^{232}_{92}\mathrm{U} \tag{2.2}$$

$$^{232}_{90}\mathrm{Th} + ^{1}_{0}\mathrm{n} \xrightarrow[(\mathrm{n},\gamma)]{} ^{233}_{90}\mathrm{Th} \xrightarrow[\beta^-]{} ^{233}_{91}\mathrm{Pa} \xrightarrow[(\mathrm{n},2\mathrm{n})]{} ^{232}_{91}\mathrm{Pa} \xrightarrow[\beta^-]{} ^{232}_{92}\mathrm{U} \tag{2.3}$$

$$^{232}_{90}\mathrm{Th} + ^{1}_{0}\mathrm{n} \xrightarrow[(\mathrm{n},2\mathrm{n})]{} ^{231}_{90}\mathrm{Th} \xrightarrow[\beta^-]{} ^{231}_{91}\mathrm{Pa} \xrightarrow[(\mathrm{n},\gamma)]{} ^{232}_{91}\mathrm{Pa} \xrightarrow[\beta^-]{} ^{232}_{92}\mathrm{U} \tag{2.4}$$

Uranium-232 has appeared in previous studies discussing the proliferation resistance of the thorium fuel cycle and in methods of discouraging the use of ^{233}U in weapons.

2.1.1. Radiation Hazards from the Contamination of ^{233}U with ^{232}U

Kang and von Hippel examined the contamination of ^{233}U with ^{232}U in the context of producing ^{233}U for weapons material [3]. Their study covers various aspects of ^{233}U that make it suitable for weapons, as well as the resistance of ^{233}U from the thorium fuel cycle to proliferation. In their study, they concluded that ^{233}U from LEU-thorium fueled pressurized water reactors would result in excessive dose rates [3]. A 5-kg sphere of ^{233}U with one percent ^{232}U after one year of decay and after separation would produce a dose rate of 127 rem per hour at a distance of 0.5 meters [3]. Kang and von Hippel then explained that by limiting burnup and using reactors that have fewer fast neutrons and more thermal neutron flux, the contamination of ^{232}U can be mitigated against. Such fluxes could possibly be achieved in a heavy water reactor [3]. A reprocessing procedure that removes the first daughter, ^{228}Th, can also limit the dose due to ^{208}Tl [3].

2.1.2. Radiation and Decay Heat causing Degradation of Weapons Components

A study by Moir examined two properties of ^{232}U: the gamma dose from ^{208}Tl, and heat production due to ^{232}U decay [4]. While the dose to workers has already been discussed, Moir also looked at the damage to the high explosive components in weapons due to gamma emissions [4]. Ionizing radiation may lead to the degradation of high explosives [4]. This limits the shelf life of the uranium and other components [4]. Decay heat will also degrade the components of a weapon over time [4]. One kilogram of ^{232}U produces 641 watts after purification [4]. This increases to 5322 watts per kilogram after nine years of decay [4]. This may potentially degrade components and make the material difficult to store and handle [4].

2.1.3. Proliferation Resistance of the Thorium Fuel Cycle in Conjunction with Molten Salt Reactors

Molten salt reactors are often considered for use with the thorium fuel cycle and are stated to offer proliferation resistance when used with the thorium fuel cycle. Some of these properties are due to the presence of ^{232}U. A study by Gat and Engel discusses how the properties of ^{232}U, the thorium fuel cycle as a whole, and molten salt reactors together increase the resistance of ^{233}U to proliferation [5]. Removal of undesired ^{232}U from a molten salt fuel requires an isotope separation process [5]. This fuel cycle reduces processing and handling steps, limiting diversion opportunities [5]. This study notes that the presence of ^{232}U makes covert ^{233}U diversion difficult because of the added ^{232}U being relatively easy to detect [5]. High levels of shielding and remote handling are necessary as well to minimize the gamma dose to workers [5].

It should be noted that in the above studies, the focus was on the thorium fuel cycle and the intrinsic presence of ^{232}U and the 2.6 MeV gamma rays from ^{208}Tl making fissile material from this fuel cycle hazardous to work with. While detection was briefly noted, these studies looked more closely at the dose to individuals and spiking fissile material to prevent proliferation. These studies also did not consider the concept of adding ^{232}U produced elsewhere to the ^{233}U material.

2.2. Protection of ^{235}U Enriched Uranium with ^{232}U

Using ^{232}U to protect ^{235}U has been previously studied before, but once again, the focus of these studies is more on the use of ^{232}U as a hazardous deterrent to individuals handling such material or for degrading weapon components. Although, tracer use has been considered here as well. Sources of ^{232}U considered focus on ^{232}U recovery during light water reactor fuel reprocessing, and not on production sources outside of recovery from uranium.

2.2.1. Proliferation Resistance of ^{235}U via Excessive Dose and Decay Heating

Lloyd and Goddard extensively studied the use of ^{232}U in deterring the use of ^{235}U for weapons via the decay heat and gamma emissions [6] . They looked at the effects of including ^{232}U in the material of a uranium pit implosion type device [6]. That study focused on heat degradation of such a device due to ^{232}U [6]. Sufficient heating can degrade components, and potentially detonate the high explosives [6]. They also looked at how ^{232}U concentration changes when added to uranium before enrichment [7]. They calculated when that natural uranium with an added ^{232}U concentration of 0.03 percent was enriched to 90 percent ^{235}U, the ^{232}U percentage increased to 6.241 percent [7]. They also conducted an extensive figure of merit analysis on the attractiveness of uranium containing ^{232}U over time [8]. Lloyd and Goddard focused on the decay heat as the primary factor in using uranium containing ^{232}U, and did not discuss detection. They also did not focus on the production source of ^{232}U for protecting enriched uranium.

2.2.2. Sourcing ^{232}U from Reprocessed Uranium to Protect LWR Fuel

Studies on calculating the buildup of ^{232}U in light water reactors have been conducted in the past. A few of such studies are explored here, with one study examining WWER reactors, and the other studies examining PWRs and BWRs.

In a study by Gusev, Smirnov, Nevinitsa, and Volkov, the use of ^{232}U emissions from reprocessed uranium was discussed [9]. This study looked at a hypothetical scenario involving the diversion and enrichment of WWER reactor fuel rods made of reprocessed uranium [9]. Their conclusions were that fuel rods made with reprocessed uranium, which inherently contains ^{232}U, is easier to detect, and more resistant to diversion [9]. In the case of removed fuel rods from a new fuel assembly, if the ^{232}U concentration is measured and does not match an expected concentration based on the reprocessed uranium used, it can be determined whether diversion has occurred [9]. While this study does discuss improving the detection of enriched uranium rather than increasing dose to workers, the ^{232}U is obtained from reprocessed uranium [9]. This paper does not discuss adding ^{232}U to fresh uranium enriched from natural material.

A pair of studies written by W. B. Arthur focused on PWRs and BWRs produced by Westinghouse and General Electric, respectively. One such study looked a standard fueled PWRs and BWRs, and examined scenarios under which the ^{232}U concentration grows in excess of 110 ppb [10]. This concentration can be limited by limiting thorium and ^{236}U, or limiting aging time after irradiation. Another study examined denaturing fuel with thorium, with enriched fresh fuel having ^{223}U concentrations ranging from 135 to 260 ppm [11]. For thorium bread fuel, the ^{232}U concentrations varied from 411 to 512 ppm [11].

2.2.3. Previous Examinations on Producing ^{232}U from ^{230}Th and ^{231}Pa

A couple of studies have looked at producing ^{232}U from ^{231}Pa and ^{230}Th. By using ^{231}Pa and ^{230}Th, these studies have examined ^{232}U production independent of the thorium fuel cycle and without requiring spent nuclear fuel. These studies may provide notable comparisons in results.

A study by Dominguez, Jodra, and Gonzales in Spain modeled using the BR-2 reactor in Belgium for ^{232}U production from ^{230}Th and ^{231}Pa [12]. This study focused on the use of ^{232}U for thermal spiking of nuclear material. The authors modeled irradiations with flux levels ranging from 10^{12} to $5*10^{14}$ neutrons/(cm^2*s). Several ^{230}Th enrichments were examined by the authors, ranging from 0.5 percent ^{230}Th to 15 percent ^{230}Th. This study also examined ^{232}U production optimization with the recovery and recycling of ^{231}Pa and ^{230}Th.

An earlier study by Sakanoue and Komura in 1961 looked at producing ^{232}U from ^{231}Pa irradiations the JRR-2 reactor [13]. The authors modeled irradiations of ^{231}Pa with the fluxes of 10^{13}, 10^{14}, and 10^{15} neutrons per cm^2 per second. The authors considered ^{232}U as a tracer, but did not determine usable tracer quantities, and also considered direct alpha spectrometry of ^{232}U rather than gamma emissions from ^{208}Tl decay daughters. The authors also conducted an experiment in which a sample of ^{231}Pa was irradiated in the JRR-2 reactor. With this experiment, the authors examined ^{231}Pa irradiation and chemical processing of ^{232}U, as well as the buildup of fission products during irradiation.

2.3. Literature Review Summary

Based on the reviewed literature, the focus on previous work has been the use of higher concentrations of ^{232}U for inducing a radiation hazard or excess heating, with the benefit of increasing detectability. Tracer use of ^{232}U has been discussed, but minimizing additional dose has not appeared to have been a focus. Sources of ^{232}U have been so far from breeding, reprocessing, or recovery of ^{232}U from previously irradiated fuel or breeding material, such as reprocessed ^{235}U fuel, or ^{233}U recovered from thorium breeding targets.

The concept studied in this dissertation aims to only increase the detectability of enriched uranium. The significant increases in dose due to the 2.6 MeV gammas from higher concentrations of ^{232}U are not desired. Also, since the thorium fuel cycle has not been widely utilized, ^{232}U from this cycle is minimal. Reprocessed uranium is not available in the United States, and only a few nations perform reprocessing. Because of this, ^{232}U is not considered available from reprocessing in this dissertation. Whether from the thorium fuel cycle or from reprocessed uranium, such ^{232}U sources also do not protect fresh uranium milled and enriched from ore. Therefore, ^{232}U must be produced from irradiation of specialized targets.

2.4. Originality of Work Compared to Previous Studies.

The novel aspects of this dissertation involve quantifying the amount of ^{232}U to add to uranium materials to minimize dose, and the sourcing of ^{232}U from ^{231}Pa and ^{230}Th irradiation, rather than from reprocessed ^{235}U or from ^{233}U breeding. Spiking applications were the primary application previously considered and reprocessing sources have been studied previously, as discussed throughout this chapter.

Previous studies on the addition of ^{232}U have primarily been adding quantities sufficient to pose a significant hazard to personnel in the vicinity of such material due to high radiation doses. These studies have also considered the use of decay heat to degrade nuclear materials. Both of these applications require significant quantities of ^{232}U, whereas the objective of this study is to only use enough ^{232}U to increase detection while

keeping the increase in ambient dose rate to a minimum. While increasing detectability has been discussed in previous studies, minimizing dose has not been a focus. This study aims to minimize the hazard by modeling various systems containing uranium and determining the minimum concentration from which a dose increase is observed. This will also provide the production requirements for ^{232}U, assuming that the minimum quantity that increases dose is the minimum quantity of ^{232}U that can be detected.

Uranium-232 is a byproduct of the breeding of ^{233}U in the thorium fuel cycle, and can also be sourced by reprocessing irradiated ^{235}U fuel. A few studies mentioned here previously in this chapter have discussed thorium fuel cycle and ^{235}U reprocessing sources. Using ^{230}Th and ^{231}Pa have been studied previously, however this study was conducted with a different modeling method, and considering a different reactor facility.

This dissertation examines sourcing ^{232}U by directly producing this isotope by irradiation of the isotopes ^{231}Pa and ^{230}Th. This study examines using the High Flux Isotope Reactor and will use the SCALE 6.2 ORIGEN module to provide a more sophisticated examination of ^{232}U production in a different facility using modern modeling techniques.

CHAPTER 3.
RADIOACTIVE DECAY CHAINS, ISOTOPE PRODUCTION, AND COMPUTATIONAL TECHNIQUES UTILIZED

For understanding the production, occurrences, and applications of ^{232}U, it is important to know the principles of neutron interactions and radioactive decay. Neutron interactions play a key role in the production of ^{232}U. Radioactive decay also plays a key role in production, and is necessary in the use of ^{232}U as a tracer. It is also important to understand the computational techniques used for modeling isotope production and decay for this study.

3.1. Radioactive Decay of ^{232}U and ^{208}Tl

A key property of radioactive materials is radioactive decay. Radioactive decay is the process by which certain atomic nuclei undergo a disintegration releasing energy. The energy released by the nucleus is in the form of particles or photons as a means for the nucleus to transition from a higher energy state to a lower energy state.

3.1.1. Alpha and Beta Decay

Several aspects of this dissertation are dependent on radioactive decay and the transmutation processes that occur as a part of radioactive decay. Several different types of radioactive decay exist, with each type causing a different transition in the nucleus. As shown in Figure 1.1, the ^{232}U decay chain consists of two types of decay that cause transmutation: α decay, and β^- decay. The general equation for alpha decay is shown in Equation 3.1:

$$ {}^{A}_{Z}X \rightarrow {}^{A-4}_{Z-2}D + {}^{4}_{2}\alpha \tag{3.1} $$

where, ${}^{A}_{Z}X$ is the parent nucleus, ${}^{A-4}_{Z-2}D$ is the daughter nucleus, and ${}^{4}_{2}\alpha$ is the emitted alpha particle, which is equivalent to a ${}^{4}_{2}$He nucleus. Most of the nuclides in the ^{232}U decay chain are heavy nuclides that undergo alpha decay.

Thallium-208 is one of the two nuclides in the ^{232}U decay chain that undergo beta decay. The other nuclide, ^{212}Bi, has branched decay, undergoing alpha decay 36 percent of the time, and beta decay leading to ^{208}Tl occurring 64 percent of the time [1]. Beta decay is the conversion of a neutron in the nucleus in to a proton, emitting an electron and an antineutrino. The general equation for beta decay is shown in Equation 3.2:

$$ {}^{A}_{Z}X \rightarrow {}_{Z+1}^{A}D + e^{-} + \bar{\nu} \tag{3.2} $$

In this equation, ${}^{A}_{Z}X$ is the parent nucleus, ${}_{Z+1}^{A}D$ is the daughter nucleus, e^{-} is the electron, and $\bar{\nu}$ is the neutrino.

It is also important to note the terms half-live ($t_{1/2}$), decay constant (λ), and activity (A). Half-life is the time needed for half of a quantity atoms to undergo radioactive decay. As noted in chapter one, ^{232}U has a half-life of 69.8 years. This means that it would take 69.8 years for half of a quantity of ^{232}U atoms to undergo alpha decay. As radioactive decay is an example of exponential decay, the rate of decrease is proportional to the current value. The decay constant is the constant of proportionality for this process. The decay constant is related to half-life by Equation 3.3.

$$ \lambda = \frac{\ln 2}{t_{\frac{1}{2}}} \tag{3.3} $$

Equation 3.3 gives the decay constant the units of inverse time. When the decay constant is multiplied by the number of atoms (N), this gives the number of atoms disintegrating per second.

Accordingly, this is the activity (A) of an isotope, as shown in Equation 3.4:

$$A = N\lambda \tag{3.4}$$

3.1.2. Gamma Decay

As an isotope undergoes alpha or beta decay, the resulting nucleus is often left in an excited state. Transitioning to the ground state involves the release of gamma rays. Some isotopes are able to stay in such an exited state for extended periods of time, which is known as a metastable state or isomer. Otherwise, the gamma emission is considered prompt. As stated before, this dissertation involves the 2.614 MeV photons emitted from the decay of ^{208}Tl. The decay scheme for ^{208}Tl is shown in Figure 3.1 [14].

3.2. The Bateman Equation

As a quantity of atoms of a given isotope undergo radioactive, the number of atoms of the parent isotope are constantly changing, as well as the number of atoms for each daughter isotope. This is described for a single isotope in the differential equation in Equation 3.5.

$$\frac{dN_n}{dt} = N_m\lambda_m - N_n\lambda_n \tag{3.5}$$

In this equation, $N_m\lambda_m$ is the activity of the parent isotope, and $N_n\lambda_n$ is the activity of the daughter isotope.

Equation 3.5 can be simply solved analytically to provide the number of atoms of isotope n (N_n). The number of atoms for each isotope in a decay chain can be mathematically described with the Bateman equations [15]. The Bateman equation for a general case is shown in Equation 3.6.

$$N_n(t) = \sum_{i=1}^{n}\left[N_i(0)\left(\prod_{j=i}^{n-1}\lambda_j\right)\left(\sum_{j=1}^{n}\left(\left(\frac{e^{-\lambda_j t}}{\prod_{p=i,p\neq j}^{n}(\lambda_p-\lambda_j)}\right)\right)\right)\right] \tag{3.6}$$

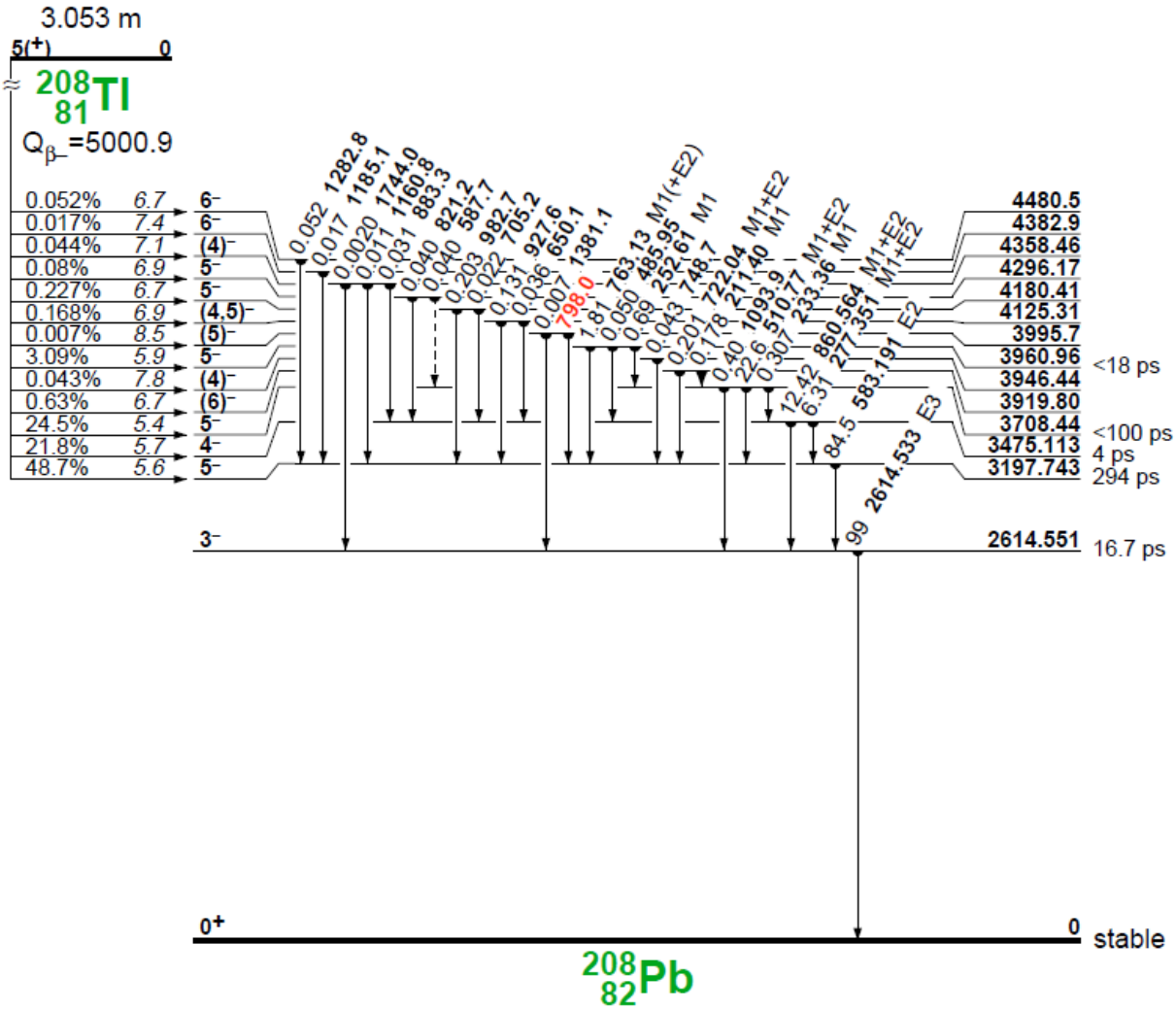

Figure 3.1 Gamma decay level scheme for ^{208}Tl [14].

This equation provides an analytical approach to solve for the activity of all of the isotopes in a decay chain. For production and loss terms due to neutron bombardment in a reactor, a similar equation is formed where production and loss for a given isotope are described by the reaction rate given in Equation 3.7.

$$\frac{dN_2}{dt} = N_1(t)\sigma\dot{\phi} - \lambda_2 N_2 \tag{3.7}$$

Note that this equation is very similar to the decay activity Equation 3.4, but the decay constant is replaced by the multiplication of σ (reaction cross-section with units of cm^2) and ϕ (neutron flux, with units of $cm^{-2}*s^{-1}$). These terms can be placed in the Bateman equation in a similar or additive manner, depending on whether an isotope undergoing bombardment is undergoing decay.

For a case involving a single decay chain, solving the Bateman equation by hand is fairly simple. However, as a target undergoes neutron bombardment in a reactor, what was once a homogeneous material becomes several different isotopes. Each isotope may have its own decay chain, and each daughter isotope has its own neutron interactions. This results in significant complexity in a Bateman equation problem that requires computational methods and software such as SCALE 6.2 ORIGEN to solve.

3.3. SCALE 6.2 ORIGEN Overview

The above complexity of the production and decay of ^{232}U and gamma emissions of ^{208}Tl and other isotopes makes determining the dose and production methods cumbersome to perform by hand. The activity of each isotope is constantly changing, which in turn changes gamma intensities. A tool that is capable of tracking the production and loss of many isotopes from both neutron interactions and radioactive decay, as well as track gamma source terms is needed to study the production and decay of ^{232}U. For this dissertation, SCALE 6.2 ORIGEN is used.

ORIGEN is a point-reactor calculation code that solves differential equations of the form like Equation 3.5 for decay or neutron interactions, and like Equation 3.7 cases where both decay and neutron bombardment are combined [16]. Based on the calculated activities and the decay schemes for a given isotope, ORIGEN is also capable of calculating gamma source terms. To perform these calculations, ORIGEN solves the differential equations for isotopes in matrix form. This is given in Equation 3.8 [16].

$$\frac{d\vec{N}}{dt} = \boldsymbol{A}\vec{N}(t) + \vec{S}(t) \tag{3.8}$$

Note that the term $\boldsymbol{A}$ is the transition matrix, which contains energy averaged cross-sections and decay constants [16]. The term $\vec{S}(t)$ is a source term for N [16].

In cases where the transition matrix requires neutron cross-sections, the cross-section data can be averaged by energy using input neutron spectra using the COUPLE module in SCALE [16]. COUPLE uses flux spectra to collapse cross-section data into the energy averaged cross-sections used in the transition matrix [16]. Flux spectra can be sourced from measurements, or from a particle transport simulation like an MCNP model. For this dissertation, the standard 238-group energy structure found in from JEFF3.0/A was used [16].

3.4. Chapter Conclusions

With the focus on the ^{232}U decay chain, production of ^{232}U through neutron bombardment, and the gamma emissions of ^{208}Tl, it is important to understand the concepts of radioactive decay and nuclide transmutation. As SCALE 6.2 ORIGEN plays a significant role in this work, the principles behind its operation are also important. The dosimetry calculations will require gamma source terms from ORIGEN. The production calculations would require neutron spectra from the High Flux Isotope Reactor to perform production simulations.

CHAPTER 4.
EXAMINING THE DOSE RATE INCREASE DUE TO THE ADDITION OF URANIUM-232 TO THE URANIUM FUEL CYCLE

A version of this work was submitted as a conference proceeding to the 2021 American Nuclear Society Annual Meeting by Joshua H. Rhodes, Brandon Grogan, Alan Krichinsky, Brad Patton, and G. Ivan Maldonado:

J. H. Rhodes, B. Grogan, A. Krichinsky, B. Patton and G. I. Maldonado, "Modeling Additional Dose from Adding Uranium-232 to the Uranium Fuel Cycle," in *Transactions of the American Nuclear Society*, 2021.

The body of this work was performed by J. Rhodes, with the other authors providing guidance and information used for performing this work. This work has been expanded on, going into greater detail background material, on the work performed, and the results from the models used.

4.1. Chapter Abstract

This chapter examines the dose rate from different uranium materials that ^{232}U has been added to. Several materials and their respective storage geometries are modeled for particle transport calculations. The objective of this study is to determine the dose rate from various forms of stored uranium with varying concentrations of ^{232}U added to the uranium. For each material and ^{232}U concentration, gamma source terms were generated using SCALE 6.2 ORIGEN. These source terms were then used in MCNP for each material and geometry. Upon analysis, it was determined that the baseline dose from enriched uranium dominates until the ^{232}U concentration reaches about one part per trillion (ppt), after which the dose rate increases linearly.

4.2. Chapter Introduction

As stated before, the lower energy gamma rays of ^{235}U are easily shielded, allowing for the possibility of concealment of special nuclear material. The highest intensity gamma ray of ^{235}U has an energy of 185.72 KeV [1]. This lower energy can be attenuated with significantly less material when compared to the 2.614 MeV gamma rays of ^{208}Tl grown in due to the decay of ^{232}U. The presence of these gammas could possibly by correlated to the presence of ^{235}U. If the quantity if of ^{232}U added is known along with the material age, the intensity of these gammas could possibly be used to quantify the material. If the ^{232}U is added before enrichment, the lower mass of the ^{232}U will cause the ^{232}U to enrich along with the ^{235}U, causing higher ^{235}U enrichments to have higher ^{232}U concentrations.

These properties raise the possibility of using ^{232}U additives for a few different applications. One application is locating material that is being smuggled or diverted, as uranium would be more difficult to conceal. More gammas would escape, or the presence of increased shielding would alert personnel tasked with implementing safeguards. The enrichment of ^{232}U alongside the ^{235}U allows for a ^{208}Tl gamma intensity to be correlated to the ^{235}U enrichment. This would allow for determining uranium enrichment, which could possibly be used to determine if a sample of uranium has been over-enriched for illicit strategic purposes.

However, the addition of a high energy gamma emitter such as ^{232}U at sufficient activity has complications. As stated earlier in Chapter 1, the addition of such a tracer that emits such high energy gammas at such intensities may expose legitimate workers to an increased gamma dose rate. Also, the higher specific activity of ^{232}U results in higher gamma intensities, even for lower energy gamma rays from ^{232}U decay. This increases the risk of health problems due to radiation exposure, and could lead to workers exceeding the occupational dose limit of 5 rem per year as stated by 10 CFR 20 while within typical working conditions [17]. However, if too little ^{232}U is added, the emissions from the decay of the other uranium isotopes may be more significant to the point that the ^{232}U is not detected at all. Therefore, it is important to determine the dependence of dose rate on the concentration of ^{232}U at each stage of the fuel cycle.

4.3. Dosimetry Modeling and Methodology

This study examines several steps of the uranium fuel cycle, and several models are needed for the uranium compounds and storage form factors found at each step. For each model, the ^{232}U concentration will have to be varied. This will provide the dose due to ^{232}U from each ^{232}U concentration for each model. The results of these will indicate what dose rate workers would expect to be exposed to when working with a given uranium compound in its appropriate storage form factor. This study will focus on the front end of the uranium fuel cycle, as the back-end post irradiation is expected to be dominated by fission product emissions which already require heavy shielding. For this study, dosimetry modeling was performed using Monte-Carlo photon transport in MCNP 6.2, with gamma source terms generated using SCALE 6.2 ORIGEN [16] [18].

4.4. SCALE 6.2 ORIGEN Gamma Source Terms

To generate the gamma source terms from the decay of uranium with varying concentrations of ^{232}U, SCALE 6.2 ORIGEN was used. When using ORIGEN for decay only calculations, a decay library is used to generate the transition matrix [16]. As stated earlier, ORIGEN is capable of calculating the gamma decay source terms for multiple isotopes over time [16]. Prominent gammas from ^{232}U decay are shown in Table 4.1 [1].

As the uranium ages, each of the uranium isotopes present undergo decay, and their respective decay daughters grow in. At lower concentrations, these decay daughters may overshadow the gammas from ^{232}U decay. The emissions of these uranium daughters are considered a baseline for this study. To capture the spectrum of photon energies that may grow in, the energy bins used in ORIGEN range from 10 keV to 3.5 MeV in 10 keV increments. To capture the buildup of ^{208}Tl and other decay daughters over time, several time steps are used: zero (immediately after adding ^{232}U), 1 month, 3 months, 1 year, 3 years, and 10 years. The mass of elemental uranium in each ORIGEN calculation is one kilogram, from which the concentration of ^{232}U can be altered as fractions of one kilogram. The ^{232}U concentrations ranged from one part per quadrillion (ppq) to one part per thousandth (ppth). The full list of concentrations is shown in Table 4.2.

Table 4.1. Prominent Gamma Energies and Intensities of the ^{232}U Decay Chain

Isotope	E (keV)	Intensity (%)
U-232	57.78	0.1999
	129.08	0.0682
Th-228	84.373	1.19
	215.983	0.247
	131.613	0.127
	166.41	0.101
Ra-224	240.986	4.1
Rn-220	549.73	0.114
Po-216	804.9	0.0019
Pb-212	238.632	43.6
	300.087	3.3
Bi-212	39.857	1.06
Po-212	2610	2.6
	570	2
Tl-208	2614.511	99.754
	583.137	85
	510.77	22.6

Table 4.2. List of ^{232}U Concentrations Examined

U-232 Concentration	U-232 Mass Fraction
zero	0
ppq	1.00E-15
3 ppq	3.00E-15
10 ppq	1.00E-14
30 ppq	3.00E-14
100 ppq	1.00E-13
300 ppq	3.00E-13
ppt	1.00E-12
3 ppt	3.00E-12
10 ppt	1.00E-11
30 ppt	3.00E-11
100 ppt	1.00E-10
300 ppt	3.00E-10
ppb	1.00E-09
3 ppb	3.00E-09
10 ppb	1.00E-08
30 ppb	3.00E-08
100 ppb	1.00E-07
300 ppb	3.00E-07
ppm	1.00E-06
3 ppm	3.00E-06
10 ppm	1.00E-05
30 ppm	3.00E-05
100 ppm	1.00E-04
300 ppm	3.00E-04
ppth	1.00E-03

Uranium enrichment must be considered as well for each stage of the fuel cycle. At the front end of the fuel cycle, the significant ^{235}U enrichments are natural uranium and 5 percent low-enriched uranium (LEU). To determine the source strength for each MCNP model, the ORIGEN source strength, calculated for one kilogram of uranium, is multiplied by the mass of uranium in the appropriate model. The calculated spectra provide the probability for each gamma energy in the MCNP source definition. Example ORIGEN input files used for this study are included in Appendix A:.

4.5. MCNP Model Geometry and Materials

As stated earlier, this study focuses on the front end of the fuel cycle. The compounds examined in this study are: U_3O_8 representing yellowcake in a 55-gal steel drum, UF_6 in the 30B and 48Y cylinders, and UO_2 in a Westinghouse 17 × 17 fuel assembly. Each of these compounds and their respective containers or form factors represents a different part of the fuel cycle: milling, UF_6 conversion, enrichment, and fuel fabrication. Each MCNP model is discussed below. As an example of the methods applied, an MCNP input file for the 55-gallon drum geometry is included in Appendix A:.

4.5.1. 55-gallon Drum of Yellowcake

Yellowcake, represented as U_3O_8 stored in a 55-gallon steel drum, represents the form that uranium is in after milling the uranium from ore, before being converted to UF_6 for the enrichment process. As this step is before enrichment, the uranium is still at the natural ^{235}U enrichment. The geometry in the MCNP model is shown below in Figure 4.1

4.5.2. Uranium Hexafluoride Cylinders

In order to enrich the uranium for use in a reactor, the yellowcake undergoes conversion to UF_6. The UF_6 is stored in special cylinders and shipped to an enrichment plant such as the centrifuge plant run by URENCO USA in New Mexico [19]. These cylinders are also used around the world, and the source terms from typical cylinders have been studied extensively [19] [20]. After enrichment, the enriched uranium is shipped to be converted to UO_2 and be fabricated into fuel. Several different cylinder types are used, and each as a

limit on the maximum uranium enrichment. This study focuses on the 30B and 48Y cylinders. In this study, the 30B cylinder will be modeled with both natural uranium and five percent LEU. The 48Y cylinder is assumed to only have natural uranium contents. [21] [22] The primary difference besides the enrichment of the contents is the size of each cylinder. The 30B cylinder has a 30-inch inner diameter, and the 48Y cylinder has a 48-inch inner diameter [21] [22]. The MCNP geometry of the 30B cylinder is shown in Figure 4.2, and the 48Y cylinder is shown in Figure 4.3. In each model, the UF_6 is assumed to solidify on the inner cylinder walls, leaving a cylindrical void.

4.5.3. Pressurized Water Reactor Fuel Assembly

Once the uranium is enriched, the UF_6 undergoes UO_2, which is then manufactured into fuel assemblies. These assemblies are then shipped to powerplants, where they are stored until loaded into the reactor for irradiation. To represent a typical fuel element in this stage of the fuel cycle, a Westinghouse 17 × 17 fuel assembly with 5 percent LEU was modeled [23]. The model excludes structural materials, control rods, and instrumentation. Only fuel pins are included. The fuel assembly array, as well as a single fuel pin are shown in Figure 4.4.

4.6. Dosimetry Tallies

In order to determine the dose rate from each model, F5 detector tallies in MCNP were used. These tallies can be placed anywhere in the geometry in order to measure the particle fluence at a chosen location. F5 tallies could be defined as point detectors, or as ring detectors [18]. A point detector measures the number of particles passing within a set distance to a specified point [18]. A ring detector allows for placing a ring around a geometry, essentially functioning like a ring of point detectors [18]. Like point detectors, ring detectors have an exclusion radius where the detector counts particles within a certain distance of the ring [18]. If placing a tally around a cylinder or other geometry that has axial symmetry, this allows for averaging across the entire azimuthal direction to determine the flux at a specified distance from an axially symmetric geometry.

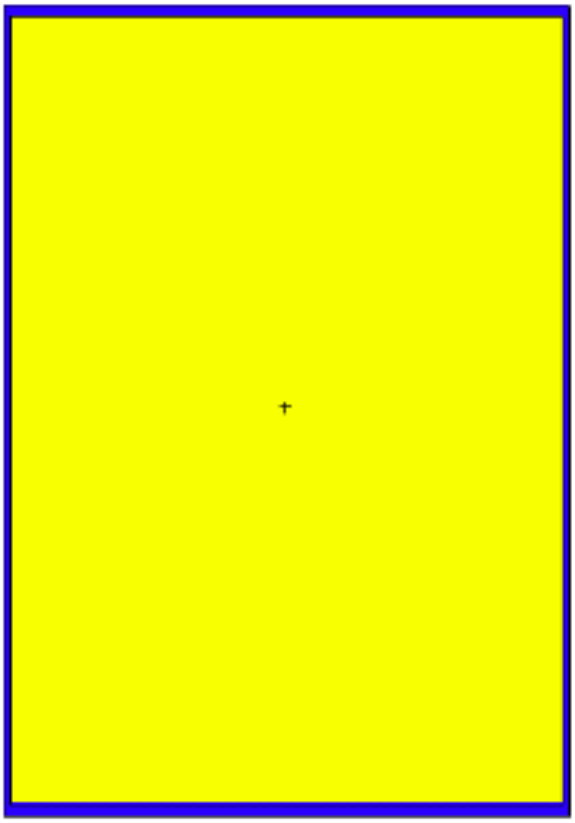

Figure 4.1. MCNP geometry of a 55-gal drum. Yellow represents U_3O_8. Blue is structural material. The wall thickness is 6 mm (0.24 in).

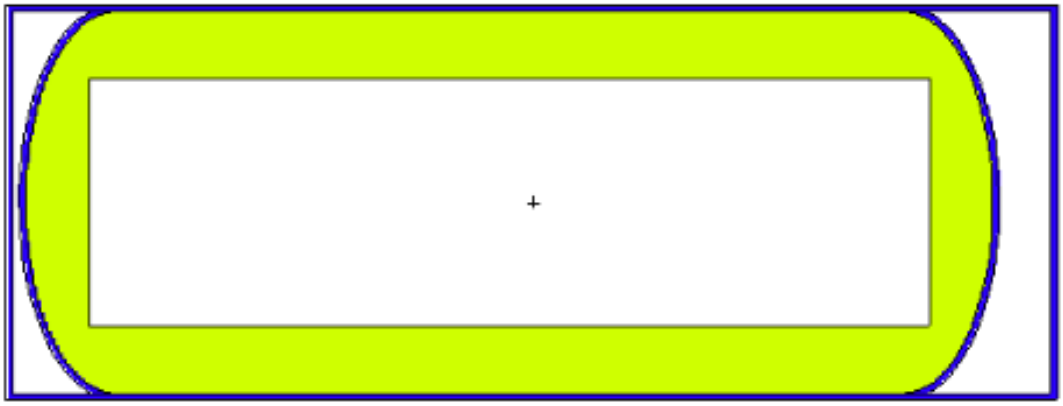

Figure 4.2. 30B cylinder. The UF_6 (green) is assumed to have accumulated on the cylinder wall (blue). The wall is 13 mm (0.5 in) thick.

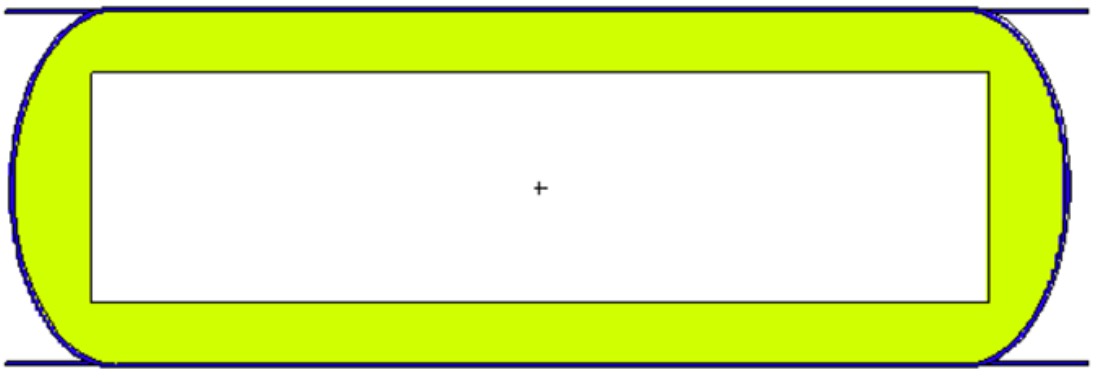

Figure 4.3. 48Y cylinder. The UF_6 (green) is assumed to have accumulated on the cylinder wall (blue). The wall is 16 mm (5/8 in) thick.

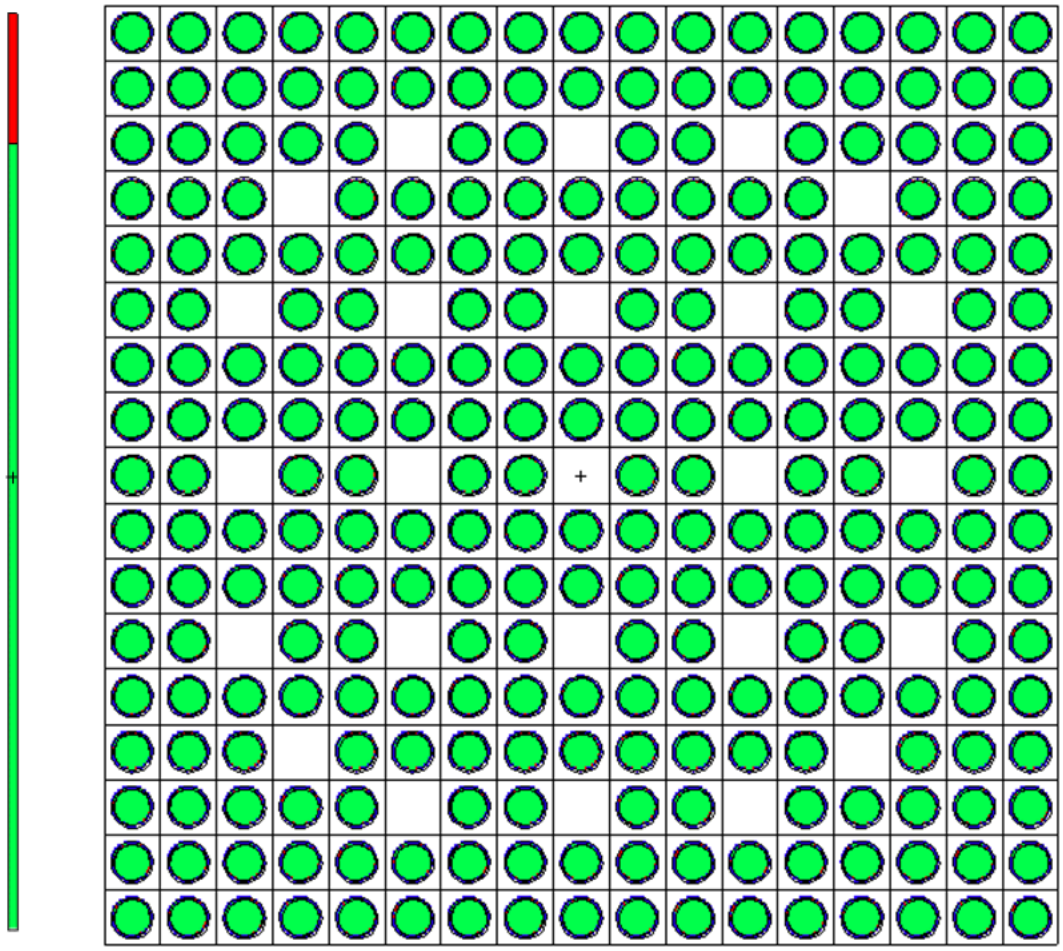

Figure 4.4. Westinghouse 17 × 17 fuel assembly and single fuel pin. Green is UO_2 fuel, red is the helium plenum, and blue is zirconium alloy cladding.

For each model, point detectors were placed axially in each model from zero to 90 cm in 30 cm increments from each geometry. For axially symmetric models, ring detectors were placed at the axial mid-point from zero to 90 cm in 30 cm increments. The 55-gallon drum and the 48Y cylinder also included detectors at distances of 10 and 20 cm. The 48Y cylinder also had detectors at 120 cm. The fuel assembly model lacks radial symmetry, so point detectors from one side of the fuel assembly were used.

Detector tallies track particle fluence per source particle [18]. This fluence must be converted to a dose rate. Multiplying by the result by the intensity provides a particles per second component to obtain flux with the units of particles/(cm^2*s). Dose conversion factors converts the number of particles to dose. ICRP 116 provides effective dose per fluence conversion factors to convert fluence to dose with the units of picosieverts * cm^2 [24]. Multiplying the above flux by these dose conversion factors provides a dose rate with the units of picosieverts per second. This result is then converted to rem per hour.

4.7. Model Results

Each model was run and the results were examined to determine the effects of ^{232}U decay on the dose rate from each model. It is important to know how the dose rate changes with distance for a given model, age, and ^{232}U concentration, and how the dose for a given ^{232}U concentration and distance changes with age. However, it is of particular interest to determine how the dose rate at a given distance for each model.

4.7.1. 55-gallon Drum

Figure 4.6 shows the dose rate in rem per hour versus the ^{232}U concentration in the modeled 55-gallon drum of U_3O_8. This plot shows the radial dose rate at 30 cm for all ages. Note that both scales are logarithmic. It is immediately observed that with respect to the ^{232}U concentration, two distinct regions are observed. For lower ^{232}U concentrations, the dose rate is constant for a given material age. However, as the ^{232}U concentration increases past 100 ppt, the dose rate begins to increase, developing a linear relationship at higher ^{232}U concentrations. Tabular data for these results is given in Appendix A, Table A.1.

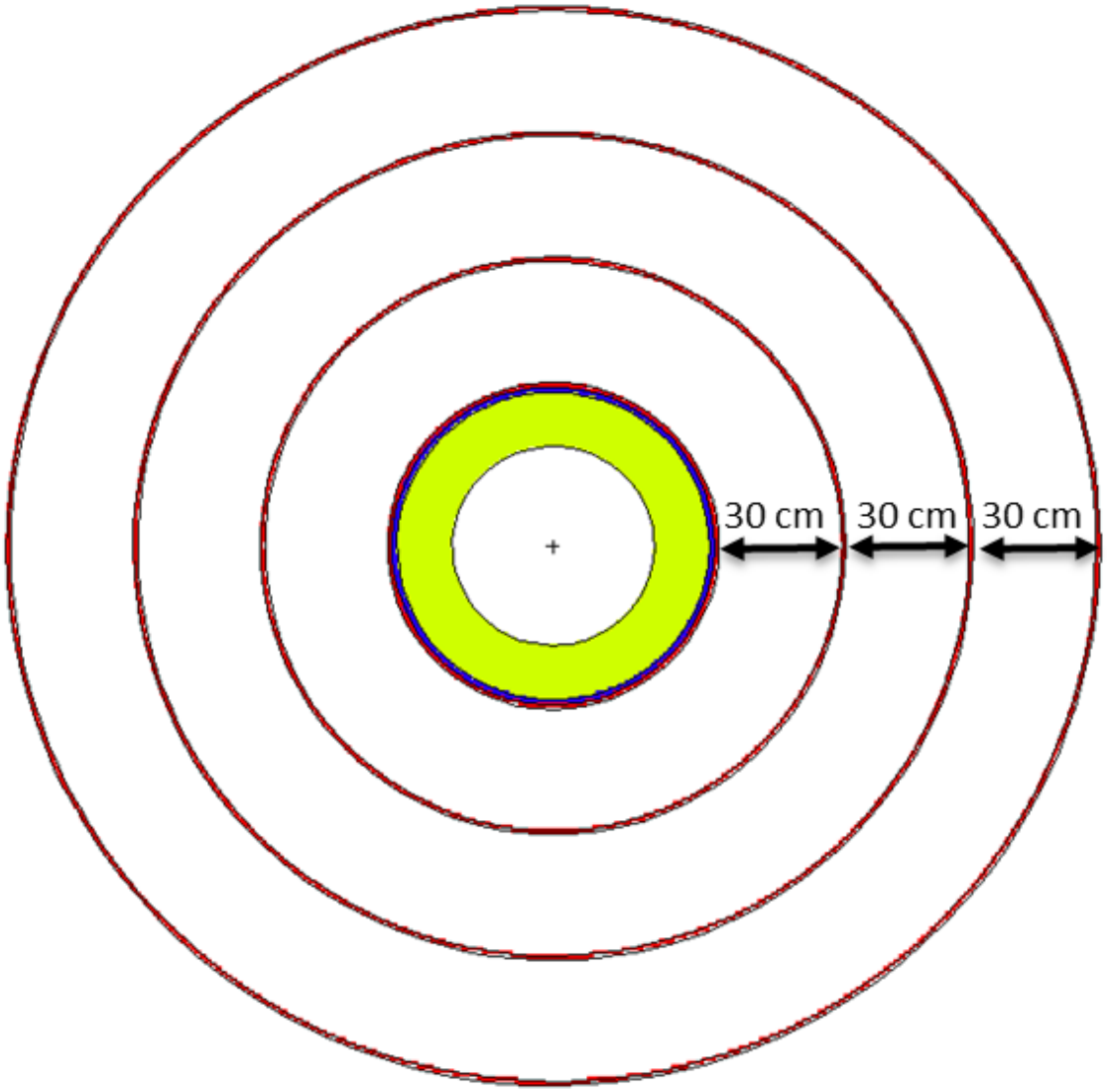

Figure 4.5. Ring detectors for the 30B cylinder model (top view).

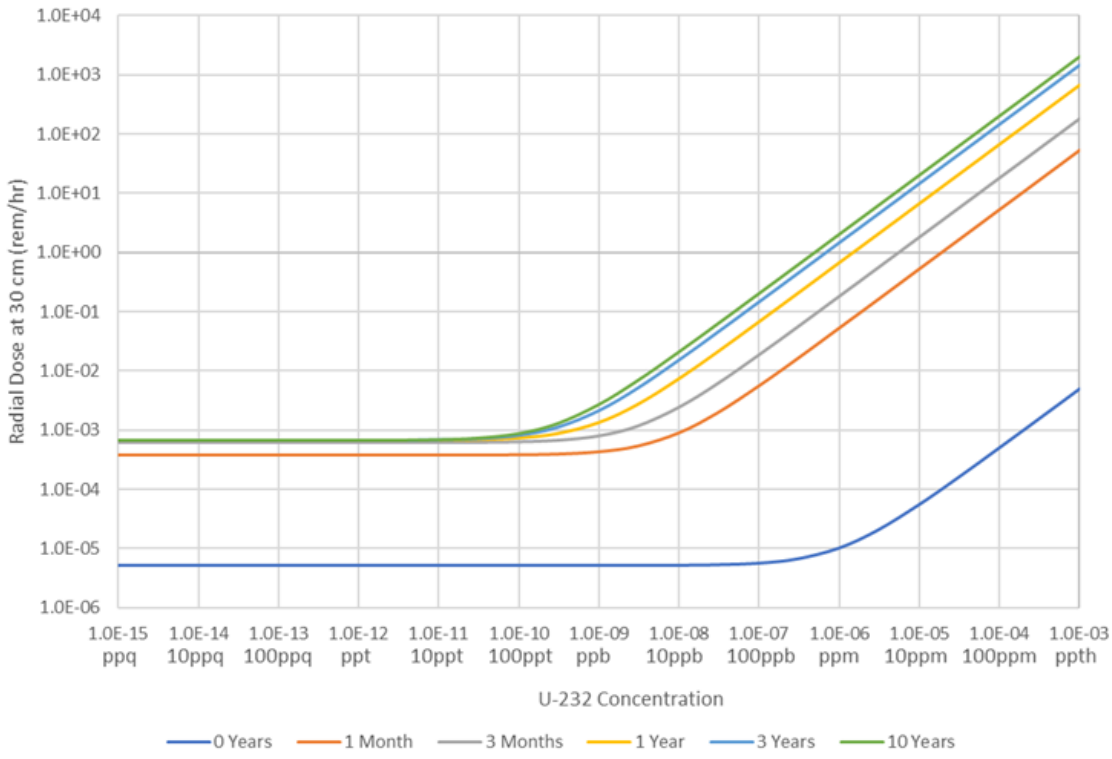

Figure 4.6. Radial Dose Rate at 30 cm vs. U-232 Concentration for a 55-gallon Drum of U_3O_8.

4.7.2. 30B Cylinder

The results for the 30B cylinder are shown below for both natural uranium feed material, as well as five percent enriched product material. The results for natural uranium shown in Figure 4.7, and the results for the five percent enriched uranium are shown in Figure 4.8. Due to the different ^{235}U enrichment, the initial dose rate at zero years is lower for the natural uranium. After aging, both cylinders have similar behavior as their decay daughters grow in. Once again, two distinct regions of decay behavior are observed, with a region of constant dose rate at lower ^{232}U concentrations followed by a linear region developing at higher concentrations. Tabular data for the natural uranium 30B cylinder is provided in Appendix A, Table A.2, and data for the 5% enriched uranium 30B cylinder is provided in Appendix A, Table A.3.

4.7.3. 48Y Cylinder

The results for the 48Y cylinder are shown in Figure 4.9. As this cylinder has natural uranium contents, it behaves similarly to the 30B cylinder, but with higher dose rates due to the greater mass or uranium. The two distinct dose rate regions are exhibited again, with a constant region at lower concentrations and a linear region at higher concentrations. Tabular data for these MCNP results is provided in Appendix A, Table A.4.

4.7.4. Fuel Assembly

The 17x17 PWR fuel assembly results are shown in Figure 4.10. It is important to remember that for the fuel assembly MCNP model, the square profile of the fuel assembly makes the use of point detectors from the side of the fuel assembly preferred. The same two region dose rate behavior is observed again. Tabular data is provided in Appendix A, Table A.5.

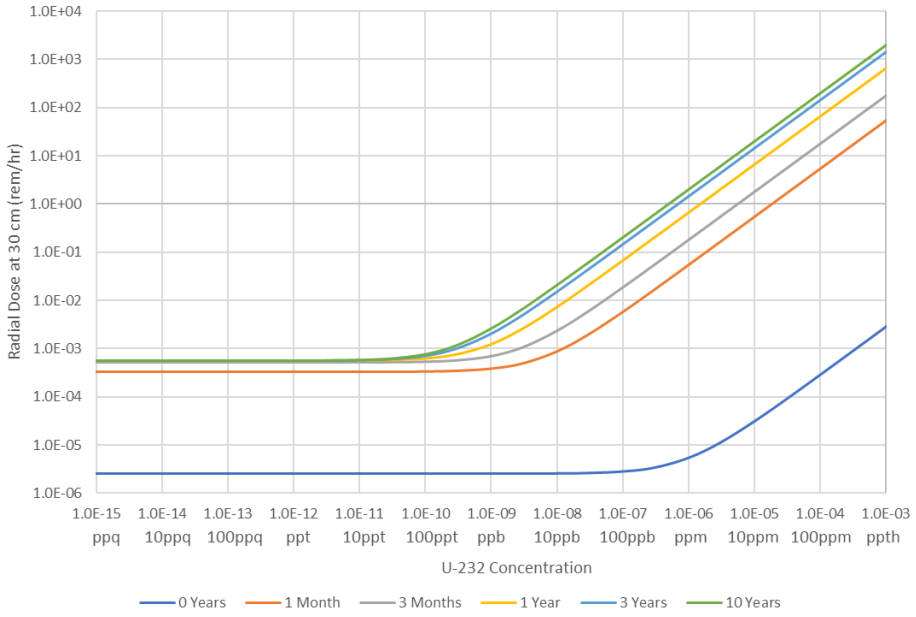

Figure 4.7. Radial Dose Rate at 30 cm vs. U-232 Concentration for a 30B Cylinder with natural uranium.

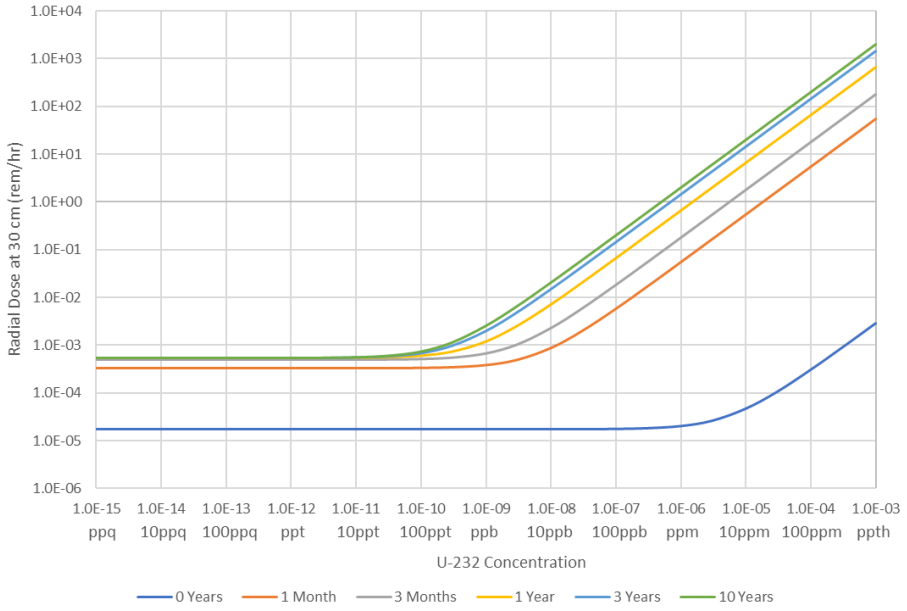

Figure 4.8. Radial Dose Rate at 30 cm vs. U-232 Concentration for a 30B Cylinder with 5 percent LEU.

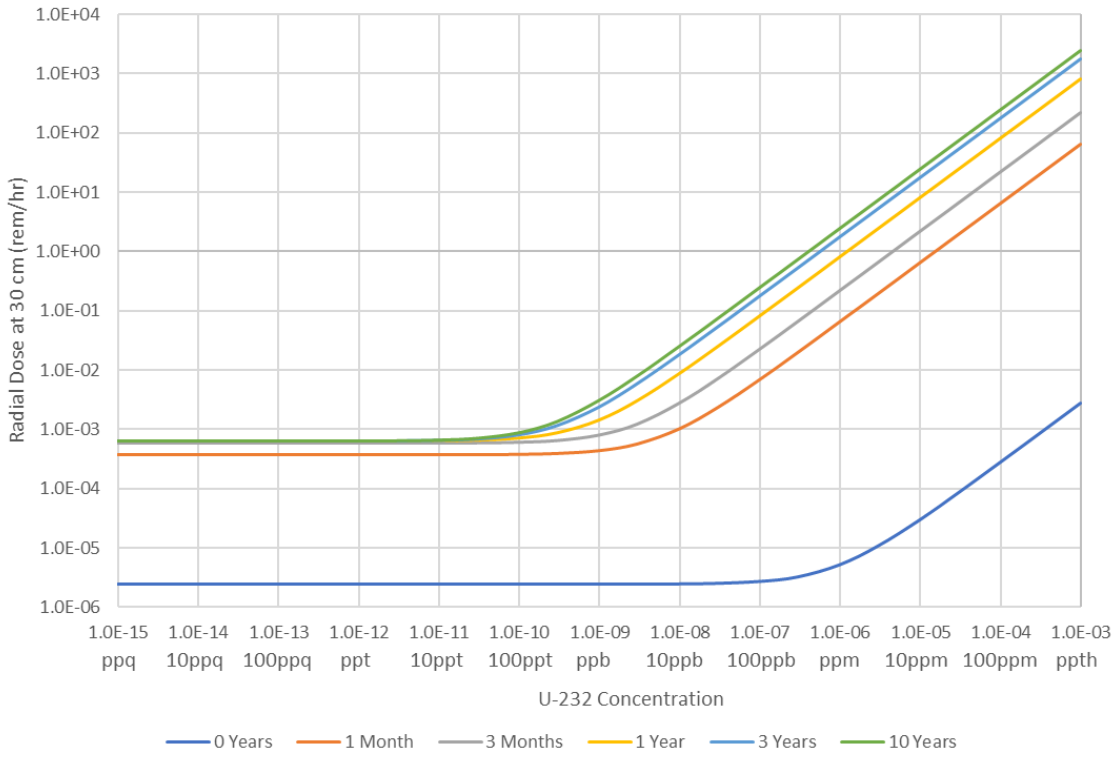

Figure 4.9. Radial Dose Rate at 30 cm vs. U-232 Concentration for a 48Y Cylinder with natural uranium.

4.8. Effects of Varying ^{232}U Concentration

Based on the discussed results above, several key trends are observed as the ^{232}U concentration is changed in each model. Combined results for each model are shown in Figure 4.11. These results are for one year of decay at a radial distance of 30 cm from the surface of the model. From Figure 4.11, it is observed that, as noted earlier for each of the models, dose rate forms two distinct regions based on ^{232}U concentration. At lower ^{232}U concentrations, the dose rate is constant with respect to ^{232}U concentration. This indicates that at lower ^{232}U concentrations, the decay of the other uranium isotopes present is the primary contribution to the gamma emissions, and not the ^{232}U.

At higher concentrations of ^{232}U, the dose rate is observed to linear with respect to ^{232}U concentration. This indicates that the emissions due to ^{232}U decay are the primary contribution to the dose rate. Between these two regions, a transition region exists whereas the ^{232}U concentration increases, the gamma emissions from ^{232}U decay increase to the point of exceeding the baseline emissions. It is this region where the dose rate transitions from a constant dose rate at lower ^{232}U concentrations to a linearly increasing dose rate at higher concentrations. This transition occurs at a ^{232}U concentration of approximately 100 parts per trillion.

This observation of two distinct regions where different gamma emissions dominate with a transition in between has occurred in every model. To determine if the linear behavior of the ^{232}U emissions continues into the constant dose rate region, the baseline dose rate can be subtracted away. This is shown to be the case in Figure 4.12, where the dose rate at 10 years aging at 30 cm is shown with the respective baseline dose rate subtracted for the 55-gallon drum.

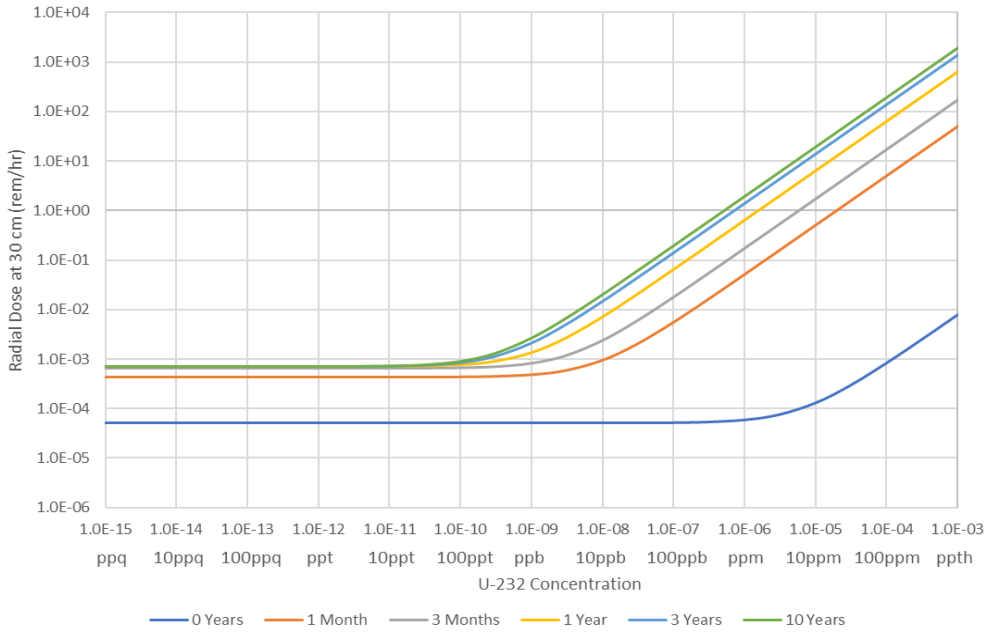

Figure 4.10. Side Dose Rate at 30 cm vs. U-232 Concentration for a 17x17 PWR fuel assembly with 5 percent enriched uranium.

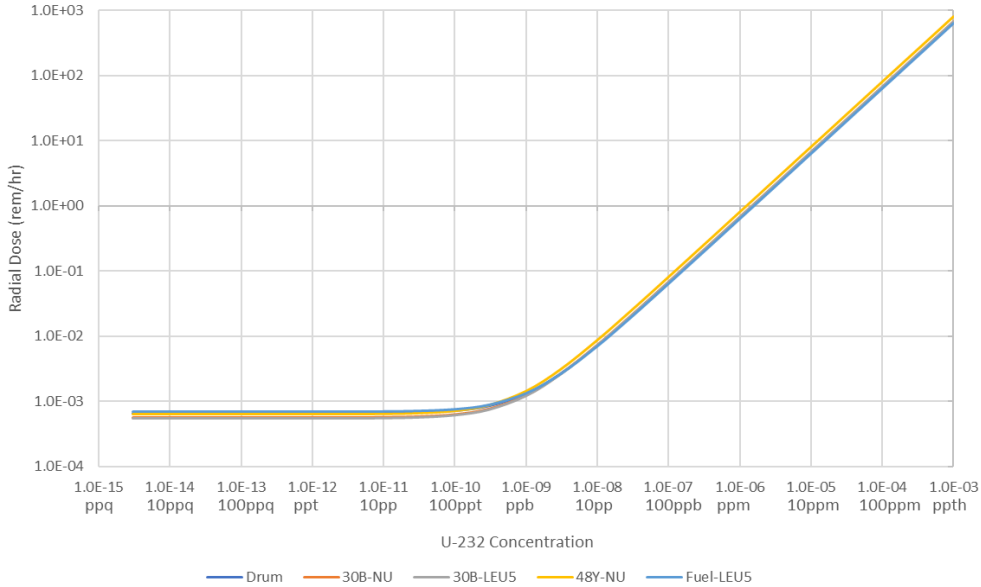

Figure 4.11. Dose rate vs. ^{232}U concentration for each model at a 30 cm distance after 1 year of aging.

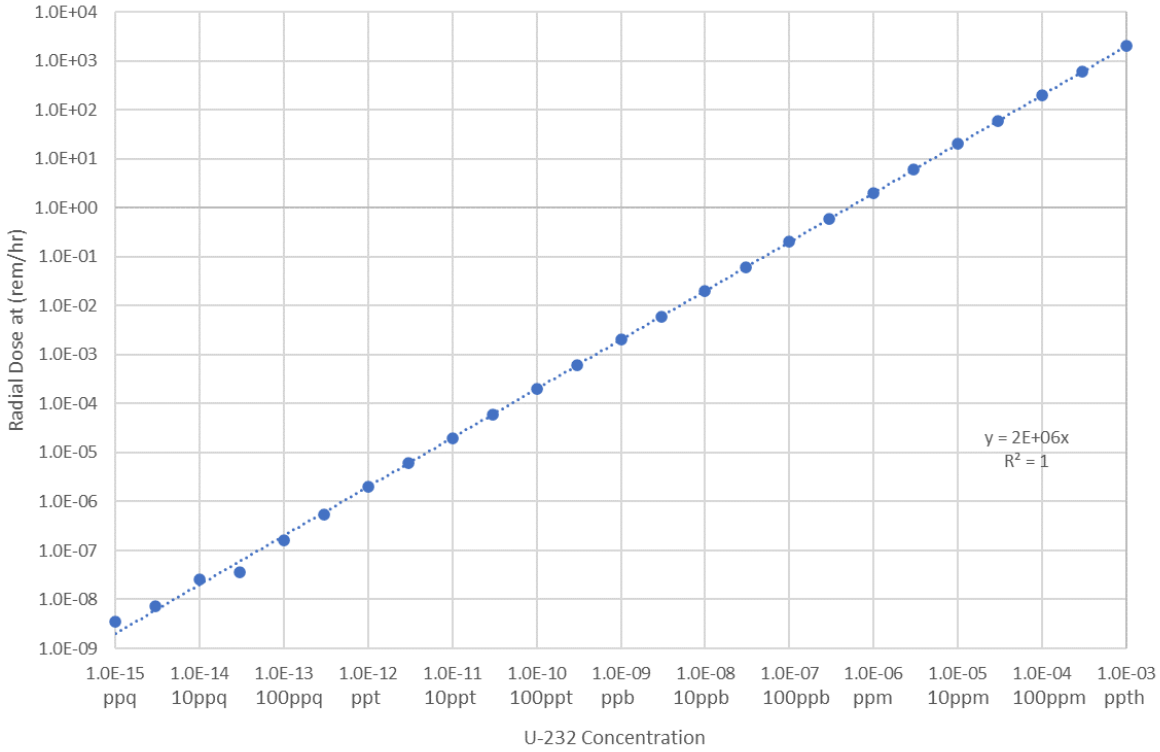

Figure 4.12. Dose rate vs. ^{232}U concentration for the 55-gal drum of U_3O_8, when baseline uranium dose is subtracted. This is for 10 years of decay at 90 cm.

4.9. Material Aging and Decay

As the uranium ages, the decay daughters approach secular equilibrium. As the half-lives of ^{235}U differ by several orders of magnitude, the significantly different decay activities will cause each uranium isotope to reach secular equilibrium with its daughters at different rates. Therefore, for each of the models, it is important to observe each ^{232}U concentration at each time step to determine how the dose rate from ^{232}U decay emissions changes with time. In the results for each model above, observe how the dose rate increase in the higher concentration region versus the lower concentration region.

In the low ^{232}U concentration region, most of the models observe a dose rate increase of about one order of magnitude in the first month, while the models containing LEU experience an increase of about one order of magnitude due to greater amount of ^{235}U having a higher activity, causing a higher initial dose rate. When observing the region of higher ^{232}U concentrations, a couple of trends are observed.

The first observation is how the dose rate in this region increases with time. In this linear region, the dose rate line is seen to increase by almost four orders of magnitude. This is due to the faster decay of ^{232}U coupled with the 2.614 MeV gammas from ^{208}Tl. After aging for a year, the dose rate increase reaches almost five orders of magnitude over the initial dose rate line.

The second observation in each of the above results is that at each time step, the transition between the constant dose rate region and the linear region of higher ^{232}U concentrations is shown to shift to lower ^{232}U concentrations as the material ages. This can be seen in each of the results above. As an example of this, Figure 4.8 shows that initially, the baseline dose rate is the primary contributor until a ^{232}U concentration of one part per million is reached. After the first month, the transition region has shifted to between one and ten parts per billion. It is clear that, initially, the activity of the baseline uranium isotopes is sufficient to contribute more to the dose rate even at some higher concentrations of ^{232}U. As the ^{208}Tl grows in from ^{232}U decay, this will become more important at lower concentrations.

4.10. Chapter Conclusions

The above results indicate that several factors must be considered when using ^{232}U as an additive with respect to dose rates to workers. As keeping the additional dose to workers to a minimum is the goal of this study, care must be taken to determine the transition region from primarily baseline uranium dose rates to ^{232}U dominant dose rates. As the uranium may be in storage before being irradiated for several years, this transition region at secular equilibrium must be utilized. It is in this region that it is assumed that ^{232}U emissions would be detectable above the baseline, while having a minimal additional dose to legitimate workers. In the above results, this occurs at about 100 parts per trillion.

It should be noted that while the results of this dosimetry study assume that observing an increase in the dose rate is equivalent to detecting the ^{232}U. This assumption needs to be verified. Worker doses also need to be determined for the average worker spending an average amount of time near such materials at certain facilities where significantly more uranium in each of the modeled forms is stored. However, these issues, while of importance, are beyond the scope of this work. Going forward in this dissertation, 100 parts per trillion will be assumed to be the required quantity of ^{232}U to add to uranium.

CHAPTER 5.
EXPLORATION OF URANIUM-232 PRODUCTION PATHWAYS AND TARGET MATERIALS

A version of this works was submitted as a conference proceeding to the 2021 American Nuclear Society Annual Meeting by Joshua H. Rhodes, Brandon Grogan, Alan Krichinsky, Brad Patton, and G. Ivan Maldonado:

J. H. Rhodes, B. Grogan, A. Krichinsky, B. Patton and G. I. Maldonado, " Exploring Production of Uranium-232 for Use as an Additive to Nuclear Fuel," in *Transactions of the American Nuclear Society*, 2021.

The body of this work was performed by J. Rhodes, with the other authors providing guidance and information used for performing this work. This work has been expanded on, going into greater detail on the work performed and the results from the models used.

5.1. Chapter Abstract

This chapter examines the production of ^{232}U via neutron irradiation. While most previously considered sources of ^{232}U are from the recovery of irradiated ^{235}U or bred ^{233}U. This study aims to determine feasible pathways for producing ^{232}U as the primary product. An examination of the neutron interactions was performed to determine the viable target materials and irradiation reactions that lead to ^{232}U. This will determine what the best target material and the appropriate irradiation facility are. This study determined that the optimal target materials are ^{230}Th and ^{231}Pa, and that thermal neutron irradiation is the most appropriate. A more focused study looked at the irradiation of ^{230}Th and ^{231}Pa in the High Flux Isotope Reactor (HFIR), with target irradiations in the hydraulic tube in the flux trap. Based on this analysis, the optimal irradiation time for ^{231}Pa is two HFIR cycles with a peak yield of 0.35 grams of ^{232}U per gram of ^{231}Pa. For ^{231}Th, the ^{232}U yield peaked at cycle five at 0.015 grams per gram of ^{230}Th.

5.2. Chapter Introduction

As noted in chapter 2, ^{232}U has generally been produced as a byproduct of ^{233}U breeding or accumulating in previously irradiated fuel. Only a couple of studies have examined directly producing ^{232}U without the need to reprocess irradiated or spent fuel material [12] [13]. Examining production of ^{232}U by means other than fuel reprocessing is important due the use of the once-through fuel cycle used in nations like the United States. While reprocessed uranium will have some ^{232}U grown in, freshly mined material will not have this protection. Producing the ^{232}U by irradiation of another target material will produce a stream of material that can be added to fresh uranium in specific, controlled quantities in order to minimize the increased dose to workers.

It is important to note the production requirements for protecting nuclear fuel. International demand for uranium is 67,500 metric tons annually [25]. Based on the 100 ppt quantity to be added as determined in the previous, this would require 6.75 grams of ^{232}U to be produced every year. were. As the previously discussed sources from ^{233}U breeding and from fuel reprocessing are not feasible, other sources must be determined. A diagram of the potential production pathways is shown in Figure 5.1.

5.3. Potential Source Materials

As shown in Figure 5.1, several materials were considered for use as a target for ^{232}U production. For this study, only neutron irradiation is considered for production. To determine the viability of each target isotope, the potential neutron interactions and decay modes for each isotope were examined [1]. The isotopes considered for ^{232}U production targets are ^{231}Pa, ^{230}Th, ^{237}Np, ^{232}Th, and ^{233}U.

5.3.1. Protactinium-231

The most direct pathway for producing ^{232}U is through ^{231}Pa. Only a single (n,γ) reaction to ^{232}Pa, followed by a β^- decay to ^{232}U is needed [1]. Protactinium-231, a decay daughter of ^{235}U, can be found in small quantities in uranium ore [26]. The relevant cross-sections are plotted in Figure 5.2 [2].

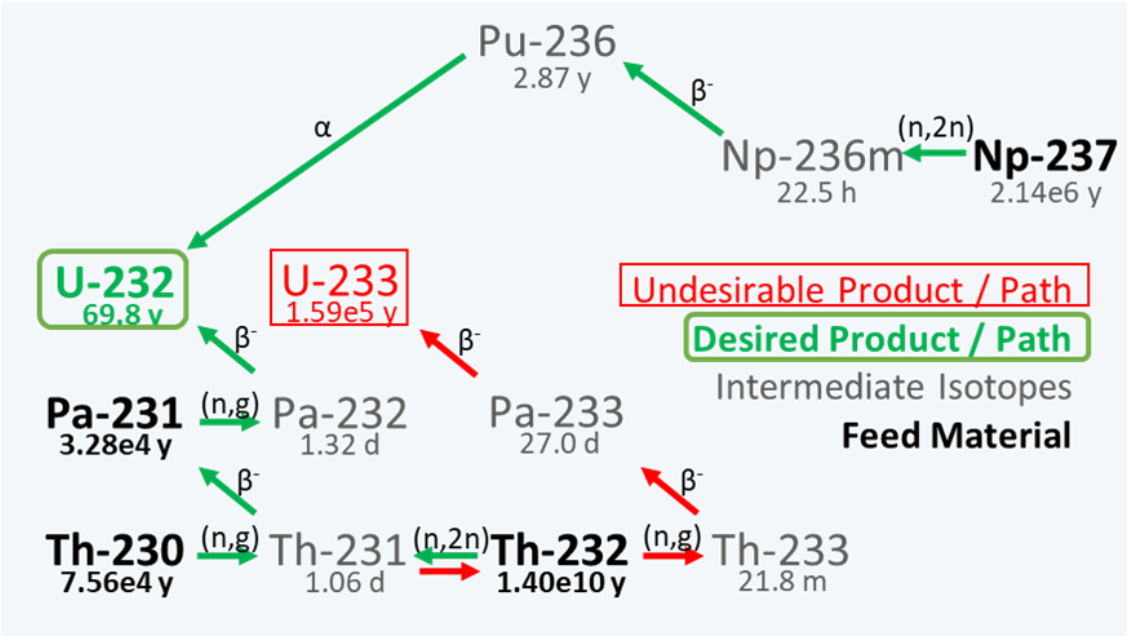

Figure 5.1. Uranium-232 and ^{233}U production pathways. Desired ^{232}U pathways are in green, and the undesired ^{233}U pathways are in red.

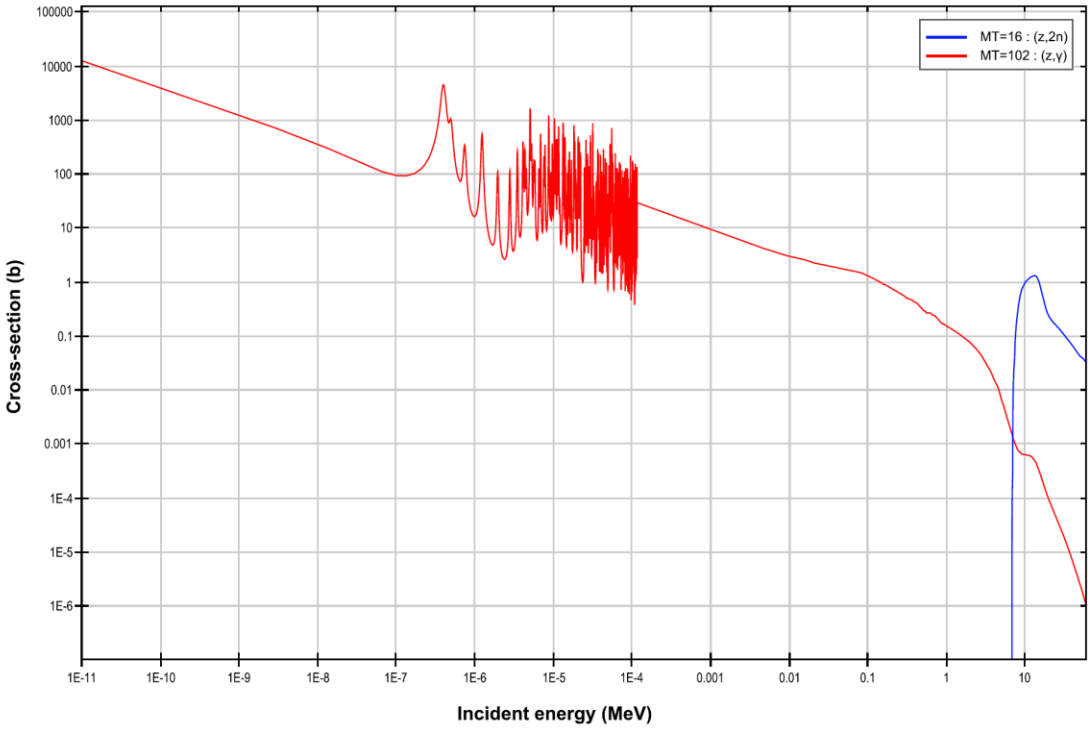

Figure 5.2.Plots of the (n,γ) (red) and (n,2n) (blue) cross-sections for ^{231}Pa [2]. Plotted using JANIS 4.0.

5.3.2. Thorium-230

The next best option for a target material is ^{230}Th. Thorium-230 is also a naturally occurring isotope found in uranium ore, and is a decay daughter of ^{238}U [26]. Thorium-230 first undergoes an (n,γ) reaction followed by a β^- decay to protactinium-231. Continued irradiation of the target then proceeds to ^{232}U as described above [1]. As producing ^{232}U from ^{230}Th requires two steps of (n,γ) and β^-, lower yields and longer irradiation times are expected than when irradiating ^{231}Pa directly. The relevant cross-sections for ^{230}Th are shown in Figure 5.3 [2].

However, ^{230}Th is has a low abundance, and ^{232}Th is significantly more common. When irradiated with thermal neutrons, ^{232}Th is the fertile material for breeding ^{233}U, as shown in Figure 5.1. Using thorium that is enriched in^{230}Th may help alleviate this. In a reactor environment, filtering out thermal neutrons in a mostly ^{232}Th target may alleviate this.

5.3.3. Neptunium-237

Neptunium-237 is used as the target material for ^{238}Pu production for radioisotope thermoelectric generators. If sufficient ^{232}U is produced, it may be possible to combine production of these isotopes. However, producing ^{232}U from ^{237}Np requires an (n,2n) reaction with a threshold of 6.58 MeV to ^{236}Np [1]. Neptunium-236 first β^- decays to ^{236}Pu, which then α decays to ^{232}U [1]. This (n,2n) reaction makes producing ^{232}U from this material difficult in the predominantly thermal neutron environment of water-cooled reactors [2]. Producing^{232}U from ^{237}Np might be more feasible using high energy neutrons. The relevant ^{237}Np cross-sections are shown in Figure 5.4 [2].

5.3.4. Thorium-232

As discussed previously, ^{232}Th is more suitable for ^{233}U breeding in a thermal neutron environment. However, as noted above, an (n,2n) reaction can used to produce ^{232}U. This reaction has a threshold energy of 6.44 MeV be induced with higher energy neutrons [2]. Following this reaction to ^{231}Th, a β^- decay will lead to ^{231}Pa, and then on to ^{232}U as discussed above. The relevant cross-sections for ^{232}Th are shown in Figure 5.5 [2].

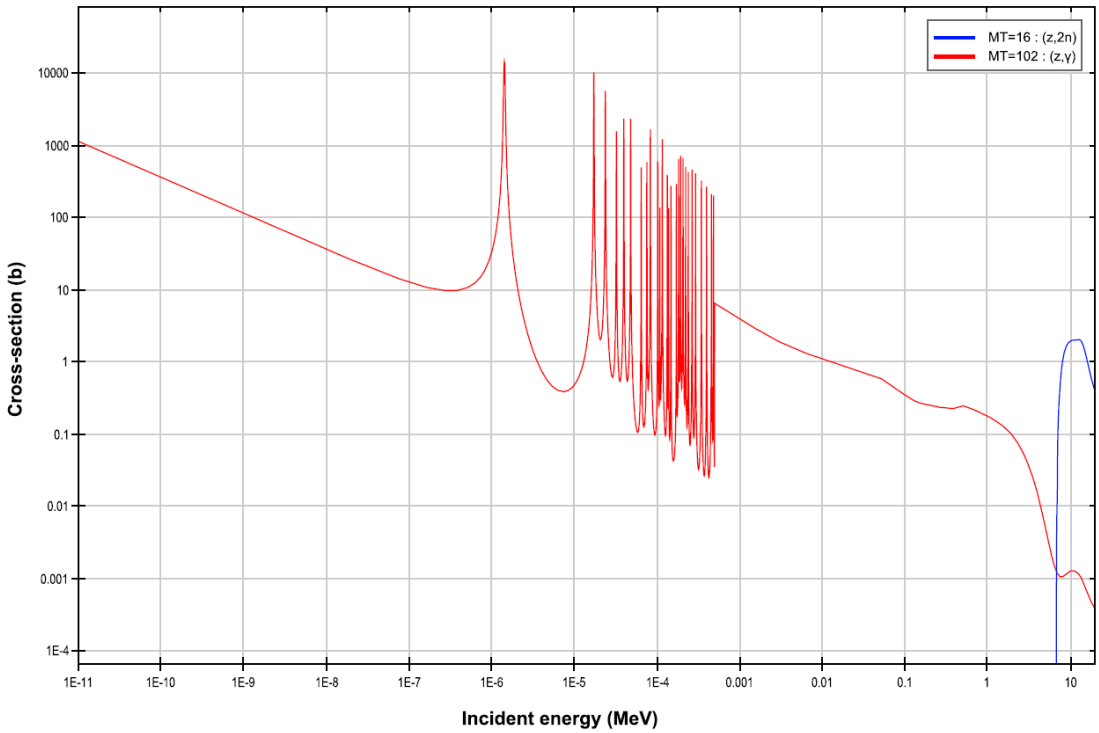

Figure 5.3. Plots of the (n,γ) (red) and (n,2n) (blue) cross-sections for ^{230}Th [2]. Plotted using JANIS 4.0.

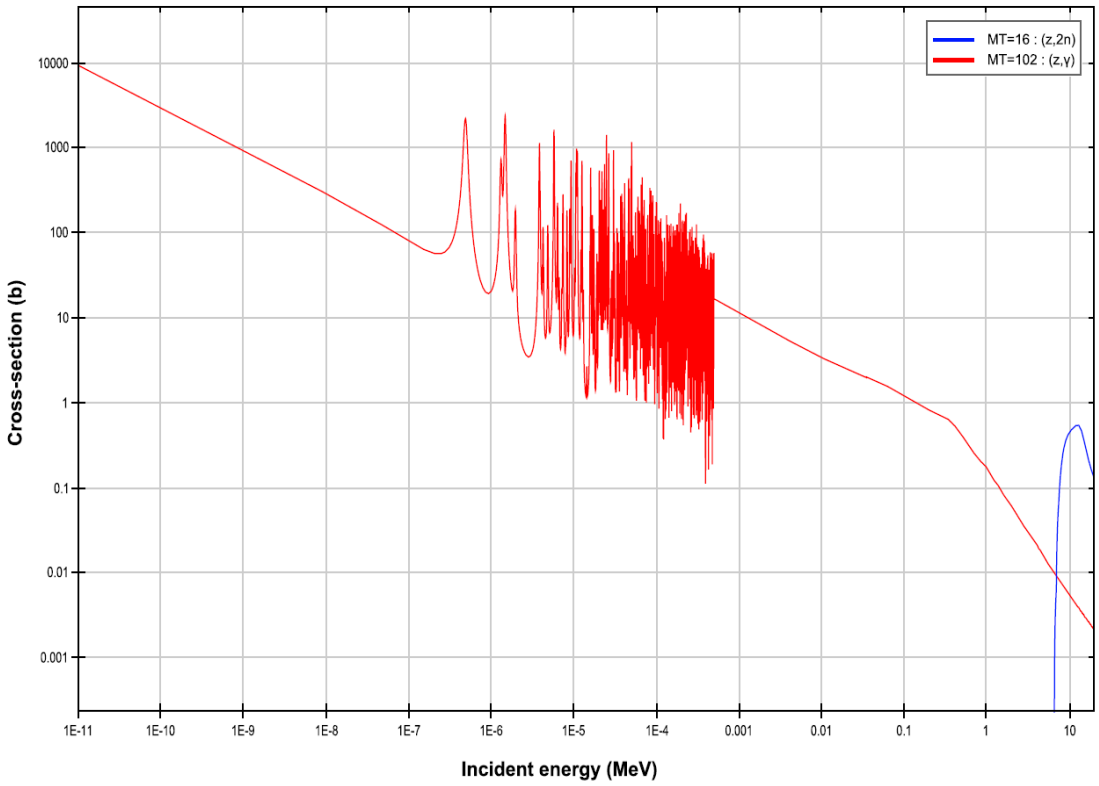

Figure 5.4. Plots of the (n,γ) (red) and (n,2n) (blue) cross-sections for ^{237}Np [2]. Plotted using JANIS 4.0.

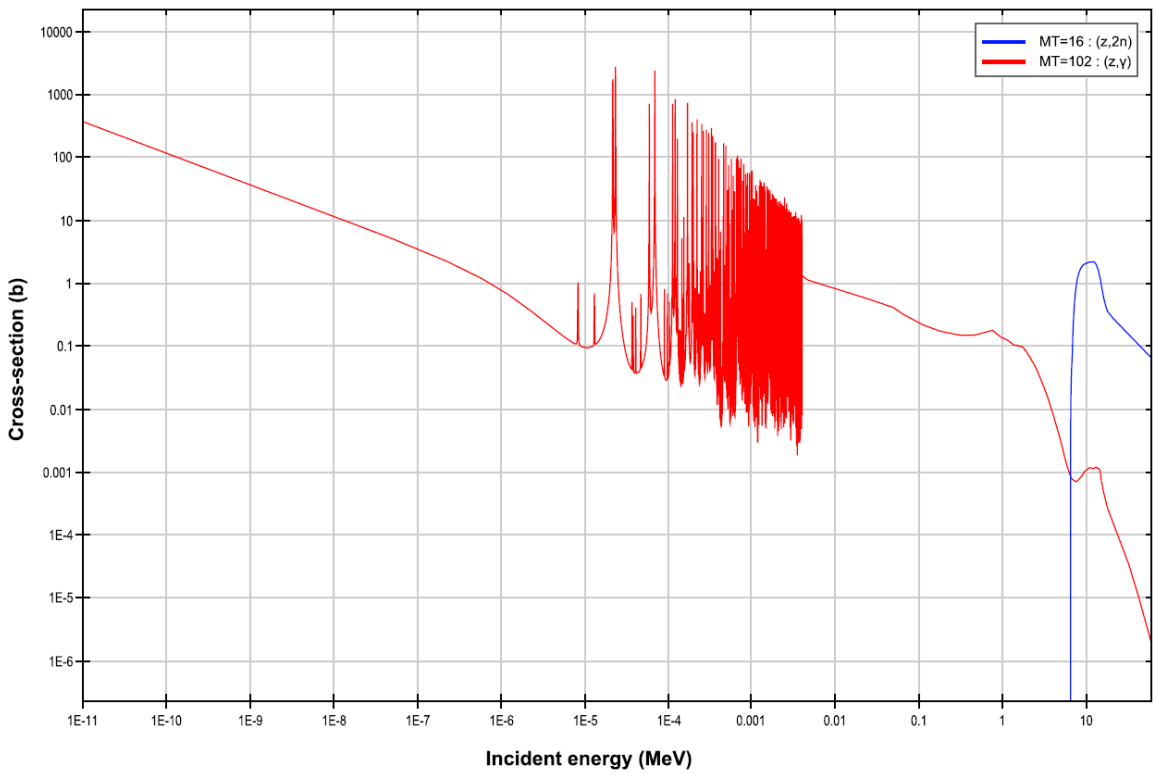

Figure 5.5. Plots of the (n,γ) (red) and (n,2n) (blue) cross-sections for ^{232}Th [2]. Plotted using JANIS 4.0.

5.3.5. Uranium-233

Uranium-233 breeding produces ^{232}U as a by-product, and ^{233}U stockpiles have quantities of ^{232}U mixed in. However, since ^{233}U is a fissile isotope, has special security requirements as a special nuclear material. Also, as ^{233}U is a fissile material, an excessive $^{233}U/^{232}U$ ratio may alter the core neutronics when added to fuel materials. The relevant ^{233}U cross-sections are shown in Figure 5.6 [2].

5.4. Initial Examination of Reactions and Physics

An initial study of the various reaction and decay pathways was performed using SCALE 6.2 ORIGEN [16] to simulate the above materials undergoing irradiation in various neutron environments. ORIGEN is capable of modeling point neutron irradiation and decay for multiple isotopes based on user-provided neutron fluxes, neutron spectra, and irradiation durations [16]. For this initial study, the following spectra were used: a thermal spectrum using a Maxwell distribution with mean energy of 0.025 eV, a fission spectrum using a Watt fission spectrum with mean energy of 2 MeV, and a high energy spectrum of 14 MeV monoenergetic neutrons. These spectra are not meant to represent any particular facility, but to provide understanding of the physics the relevant neutron interactions

Several materials are available to Oak Ridge National Laboratory for initial laboratory testing and proof-of-concept purposes. These materials examined in this study are in Table 5.1. It should be noted that these stockpiles are limited, and new sources of target material will be needed to support long-term production.

The purpose of this initial examination was to determine which materials had higher ^{232}U yield, as well as minimal ^{233}U buildup. Producing fissile material such as ^{233}U as a byproduct is not desired. The criteria for choosing the preferred target material were: a ^{232}U yield of at least 10^{-4} grams of ^{232}U per gram of target material, as well as a ^{233}U to ^{232}U ratio of 10. The ^{232}U yield is shown in Table 5.2, and the ^{233}U ratio is shown in Table 5.3.

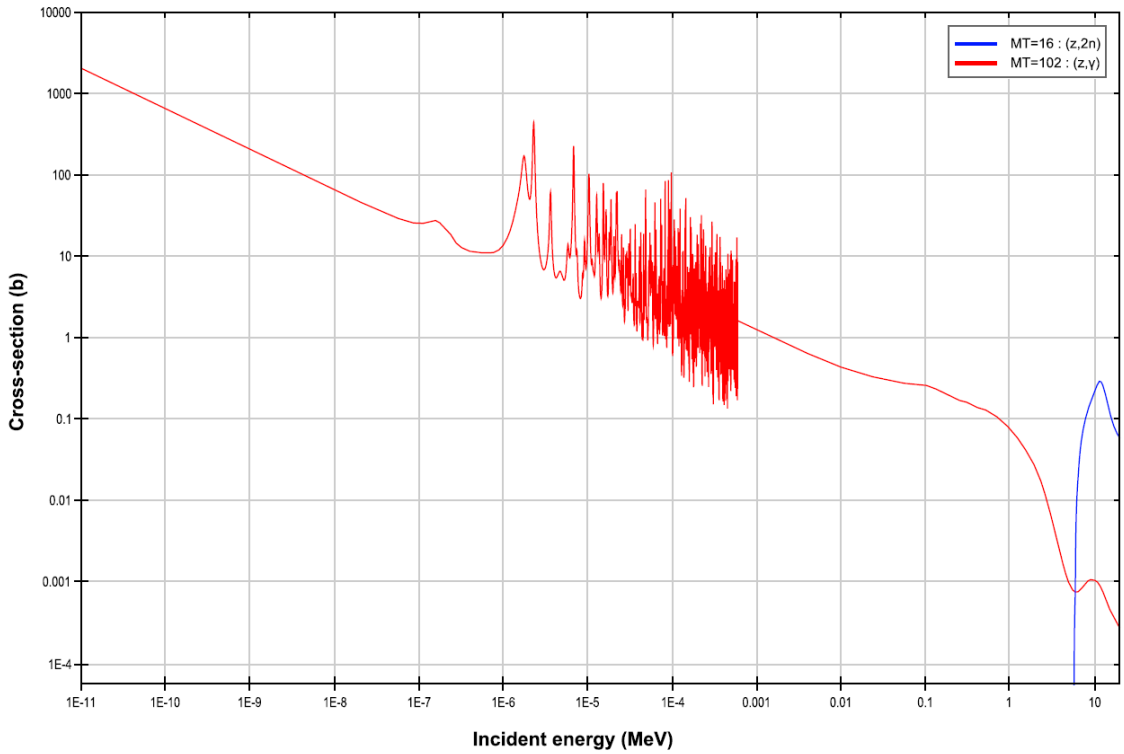

Figure 5.6. Plots of the (n,γ) (red) and (n,2n) (blue) cross-sections for ^{233}U [2]. Plotted using JANIS 4.0.

Table 5.1. Source materials for initial ^{232}U production scoping study.

Isotope	**Note**
Th-230	84% ^{230}Th and 16% ^{232}Th by mass
Th-232	
Pa-231	
U-233	Contains 150 ppm ^{232}U
Np-237	

Table 5.2. Scoping study ^{232}U yield. Units are grams of ^{232}U per gram of source material. Yields greater than 10^{-4} are highlighted in green. Uranium-233 thermal irradiations, consume more ^{232}U than produced.

	Source Material				
Spectra	**Th-232**	**Th-230**	**U-233**	**Np-237**	**Pa-231**
Thermal	1.15E-06	**3.55E-03**	1.44E-04	6.98E-09	**1.40E-01**
Watt	3.86E-08	3.48E-08	**1.93E-04**	3.40E-08	**1.05E-03**
14-MeV	1.78E-08	2.91E-09	**2.10E-03**	5.41E-06	4.47E-06

Table 5.3. Ratio of 233U to 232U. Highlighted are ratios less than 10.

	Source Material		
Spectrum	**Th-230**	**U-233**	**Pa-231**
Thermal	**1.30E-01**	5.36E+03	**2.45E-02**
Watt	4.37E+02	5.14E+03	**1.99E-04**
14-MeV	8.63E+01	4.70E+02	**1.09E-04**

Thorium-230 and ^{231}Pa were the most viable materials with thermal neutrons. Fast neutrons made ^{233}U and ^{231}Pa viable target materials for irradiation. With 14 MeV neutrons, only ^{233}U via (n,2n) reactions met the criteria. Of the materials studied, the materials that had the least ^{233}U buildup are ^{230}Th at thermal energies, and ^{231}Pa at all three spectra. The ^{232}U yield excludes ^{231}Pa at high energy. This leaves ^{230}Th at thermal energy and ^{231}Pa at thermal and watt energies. As more reactor facilities are available and are capable of higher fluxes, reactor irradiation is preferred. Next is a focused study of producing^{232}U via irradiation of ^{230}Th and ^{231}Pa in the High Flux Isotope Reactor.

5.5. HFIR Irradiation ORIGEN Simulations

ORIGEN can be used to simulate irradiation of ^{231}Pa and ^{230}Th to determine the potential ^{232}U yield from irradiation in various facilities at the High Flux Isotope Reactor at Oak Ridge National Laboratory. The results of these calculations will help determine the optimal irradiation time and target material for maximizing ^{232}U yield.

5.5.1. The High Flux Isotope Reactor (HFIR)

The High Flux Isotope Reactor is a light water–cooled, beryllium-reflected reactor that operates at a power of 85 MW_{th} [27]. HFIR has several facilities where targets or samples can be irradiated. These include a central flux trap, reflector positions, and “rabbit” facilities that allow for samples to be quickly inserted and removed [27]. These rabbit systems in HFIR include a hydraulic facility in the flux trap and two pneumatic facilities in the reflector [27]. A schematic of the HFIR core is provided in Figure 5.7 [27].

A target will be exposed to a neutron spectrum dependent on the location in HFIR. Different flux spectra were used depending on the core position to simulate irradiation in that position to model the ^{232}U yield from that position. Flux trap and reflector positions were examined. The facilities focused on for this study are the hydraulic facility, and the vertical experimental facilities (VXF), specifically the inner small vertical experimental facilities (ISVXF) highlighted in Figure 5.7.

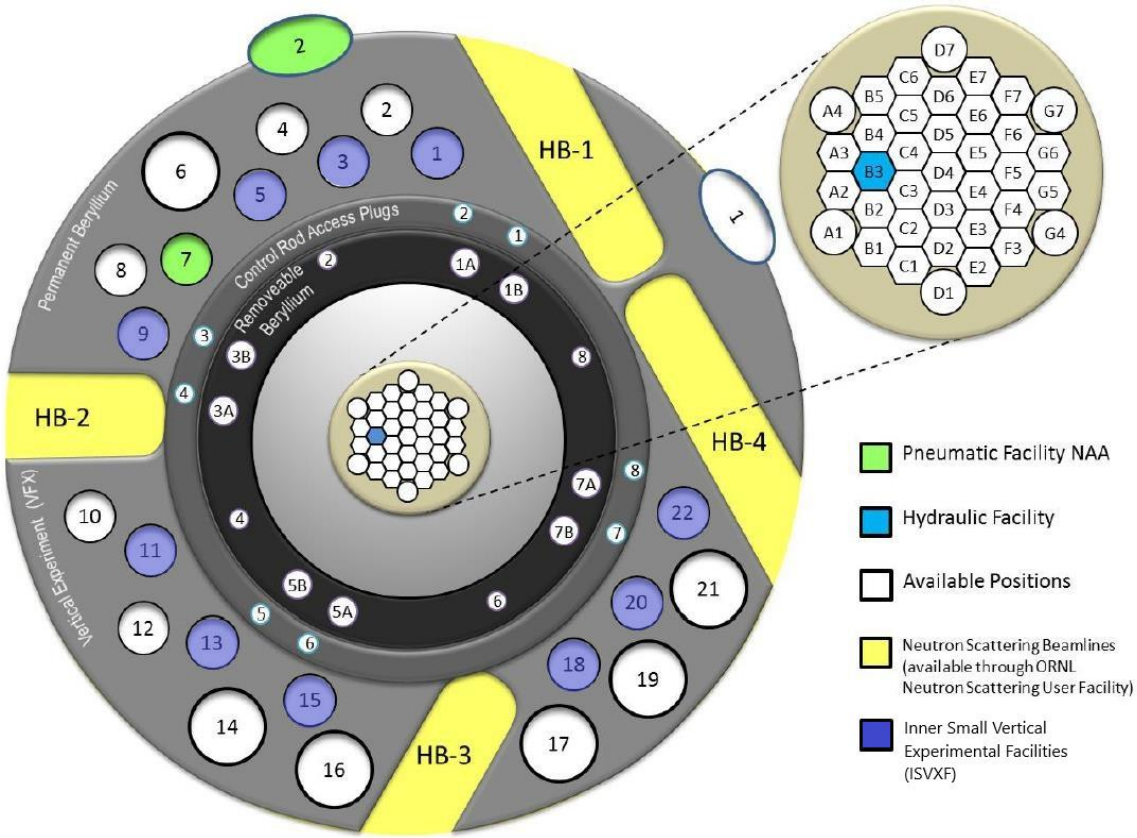

Figure 5.7. HFIR Core Diagram. This diagram has been modified to highlight in blue the ISVXF positions considered. One of pneumatic facilities, in green, is also in one of these facilities.

To represent the hydraulic tube and the ISVXF positions in HFIR in ORIGEN calculations, flux spectra generated from the cycle 400 MCNP model are used. These spectra are input into the COUPLE module to generate the libraries needed for the used to perform the irradiation calculation. ORIGEN calculations using these spectra will indicate the performance of each target material in each reactor position. The spectra used for the hydraulic tube and ISVXF are shown in Figure 5.8.

A typical operating cycle on average lasts for 24 days at power followed by a shut down time for 18 days on average. This study will consider an irradiation time of six HFIR operating cycles, for a total of 144 days of irradiation. The calculations will include the 18 days of down time between cycles, but these are not plotted in the results. The final cycle will be followed by a cooling period of 3 months. to allow for fission products to decay.

The previous results show that the best target materials are ^{231}Pa and ^{230}Th. However, because thorium recovered from ore is ^{232}Th, thorium containing a mix of ^{230}Th and ^{232}Th was also studied to determine the impact of ^{232}Th being present. For comparison, pure ^{230}Th and a thorium material enriched to 10% ^{230}Th with 90% ^{232}Th remaining are presented.

5.6. Results

The results of this study are presented for ^{231}Pa, pure ^{230}Th, and for a 10% ^{230}Th to 90% ^{232}Th mixture. These ORIGEN results are for one gram of each material irradiated for six cycles in either the hydraulic facility or the ISVXF. Examples for these ORIGEN calculations are provided in Appendix B:.

5.6.1. Hydraulic Tube ORIGEN Calculations

The results presented in by looking at each of the target materials in order of preferred material. Each of the results will examine the buildup of ^{232}U as well as the ^{233}U contamination and the efficiency of ^{232}U production in grams per reactor day. Thorium

target irradiations also include examining the intermediate ^{231}Pa production in these targets. The ^{231}Pa irradiation results are shown in Figure 5.9.

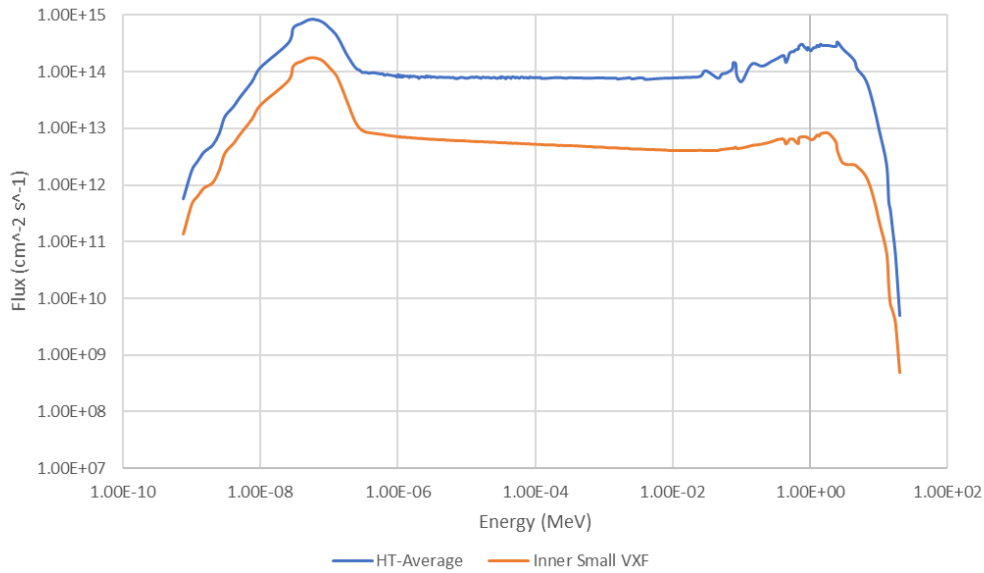

Figure 5.8. Flux per unit Lethargy Spectra for the Hydraulic Tube and Inner Small Vertical Experimental Facilities from the MCNP cycle 400 model.

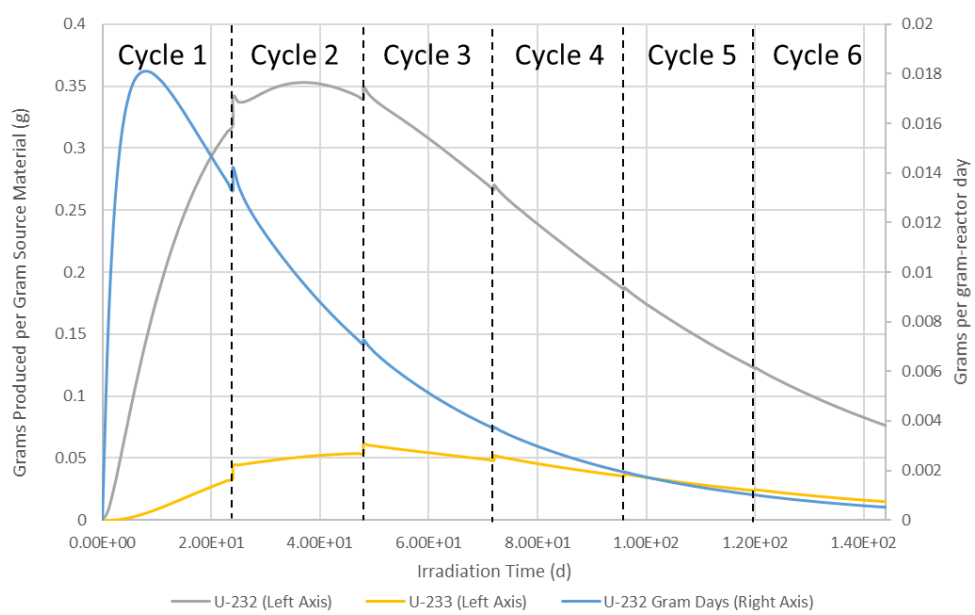

Figure 5.9. Irradiation of one gram of Protactinium-231 in the HFIR hydraulic facility for six cycles.

For ^{231}Pa target irradiations, the mass of ^{232}U peaks in cycle two at about 0.35 grams. The ^{233}U mass peaks at the beginning of cycle three. The grams of ^{232}U produced per reactor day peaked halfway through the first cycle. This indicates that the efficiency of production peaks in cycle one. Therefore, ^{231}Pa should only be irradiated in the hydraulic facility for one to two cycles.

The results of a pure ^{230}Th irradiation are given in Figure 5.10. This figure includes the masses for ^{232}U ^{233}U, and ^{231}Pa. The mass of ^{232}U peaks at the end of cycle five at about 0.15 grams. The production efficiency peaks between cycles two and three at 0.002 grams per day. Note that after cycle four, the increase in ^{232}U is small, so it may only be worthwhile to end irradiation after four cycles. It is also observed that the ^{231}Pa curve is similar to the ^{232}U efficiency curve, with the ^{231}Pa mass peaking between cycles two and three at about 0.15 grams. Because of this ^{231}Pa buildup, there is the possibility of recycling the ^{231}Pa from ^{230}Th irradiations.

The results of a 10% enriched ^{230}Th with 90% ^{232}Th are shown in Figure 5.11. Note that the behavior of the ^{232}U mass, production efficiency and ^{231}Pa mass behave similarly to the pure ^{230}Th target, but scaled to approximately one tenth of the mass. The ^{232}U mass peaks at the end of cycle five, but the produced mass is only 0.015 grams per gram of thorium. The ^{231}Pa peaks again between cycles two and three, also at 0.015 g. This material could potentially be recycled into protactinium targets. The grams of ^{232}U per day peaks between cycles two and three again, with a maximum at 0.00018 grams per day. Because this material contains a significant fraction of ^{232}Th, the buildup of ^{233}U is more significant. The ^{233}U mass reaches a maximum between cycle four and five, peaking to over 0.02 grams during the 18 days between cycles. Once again, irradiating for a fifth cycle may not be worthwhile with this material. The buildup of ^{233}U is still low, but is now a significant fraction of the uranium produced in the target. This may pose a problem for security or have an impact on fuel neutronics.

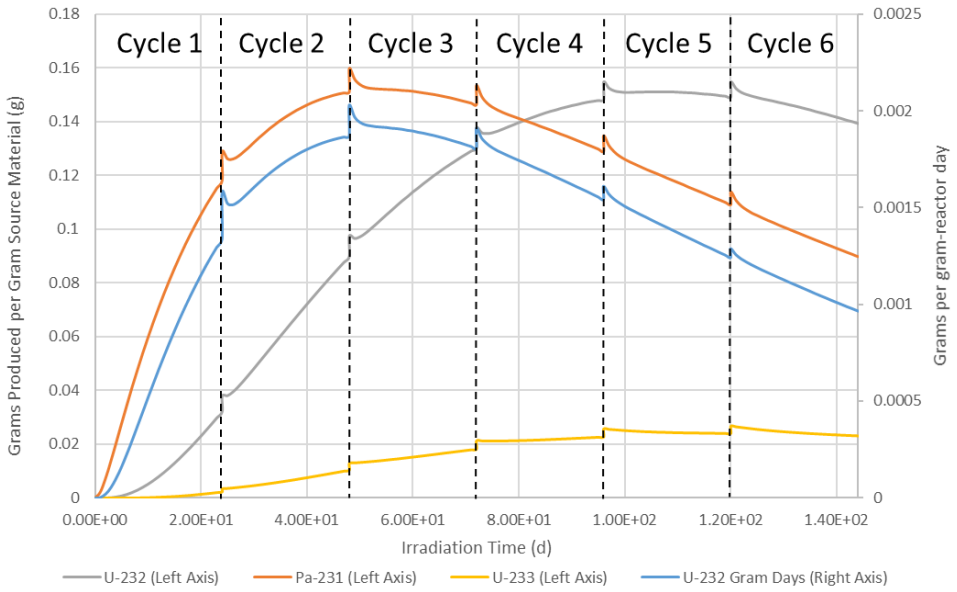

Figure 5.10. Irradiation of one gram of Thorium-230 in HFIR hydraulic facility for six cycles.

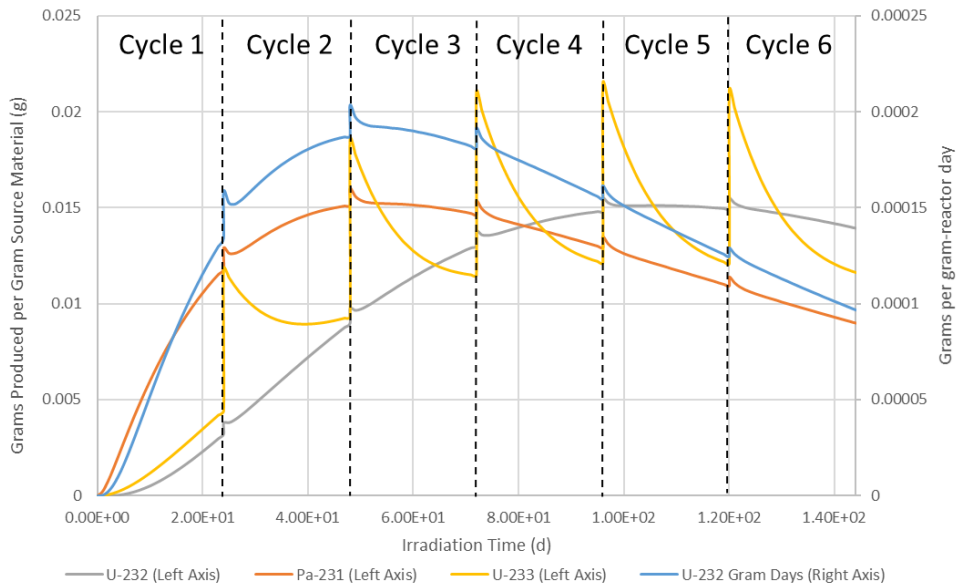

Figure 5.11. Irradiation of one gram of 10:90 ^{230}Th:^{232}Th in HFIR hydraulic facility for six cycles.

5.6.2. ISVXF ORIGEN Calculations

The results for the ISVXF facilities are presented in the same manner as the hydraulic tube results, showing the concentrations for ^{232}U and ^{233}U, as well as the ^{232}U production efficiency in grams per reactor day. Once again, ^{230}Th irradiations include the buildup of ^{231}Pa. The ^{231}Pa results are shown in Figure 5.12.

From Figure 5.12, it can be seen that even after eight HFIR cycles, the ^{232}U concentration has not reached its peak. This significantly slower buildup can be explained by the total neutron flux out in the reflector region where the ISVFX positions are located being lower in magnitude. However, it should also be noted that after the eighth cycle, the mass of ^{232}U produced is over 0.42 grams. This is more ^{232}U than the previously discussed hydraulic tube calculations. This can be explained by examining the neutron spectra in Figure 5.8. As the ISVFX positions are in the reflector, the neutron spectrum is shifted to more thermal energies than when compared to the flux trap. An examination of the radiative capture cross-section in Figure 5.2 shows that at fast energies, the radiative capture cross-section is on the order of 0.1 barns and falls significantly, limiting the buildup of ^{232}U in a faster neutron spectrum. At thermal energies, the radiative capture cross-section is on the order of hundreds of barns increasing yield when the neutron spectrum is shifted toward these energies.

Results for 100 percent ^{230}Th irradiations in the ISVFX positions are shown in Figure 5.13. Note the quantities of each isotope produced after eight cycles. After eight HFIR cycles, neither ^{232}U or ^{231}Pa reach their maximum yield. The final ^{232}U yield is 0.0522 grams per gram of target material. The amount of ^{231}Pa produced was 0.105 grams. Only 0.00442 grams of ^{233}U accumulated after eight cycles. Once again, this amount of time is prohibitively long. However, the contamination of the ^{232}U in the target is low, allowing for high purity ^{232}U and ^{231}Pa to be produced. Uranium-233 contamination may be limited even more with less irradiation cycles. As with ^{231}Pa, the yields are affected by changes in the neutron energy spectrum. It should be noted that at thermal energy, the capture cross-section for ^{231}Pa is greater than that for ^{230Th}, limiting the maximum ^{231}Pa yield as neutron capture in ^{231}Pa become significant.

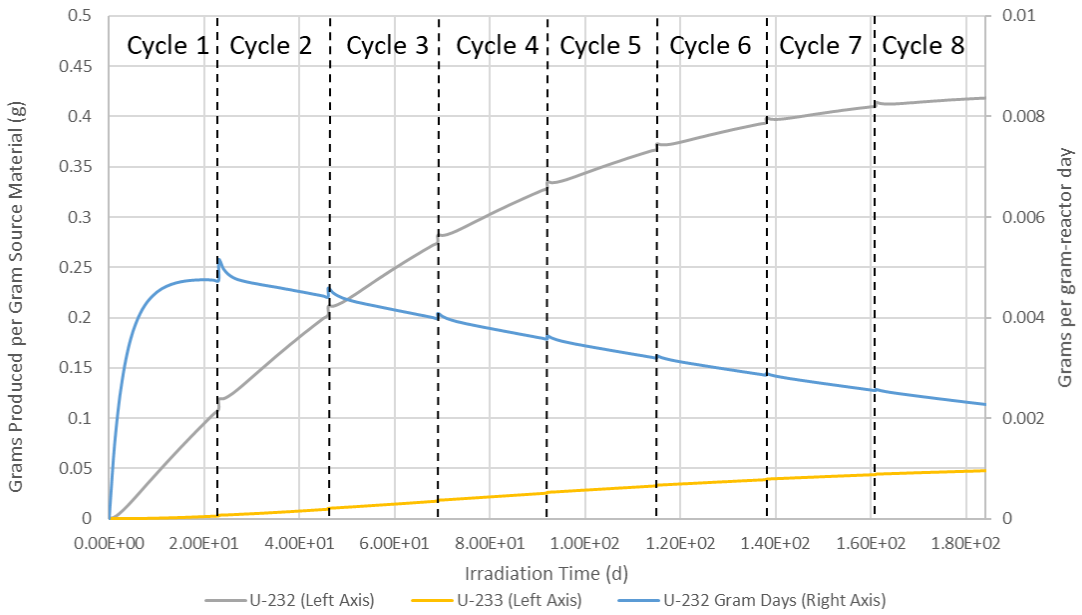

Figure 5.12. Protactinium-231 irradiation in an Inner Small Vertical Experimental Facility for eight cycles.

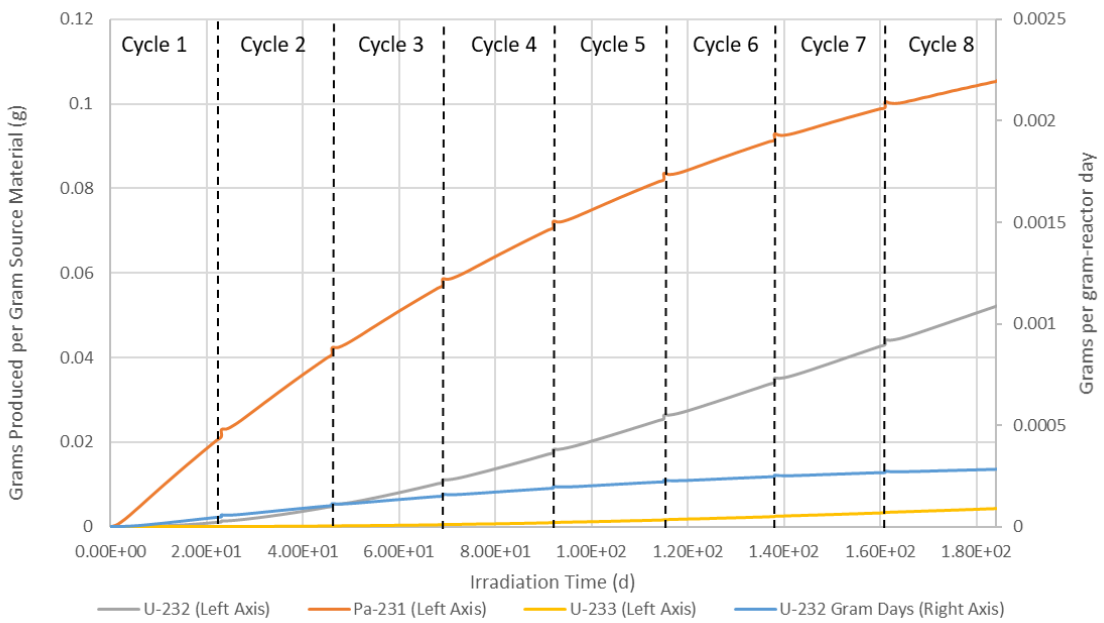

Figure 5.13. Thorium-230 irradiation in an ISVXF for eight cycles.

Results for a 10 percent ^{230}Th, 90 percent ^{232}Th target are shown in Figure 5.14. For these results, the amount of $^{-233}$U produce should be noted, as well as how this compares to the ^{232}U produced from the same source material. Once again, it should be noted that none of the isotopes reached their maximum yield within eight cycles. For these results, the amount of ^{232}U produced was 0.00523 grams per gram of source material after eight HFIR cycles. The results also show 0.0105 gram of ^{231}Pa and 0.0114 grams of ^{233}U. This combination of source material and flux spectrum strongly favor the buildup of ^{233}U over ^{232}U.

5.7. Chapter Conclusions

Based on the preceding results, the preferred material for target construction is ^{231}Pa. Protactinium-231 produces more ^{232}U per gram of target material and requires significantly less time for irradiation, requiring only two HFIR cycles to reach peak yield. Thorium-230 is also usable for a target. However, because of the two neutron captures required, the yield is significantly lower and the irradiation time is significantly longer to reach the maximum yield. It should be noted that these results discussed do not include target self-shielding, which will lower peak ^{232}U yield. This will be explored in the next chapter. These results also do not factor in the costs of mining protactinium, which is expected to be significant enough to make thorium a more cost-effective target material.

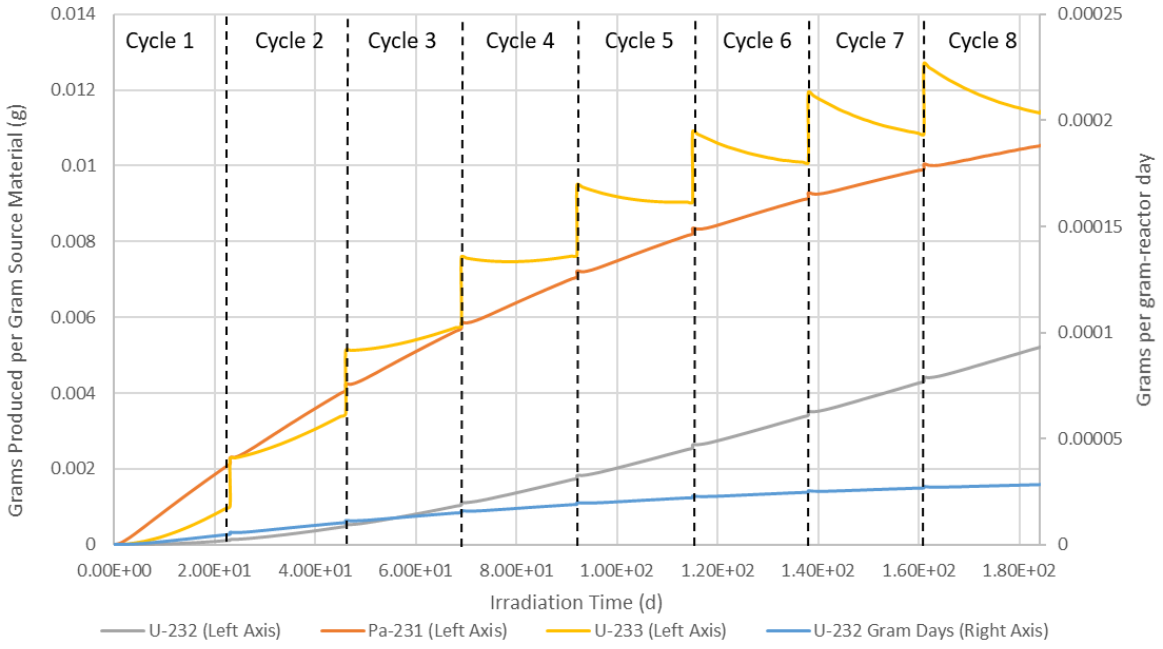

Figure 5.14. 10:90 ^{230}Th:^{232}Th Irradiation in an ISVXF for eight cycles.

CHAPTER 6.
EXAMINATION OF HFIR TARGET NEUTRONICS AND SELF-SHIELDING FOR URANIUM-232 PRODUCTION TARGETS

6.1. Chapter Abstract

This chapter builds on the work discussed in Chapter 5. This study looks at the neutronics of a HFIR target filled with ^{230}Th or ^{231}Pa. A HFIR target was modeled in MCNP, placing the target in the flux trap towards the center of the reactor. The targets were assumed to contain ^{231}Pa, or thorium with varying percentages of ^{230}Th and ^{232}Th. Flux tallies were used inside the targets to determine changes in the neutron flux from the surface towards the center of the target. These neutron fluxes were then averaged over the target volume. This flux was then used in SCALE 6.2 ORIGEN to determine the ^{232}U yield when these MCNP fluxes are used. These results are then compared to the ^{232}U yield in Chapter 5 to determine the effects of self-shielding on ^{232}U yield. Compared to the results in the previous chapter, the simulations indicate that ^{230}Th is susceptible to neutron losses to self-shielding causing a 29 percent decrease in peak ^{232}U yield after five HFIR cycles. The ^{232}U yield from ^{231}Pa irradiations was minimally affected.

6.2. Chapter Introduction

Self-shielding incorporates the concepts of resonance absorption and spatial shielding [28] [29]. Resonances of a significantly high magnitude can potentially depress the flux at a given energy [28] [29]. This results in less neutron absorption in the target. Spatial self-shielding results in the outer layers of a target absorbing neutrons, causing the interior of a target to receive less neutron flux [28] [29]. This study will determine the effects of self-shielding on the production of ^{232}U in the High Flux Isotope Reactor. This will involve using an MCNP model of HFIR and the flux trap target geometry to model targets for ^{232}U production.

6.3. HFIR Target MCNP Model

For this study, an MCNP model for the High Flux Isotope Reactor was used for neutron transport calculations for the HFIR flux trap. The model used for this study is a validated model of HFIR as configured during cycle 400 in 2004. The validation study for this model was published by N. Xoubi and R. T. Primm III in 2005 [30]. A cross-section of this MCNP model is shown in Figure 6.1 [30].

6.3.1. Flux Trap Target Positions

As discussed in the previous chapter, the flux trap of HIFR has several regions for target placement, containing six peripheral target positions (PTP) and 31 interior positions [27]. The hydraulic facility considered earlier in this dissertation to represent the flux trap is located in one of these interior positions. Those results have shown that targets are optimally irradiated for multiple cycles, which make the mid-cycle removal ability of the hydraulic tube unnecessary. For this study on target neutronics and self-shielding, a target in a standard interior flux trap position will be considered. A closer cross-section from the cycle 400 MCNP model focusing on the flux trap is shown in Figure 6.2 [30].

6.3.2. HFIR Target Composition

The targets for producing ^{232}U are assumed to be based on actinide targets for curium and californium production in the HFIR flux trap. The targets are aluminum clad, with the target material in the form of an actinide oxide in an aluminum matrix. For ^{232}U production, the respective oxides are ThO_2 and Pa_2O_5. The target material consists of 20 percent actinide oxide, 70 percent aluminum, and 10 percent void. For ^{231}Pa and ^{230}Th, this composition results in about 18 grams of actinide per target. As ^{230}Th is of low natural abundance in thorium, enrichment is expected to be utilized, and the resulting materials may vary in the fraction of ^{230}Th to ^{232}Th. The ^{230}Th enrichments examined in this study are shown in Table 6.1. A pure ^{232}Th target is included as a control to compare how the flux changes as the target is enriched in ^{230}Th.

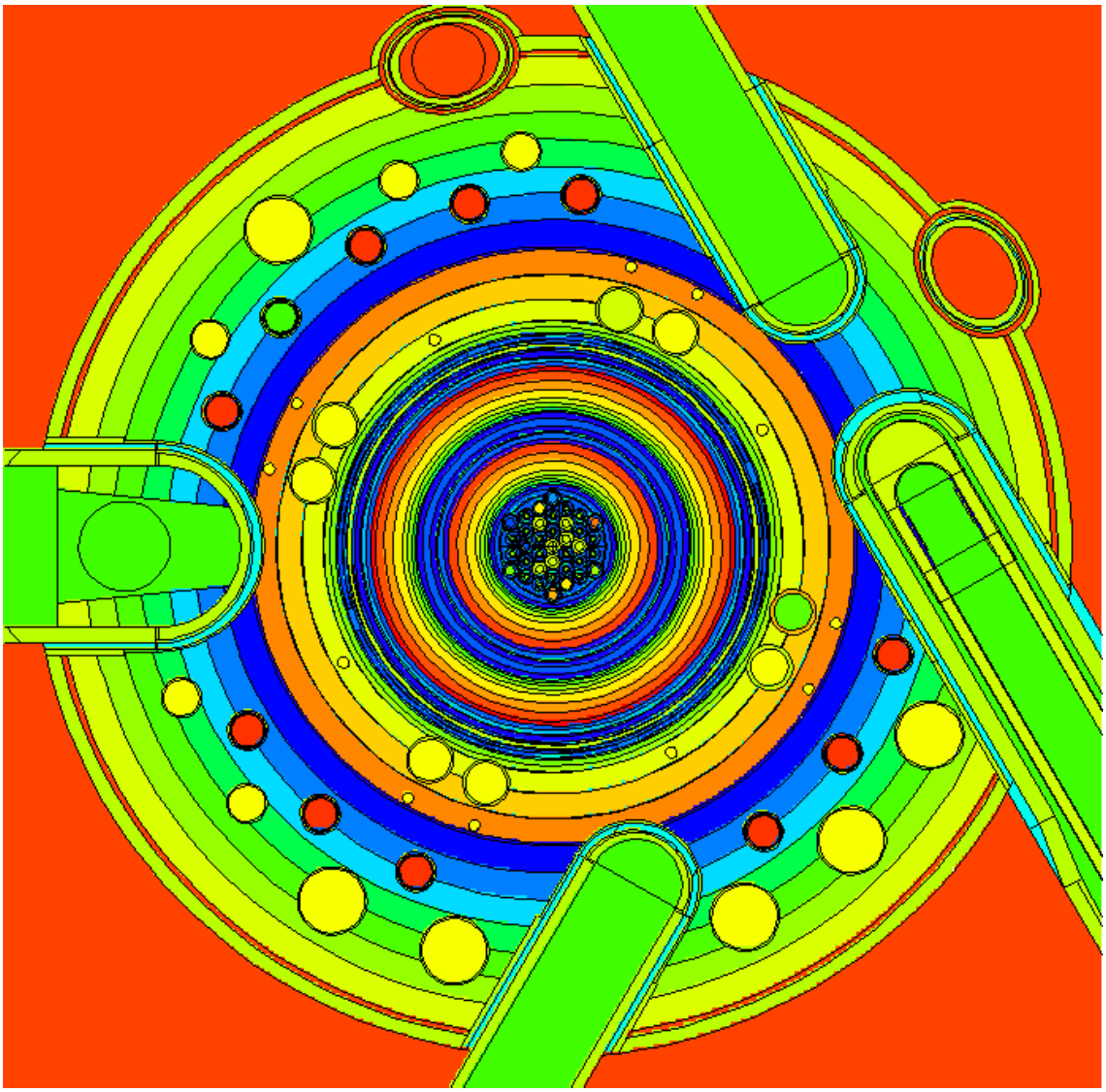

Figure 6.1. Cross-Section of the HFIR core from the Cycle 400 MCNP model.

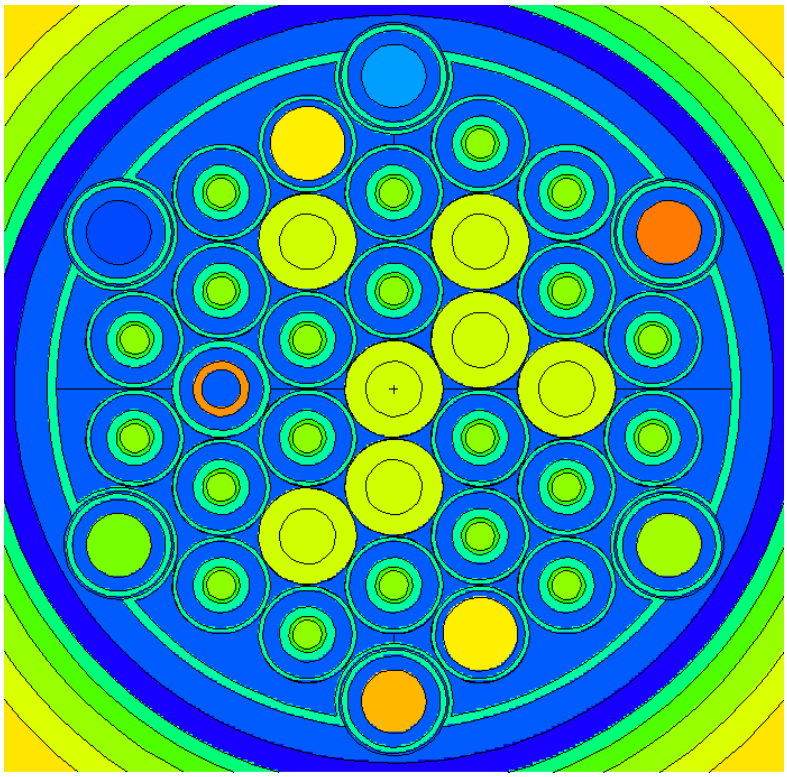

Figure 6.2. Cross-Section of the HFIR flux trap from the Cycle 400 MCNP model.

Table 6.1. Thorium-230 Enrichments Examined

Th-230 Enrichment	Th-230 Fraction	Th-232 Fraction
0% Th-230 (Pure Th-232)	0	1
3 % Th-230	0.03	0.97
10 % Th-230	0.1	0.9
15 % Th-230	0.15	0.85
20 % Th-230	0.2	0.8
30 % Th-230	0.3	0.7
40 % Th-230	0.4	0.6
50 % Th-230	0.5	0.5
60 % Th-230	0.6	0.4
70 % Th-230	0.7	0.3
80 % Th-230	0.8	0.2
90 % Th-230	0.9	0.1
100 % Th-230	1	0

6.3.3. Neutron Flux Tallies Utilized.

To determine the neutron flux in the target, the target is divided up into concentric cylinders at increments of 0.25 target radii. This will allow for observing the changes in the flux between the outer layers of the target and the target center. This tally will also use 238 energy bins, which will show the effects of resonance absorption in the target. The target geometry with the tally cells and surfaces is shown in Figure 6.3.

Once each MCNP simulation is run, the flux tallies are then normalized for reactor power. This then provides the flux spectrum for each ^{230}Th enrichment at various depths in the target. An average flux for the whole target is also tallied in MCNP.

6.4. Flux Tally Results

After running the MCNP tallies. The 238-group spectra for each depth in the target is than analyzed to determine how the flux changes as neutrons pass deeper into the target and note the presence of resonance absorption at the various target depths.

6.4.1. Protactinium-231 Results

Flux tallies in ^{231}Pa indicate that similar self-shielding effects are acting on the flux. Figure 6.4. shows the flux spectra for various depths in a ^{231}Pa HFIR target. Note that the flux is per unit lethargy.

The flux is at its maximum in the thermal region before dropping significantly as resonance energies are approached. There is also a prominent first resonance that depresses the flux at that energy. The spectrum for the outer layer is shown in Figure 6.5, and the spectrum at the inner layer is shown in Figure 6.6. Both spectra are in flux per unit lethargy.

Based on this flux data, it is expected for the ^{232}U production to deviate from the results in Chapter 5, which used flux spectral tallied from the surface of the hydraulic tube. The ^{232}U yield is expected to be lower when these resonance absorption results are accounted for.

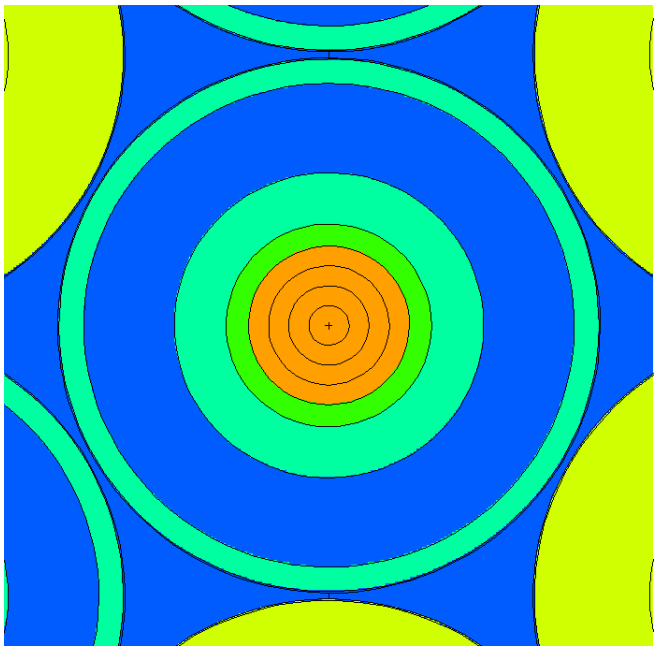

Figure 6.3. Cross-section of the HFIR target geometry. Orange is the oxide-aluminum target material, lime green is an aluminum liner, and the teal is the cladding and outer coolant shroud.

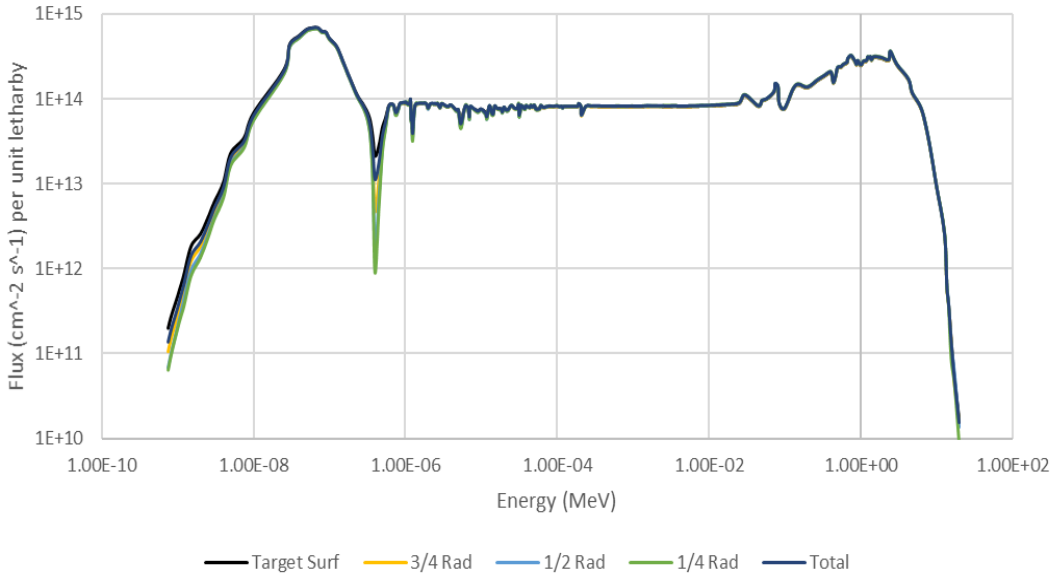

Figure 6.4. 238-group neutron spectra in flux per unit lethargy for various depths in a ^{231}Pa target.

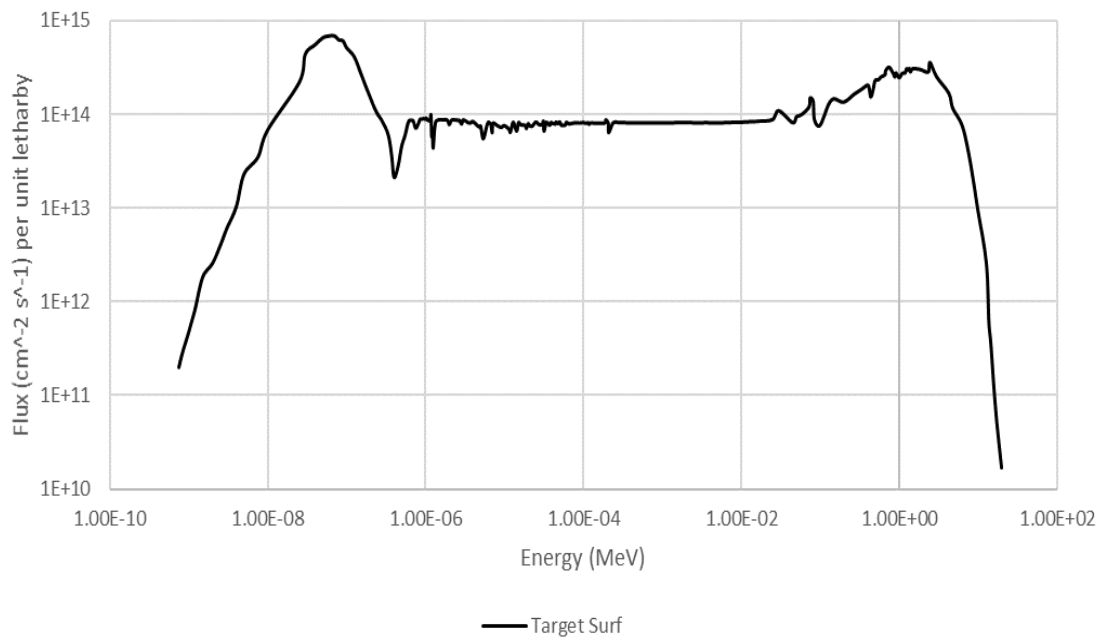

Figure 6.5. 238-group neutron spectra for the outer layer of a ^{231}Pa target.

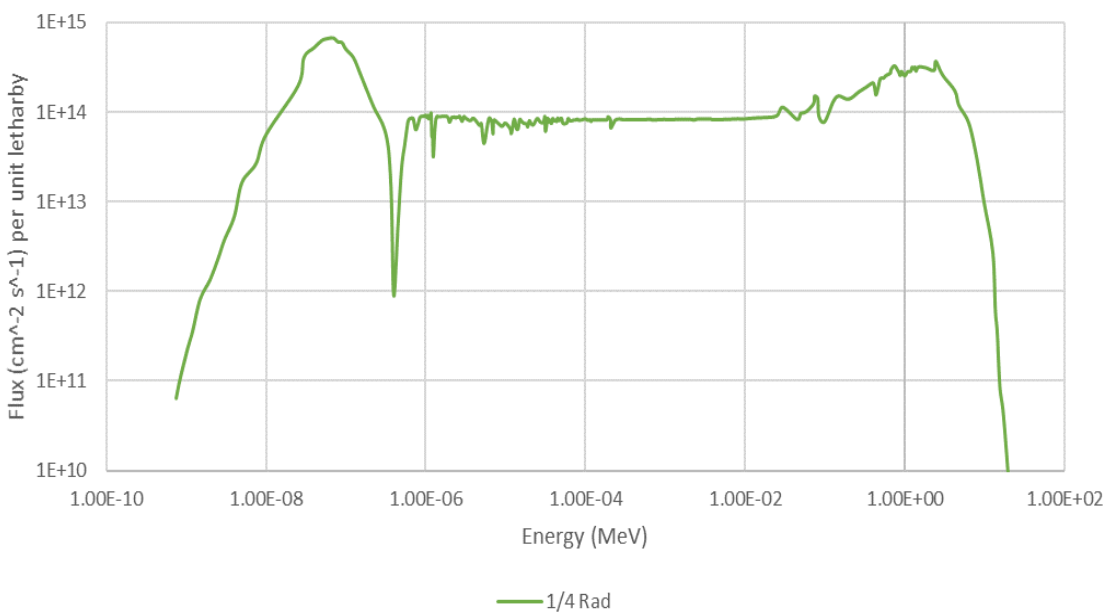

Figure 6.6. 238-group neutron spectra for the center of a ^{231}Pa target.

6.4.2. Thorium-230 Results

This section examines how resonance absorption varies with the ^{230}Th enrichment. The spectra from the ^{232}Th target are shown in Figure 6.7. From Figure 6.7. we see that the flux is highest in the thermal region, then dropping significantly as the energy increases into the resonance region. This remains true for the other ^{230}Th enrichments. However, there are changes as the ^{230Th} enrichment increases. The results for 40 percent ^{230}Th are shown in Figure 6.8.

Notice that for this target, towards the center of this target, a significant depression in the flux has emerged at 1.45 eV. This corresponds to the first resonance of ^{230}Th as shown in Figure 4.3 This depression becomes even greater as the ^{230}Th increases further. Figure 6.9. shows the spectra for 100 percent ^{230}Th.

Not only does this depression increase with ^{230}Th enrichment, but also with depth in the target. Figure 6.10 shows the flux in the outer layer of the target. Notice the flux at the first resonance energy at this depth. Figure 6.11 shows the flux in the central region of the target. At this depth, the flux at the resonance energy is depressed by about two orders of magnitude which may affect neutron capture in the interior of the target.

It should be noted that the most of the resonance absorption in the target occurs at the outer layers of the target. Figure 6.12 is the volumetric flux spectrum for between ¾ radius and ½ radius surfaces of the target. Note that the flux at the resonance has decreased most of the two orders of magnitude between the outer layer and this second layer.

These effects also impact the total flux in the target. As the ^{230}Th enrichment increases, the total flux is observed to decrease. This decrease indicates that the neutron flux that the target is exposed to is sensitive to the difference in the cross-sections of ^{230}Th and ^{232}Th, with ^{230}Th having higher cross-sections across thermal and resonance energies. The tally results discussed earlier indicate a particular sensitivity to resonance absorption in ^{230}Th at the first resonance. This is shown in Table 6.2.

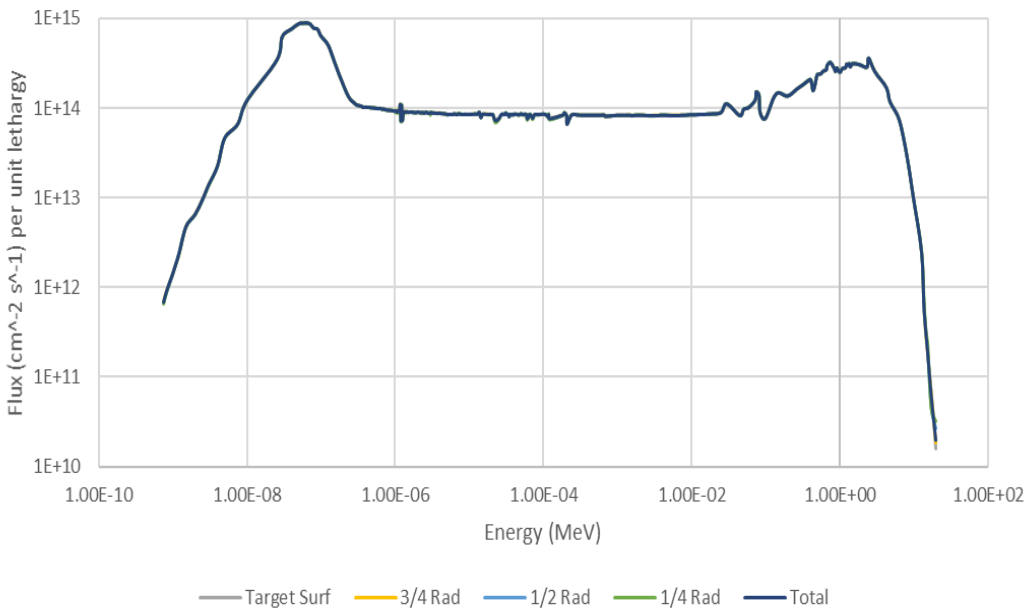

Figure 6.7. 238-group neutron spectra for various depths in a pure ^{232}Th target.

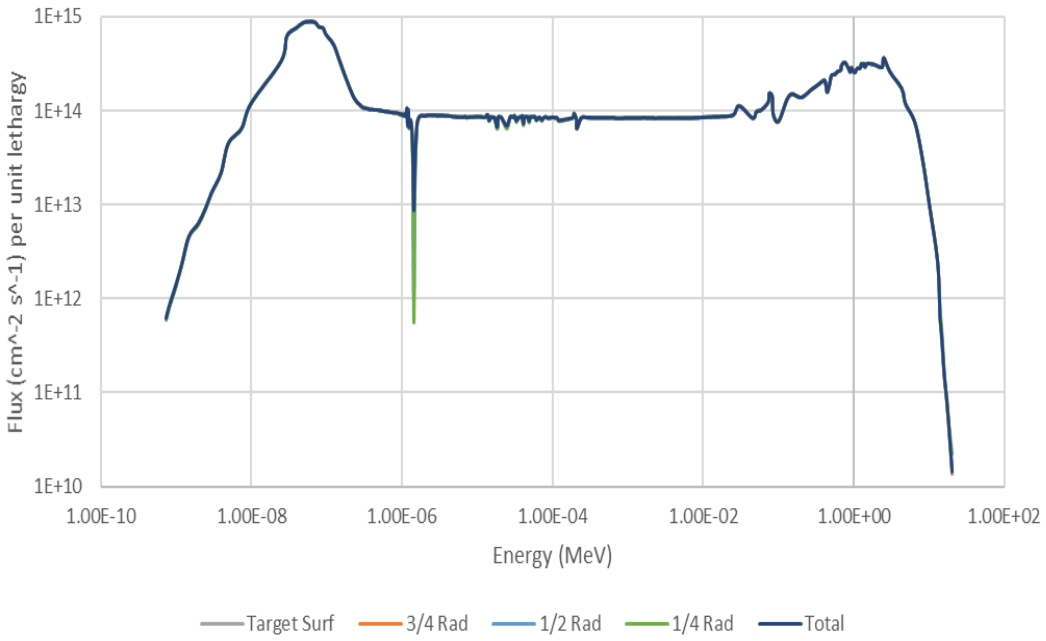

Figure 6.8. 238-group neutron spectra for various depths in a 40 percent ^{230}Th target.

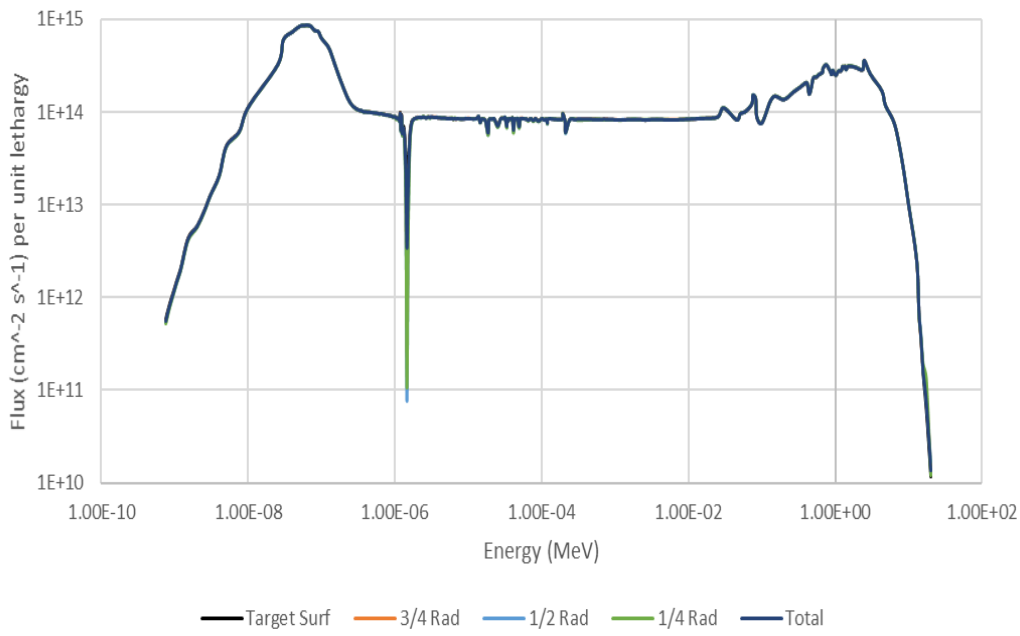

Figure 6.9. 238-group neutron spectra for various depths in a 100 percent ^{230}Th target.

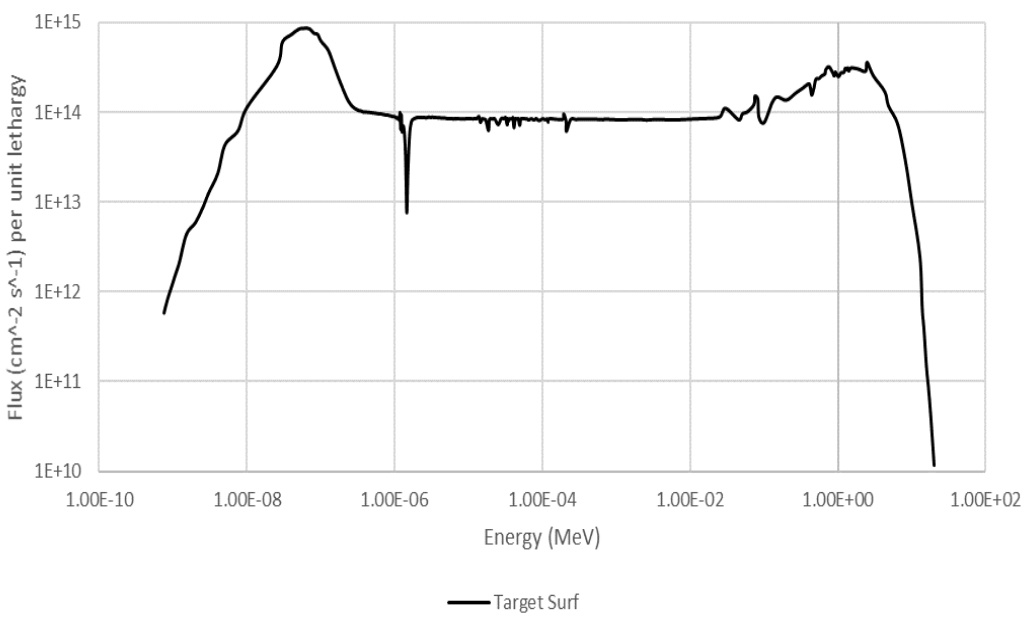

Figure 6.10. 238-group neutron spectra for the outer layer of a 100 percent ^{230}Th target.

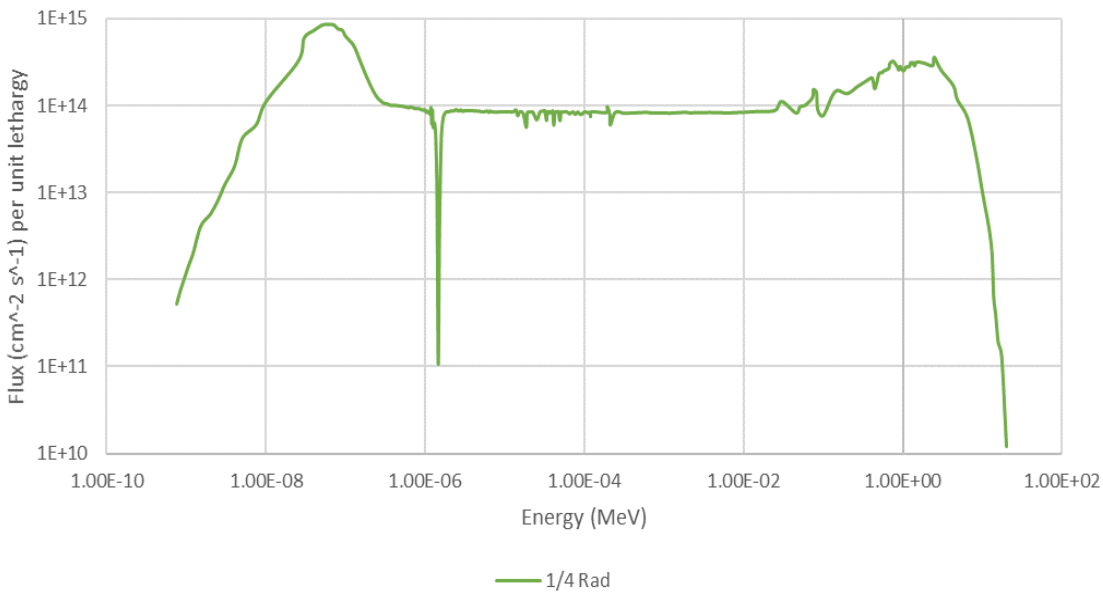

Figure 6.11. 238-group neutron spectra for the center of a 100 percent ^{230}Th target.

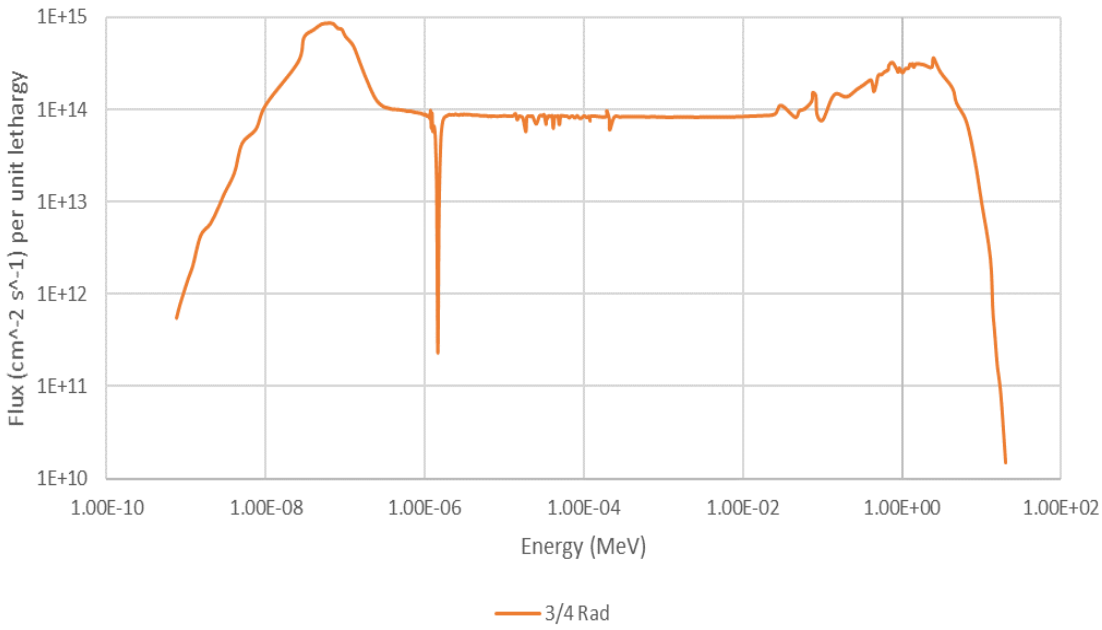

Figure 6.12. 238-group neutron spectra between ¾ radius and ½ radius of a 100 percent ^{230}Th target.

Table 6.2. Total flux tallied in the HFIR target for each ^{230}Th enrichment.

Th-230 Enrichment	Total Flux ($cm^{-2} * s^{-1}$)
0 % Th-230 (Pure Th-232)	3.77E+15
3 % Th-230	3.65E+15
10 % Th-230	3.64E+15
15 % Th-230	3.63E+15
20 % Th-230	3.63E+15
30 % Th-230	3.62E+15
40 % Th-230	3.61E+15
50 % Th-230	3.60E+15
60 % Th-230	3.60E+15
70 % Th-230	3.59E+15
80 % Th-230	3.58E+15
90 % Th-230	3.58E+15
100 % Th-230	3.57E+15

It is possible that this observation of less absorption in the resonance region could be affected by the energy bin width used in the tallies, and that absorption could be hidden by such values being averaged with regions with low absorption. However, it also possible that this region has lower absorption due to that the other resonances are lower in magnitude.

6.5. ORIGEN Results

The average flux tally results for each ^{230}Th Enrichment are then input into ORIGEN, calculating isotope production for six HFIR irradiation cycles. These results are then compared to the hydraulic tube results in Chapter 5. Examples of these ORIGEN calculations are provided in Appendix C:.

6.5.1. Protactinium-231

The ORIGEN calculation for ^{231}Pa was run for six cycles and compared to the data in Chapter 5. The results are shown in Figure 6.13. These results are similar to the previous hydraulic tube study in that the maximum yield is about 0.35 grams of ^{232}U per gram of ^{231}Pa. However, the isotope buildup does track differently than the previous study. It is clear that self-shielding does affect production, with the final yield being reached at the end of the cycle, while the hydraulic tube study reached peak yield in the middle of the cycle. A comparison of the ^{232}U yields for the hydraulic tube study and this full target study is shown in Figure 6.14. Notice that after one cycle, the MCNP data for ^{232}U production is lower than the results from Chapter 5. The ^{232}U mass does not reach the same mass until the end of cycle four.

The grams ^{232}U per gram-reactor day is also significantly lower. While this measure of efficiency peaks at the same point in cycle one, it is two orders of magnitude lower. However, the optimal irradiation time remains unchanged, with the ^{232}U mass reaching a maximum of 0.34 grams after two cycles. After two cycles, about one third of the initial ^{231}Pa is remaining. The masses of ^{231}Pa, ^{232}U, and ^{233}U are shown in Table 6.3. It should be noted that because of the isotopic purity of the protactinium, this remaining ^{231}Pa is fairly straight forward to recover and recycle.

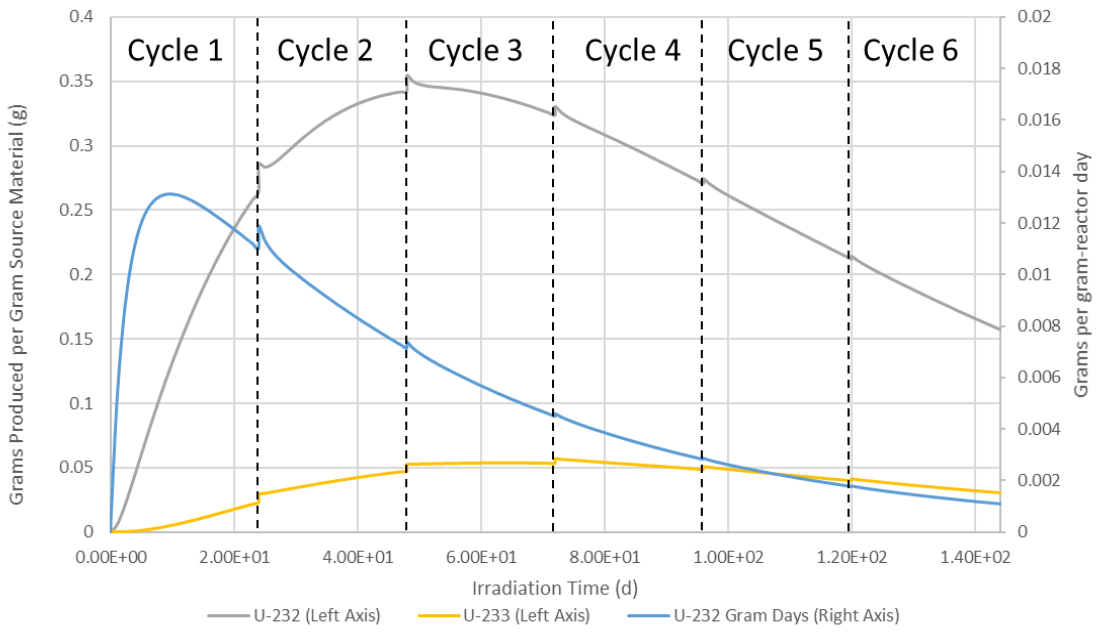

Figure 6.13. ORIGEN results for a ^{231}Pa HFIR target irradiated for six HFIR cycles.

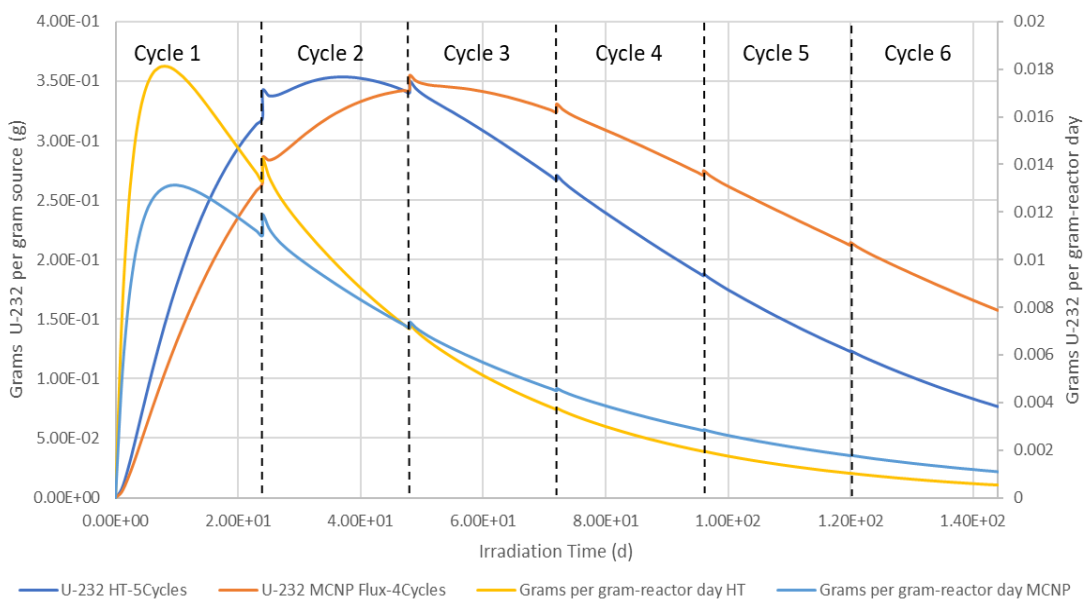

Figure 6.14. Protactinium-231 ORIGEN data for hydraulic tube data and MCNP flux data.

Table 6.3. Mass of ^{232}U, ^{233}U, and ^{231}Pa per gram of Pa Target material.

Isotope	0 Cycles	1 Cycle	2 Cycles	3 Cycles	4 Cycles	5 Cycles	6 Cycles
pa231	1.00E+00	5.77E-01	3.33E-01	1.92E-01	1.11E-01	6.41E-02	3.62E-02
u232	0.00E+00	2.65E-01	3.43E-01	3.24E-01	2.71E-01	2.12E-01	1.57E-01
u233	0.00E+00	2.29E-02	4.73E-02	5.34E-02	4.86E-02	3.99E-02	3.05E-02

6.5.2. Thorium-230

Thorium-230 irradiations using the MCNP tally fluxes result in similar decreases when compared to the hydraulic tube results in Chapter 5. It is important to note the trends in the buildup of ^{232}U over time. The ORIGEN results for 100 percent ^{230}Th are shown in Figure 6.15. Note the maximum ^{232}U yield for these results versus the results in the previous chapter.

At the end of cycle five, the mass of ^{232}U is about 0.106 grams, which is lower than the 0.15 grams in the hydraulic tube data in Chapter 5. This is decrease of 29.3 percent, which is a result of the previously discussed self-shielding effects. A comparison of this data with the HT data without self-shielding is shown in Figure 6.16.

This trend of decreased ^{232}U yield holds for the range of ^{230}Th enrichments. The results for the 10 percent ^{230}Th are shown in Figure 6.17. The amount of ^{232}U produced is 0.0126 grams, lower than the 0.015 grams produced without self-shielding in Chapter 5. This indicates that self-shielding has an impact in the final ^{232}U yield at this enrichment as well.

A comparison between these results and the HT results without self-shielding from Chapter 5 is shown in Figure 6.18. The ^{232}U yield is decreased by 16 percent when compared to the results without self-shielding. This is a lower decrease in the yield when comparing the pure ^{230}Th target results, which is in line with the previously discussed self-shielding effects. These ORIGEN results indicate that lower ^{230}Th enrichments may have better utilization. This is, however, canceled out by the significantly lower ^{232}U yield.

For each ^{230}Th enrichment, there is a maximum amount of ^{232}U produced, occurring after five HFIR cycles. However, with the increased cost and diminishing returns of irradiation, four cycles may be preferred. The amount of ^{232}U per gram of source material after each cycle for up to six cycles is shown in Table 6.5. The buildup of ^{232}U for each ^{230}Th enrichment is shown in Figure 6.19.

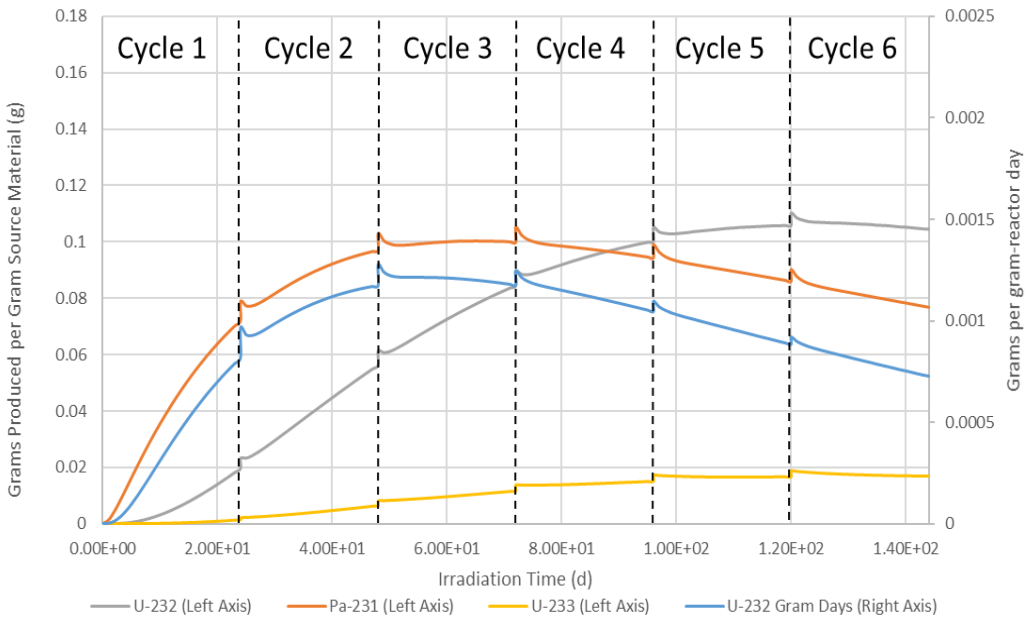

Figure 6.15. ORIGEN results for a 100 percent ^{230}Th target.

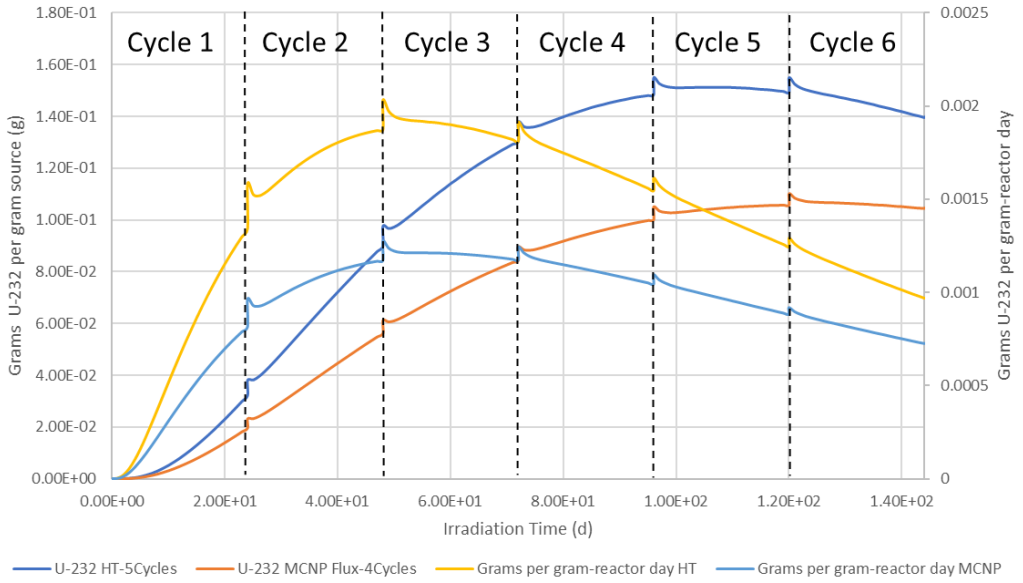

Figure 6.16. Comparison of 100 percent Thorium-230 ORIGEN data for hydraulic tube data and MCNP flux data.

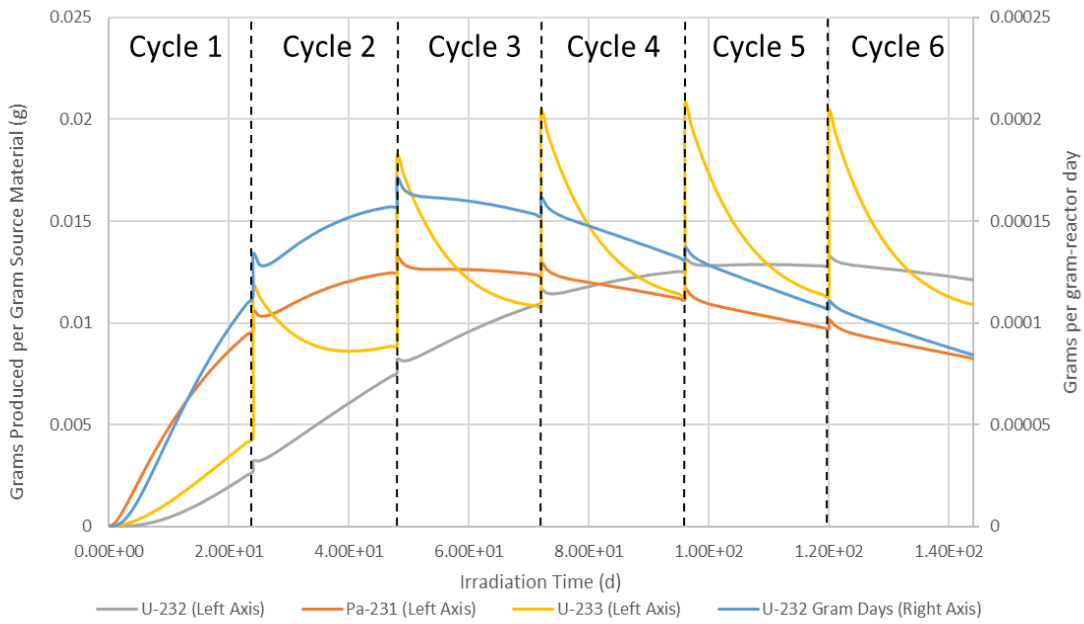

Figure 6.17. ORIGEN results for a 10 percent ^{230}Th target.

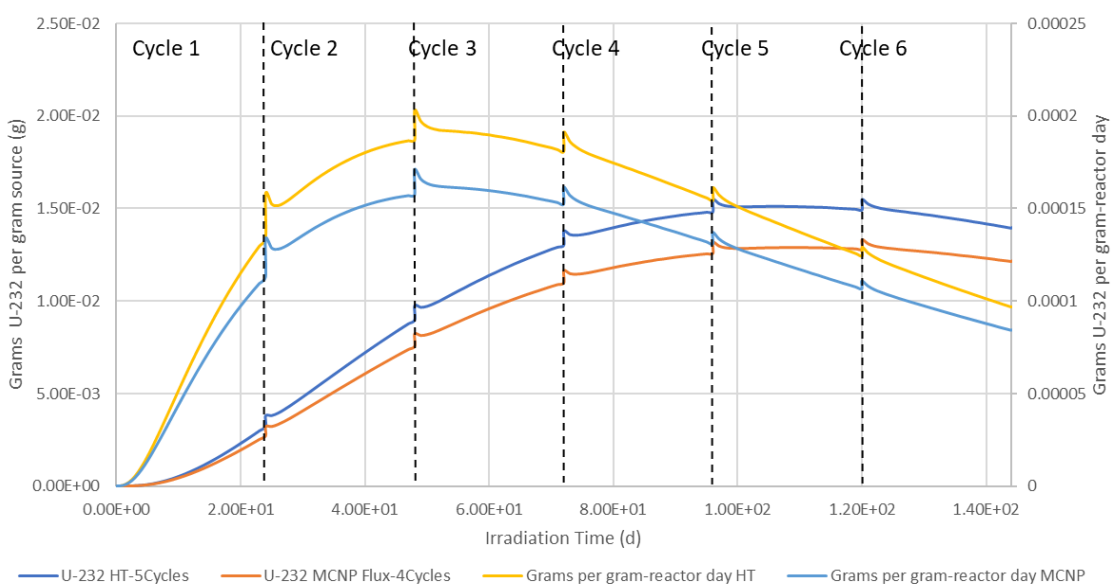

Figure 6.18. Comparison of 10 percent Thorium-230 ORIGEN data for hydraulic tube data and MCNP flux data.

Table 6.4. Uranium-232 mass (g) per Gram of Source Material for Six HFIR Cycles

Th-230 Enrichment	1 Cycle	2 Cycles	3 Cycles	4 Cycles	5 Cycles	6 Cycles
3 % Th-230	9.40E-04	2.58E-03	3.70E-03	4.17E-03	4.17E-03	3.88E-03
10 % Th-230	2.72E-03	7.56E-03	1.10E-02	1.26E-02	1.28E-02	1.21E-02
15 % Th-230	3.85E-03	1.08E-02	1.57E-02	1.81E-02	1.86E-02	1.77E-02
20 % Th-230	4.92E-03	1.38E-02	2.03E-02	2.34E-02	2.41E-02	2.32E-02
30 % Th-230	6.98E-03	1.97E-02	2.90E-02	3.37E-02	3.49E-02	3.38E-02
40 % Th-230	8.90E-03	2.52E-02	3.73E-02	4.36E-02	4.54E-02	4.41E-02
50 % Th-230	1.08E-02	3.06E-02	4.54E-02	5.33E-02	5.56E-02	5.43E-02
60 % Th-230	1.26E-02	3.59E-02	5.35E-02	6.29E-02	6.59E-02	6.45E-02
70 % Th-230	1.44E-02	4.11E-02	6.14E-02	7.24E-02	7.60E-02	7.45E-02
80 % Th-230	1.61E-02	4.62E-02	6.91E-02	8.17E-02	8.45E-02	8.45E-02
90 % Th-230	1.79E-02	5.12E-02	7.68E-02	9.10E-02	9.59E-02	9.45E-02
100 % Th-230	1.96E-02	5.63E-02	8.45E-02	1.00E-01	1.06E-01	1.05E-01

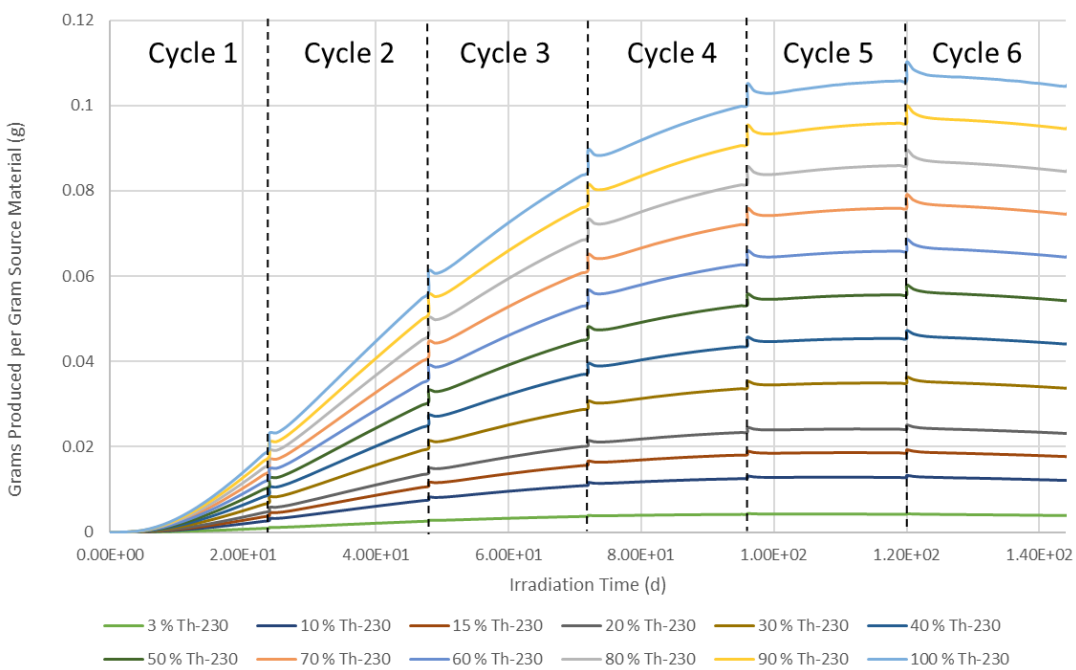

Figure 6.19. Uranium-232 Buildup for each ^{230}Th Enrichment.

As can be seen in Figure 6.19, for each ^{230}Th enrichment, most of the ^{232}U has been produced prior to cycle five. As continued irradiation would result in more target depletion for diminishing returns, ending irradiation after four cycles should be considered.

6.5.3. Thorium-230 Depletion

It is also important to examine the depletion of ^{230}Th as the target is irradiated. As noted earlier, recycling unutilized ^{231}Pa from a target conceptually straight forward. However, the presence of ^{232}Th and ^{230}Th together and the effects of self-shielding make recycling unutilized thorium more complicated. Table 6.5 contains the mass ^{232}U, ^{233}U, ^{231}Pa, and ^{230}Th per gram of target material after four cycles for each ^{230}Th enrichment. Notice the amount of ^{230}Th lost contrasted to the mass of ^{232}U produced. For a pure ^{230}Th case, almost 40 percent of the ^{230}Th is lost for only one tenth of the target mass to be converted to ^{232}U. Some ^{231}Pa builds up in the target, which may be recovered and irradiated on its own. However, it is clear that ^{230}Th has lower conversion to ^{232}U. **Error! Reference s ource not found.** contains the remaining mass of ^{230}Th for each ^{230}Th enrichment. The amount of ^{230}Th remaining should be noted when considering recycling the thorium target material, especially as self-shielding will cause ^{230}Th to undergo preferential depletion versus ^{232}Th.

It should be noted that the thorium will also accumulate other thorium isotopes during irradiation as well. Over time, the isotopes ^{228}Th and ^{229}Th will also build up in the target over time. Noting the quantities of these isotopes is important because these isotopes both decrease the overall percentage of thorium that is ^{230}Th, and pose a radiological concern to workers handling these targets. As ^{228}Th is the first daughter isotope of ^{232}U, this will expose workers to the same 2.614 MeV gammas. As these are thorium isotopes, they cannot be chemically separated. Allowing ^{228}Th to decay to daughter isotopes that can be chemically separated will take years, as ^{228}Th has a half-life of 1.9125 years [1]. Removal of ^{229}Th by allowing it to decay is not feasible, as the half-life for this isotope is 7,932 years. The mass of ^{228}Th per gram of target material is shown in Figure 6.21, and the

mass of ^{229}Th is shown in Figure 6.22. The presence of these isotopes should be considered when handling and recycling the thorium material.

Table 6.5 Isotope Buildup Mass (g) per Gram of Th-230 Source Material for Four HFIR Cycles.

Th-230 Enrichment	U-232 (g)	U-233 (g)	Pa-231 (g)	Th-230 (g)
3 % Th-230	4.17E-03	1.08E-02	3.60E-03	1.36E-02
10 % Th-230	1.26E-02	1.14E-02	1.12E-02	5.07E-02
15 % Th-230	1.81E-02	1.17E-02	1.62E-02	7.90E-02
20 % Th-230	2.34E-02	1.20E-02	2.12E-02	1.08E-01
30 % Th-230	3.37E-02	1.26E-02	3.08E-02	1.68E-01
40 % Th-230	4.36E-02	1.30E-02	4.01E-02	2.30E-01
50 % Th-230	5.33E-02	1.35E-02	4.92E-02	2.93E-01
60 % Th-230	6.29E-02	1.39E-02	5.84E-02	3.56E-01
70 % Th-230	7.24E-02	1.42E-02	6.74E-02	4.20E-01
80 % Th-230	8.17E-02	1.46E-02	7.64E-02	4.84E-01
90 % Th-230	9.10E-02	1.49E-02	8.53E-02	5.49E-01
100 % Th-230	1.00E-01	1.52E-02	9.43E-02	6.14E-01

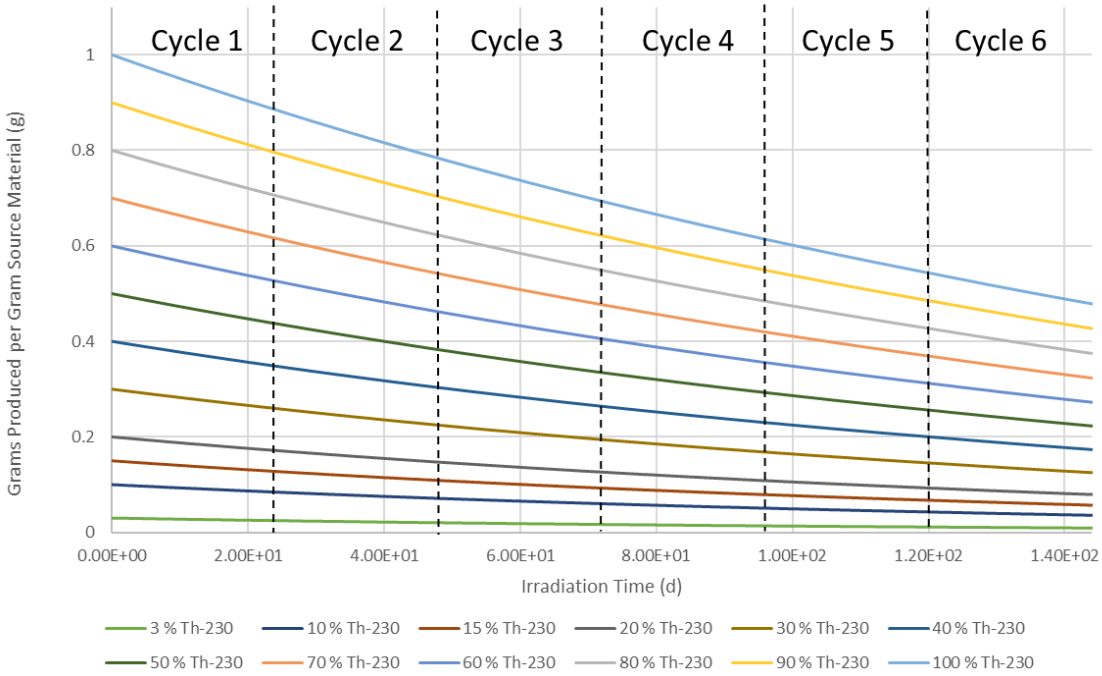

Figure 6.20. Remaining ^{230}Th mass (g) per Gram of Source Material for Six HFIR Cycles

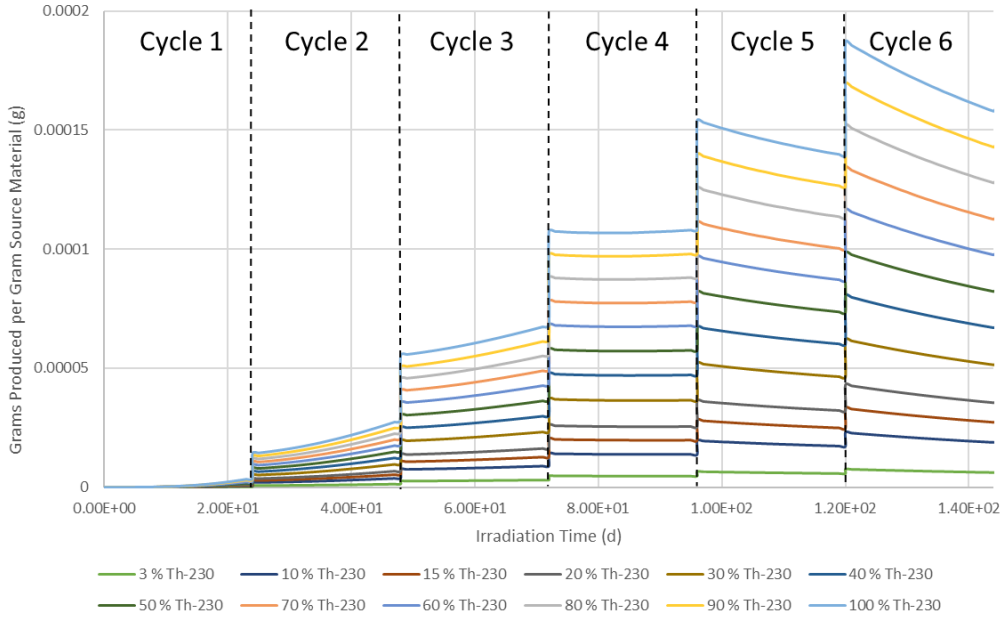

Figure 6.21. Thorium-228 mass (g) per Gram of Source Material for Six HFIR Cycles

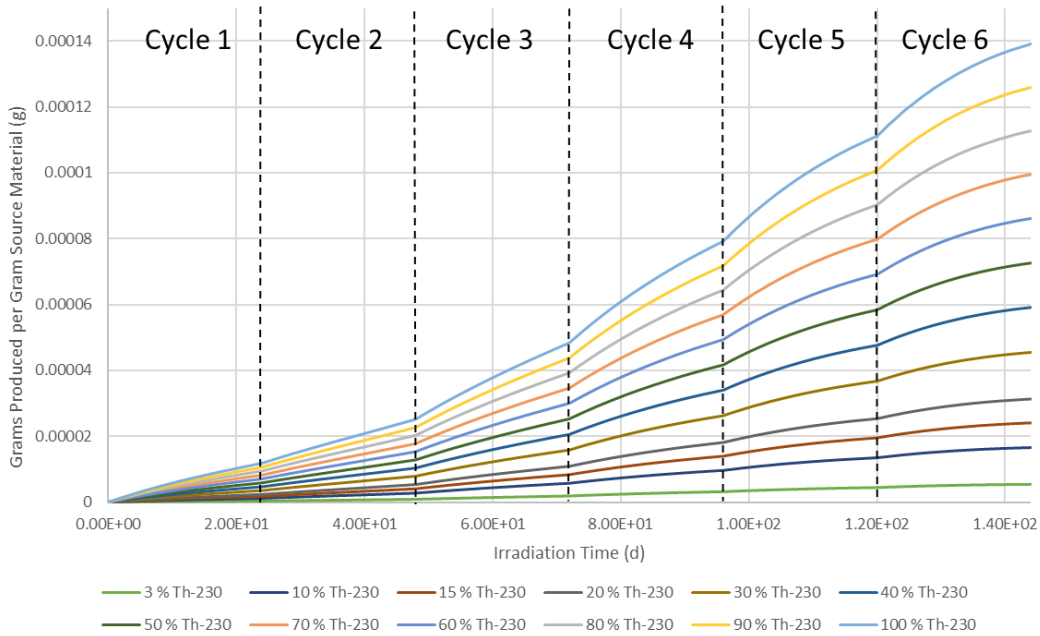

Figure 6.22. Thorium-229 mass (g) per Gram of Source Material for Six HFIR Cycles

The buildup of ^{228}Th and ^{229}Th along with the preferential depletion of ^{230}Th due to resonance absorption results in an overall decrease in the ^{230}Th assay of the remaining elemental thorium material. This decrease in the overall percentage of irradiated thorium that is ^{230}Th may result in recycled thorium material have increasingly diminished performance with each recycling. This is compounded by the loss of total elemental thorium. A significant amount of thorium is depleted, and the remaining thorium is of diminished quality. Mitigating against this reduction in the quality of the thorium target material may be accomplished by blending with fresh material, but the presence of ^{228}Th may result in difficulty working with a target containing recycled thorium. The amount of elemental thorium remaining is shown in Figure 6.23. The fraction of thorium that is ^{230}Th after each cycle is shown in Figure 6.24.

6.6. Chapter Conclusions

As indicated by the results above, the ^{232}U yield is affected by resonance absorption and spatial shielding. It is clear that to improve yield, the neutronics of target design must be carefully considered. However, target design issues such as such as material and thermal considerations are beyond the scope of this dissertation. It should be noted that the previous conclusions on irradiation time remain unchanged. The ^{231}Pa target should be irradiated up to two cycles, while the thorium targets should be irradiated for up to four cycles.

This has also provided understanding for considerations for recycling thorium, the decrease in the ^{230}Th enrichment, as well as the buildup of ^{228}Th and ^{229}Th make thorium recycling more complicated due to higher doses to workers. Protactinium recycling is comparatively more straight forward.

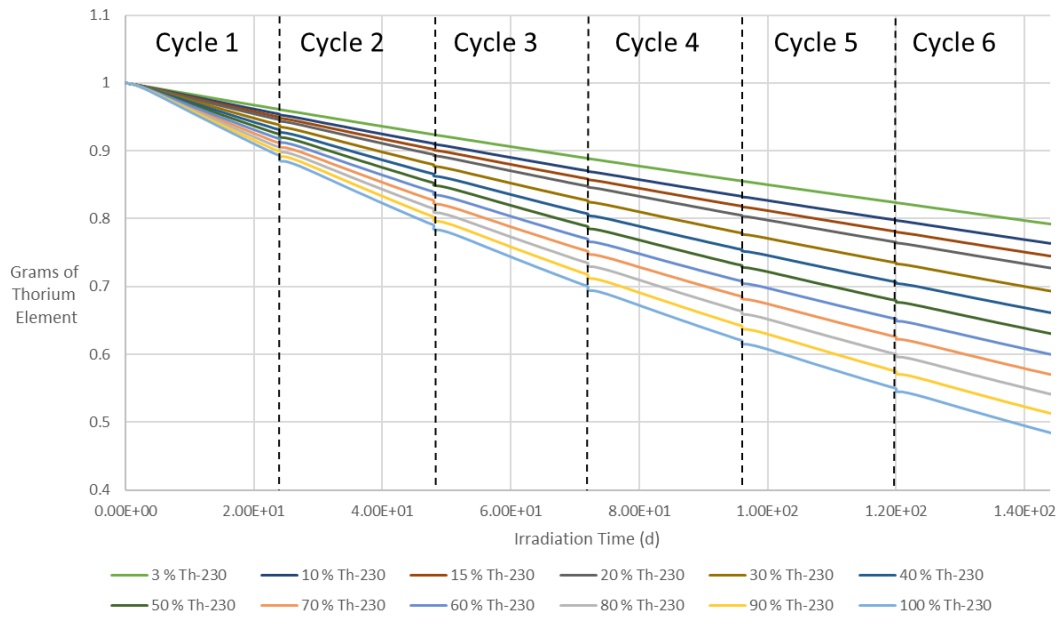

Figure 6.23. Remaining Elemental Thorium – Sum of all thorium isotopes.

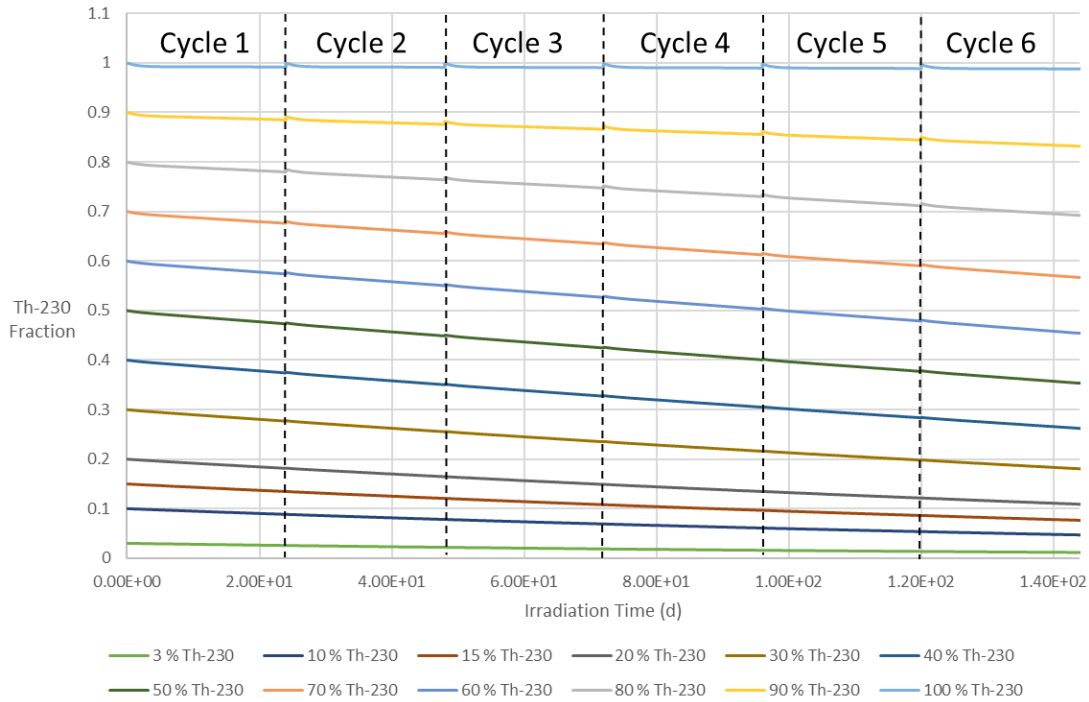

Figure 6.24. Remaining ^{230}Th Fraction in Elemental Thorium.

CHAPTER 7. ANALYSIS OF ANTICIPATED COSTS OF PRODUCING ^{232}U

7.1. Chapter Abstract

This chapter examines the associated costs of ^{232}U production based on estimates of costs for each step of production using the existing infrastructure of HFIR and ORNL. This study looks at estimated and assumed costs for each stage from extraction of raw material through irradiation and final chemical processing. Based on these estimates, various based on different target materials, protactinium and the different possible ^{230}Th enrichments, are examined based on material irradiated to determine which material and process provides the most cost-effective pathway for producing ^{232}U.

7.2. Chapter Introduction

The production of ^{232}U requires several key steps and processes, from sourcing raw material for ^{231}Pa and ^{230}Th, to final product recovery post-irradiation. Each of these steps will have an associated cost value that must be considered. Each of these steps and costs could be broken down further. However, for the purposes of this study, a few general steps will be considered. The costs for each step will be analyzed along with the self-shielded HFIR ORIGEN results from the previous chapter with the goal of determining the most cost-effective way of producing ^{232}U at HFIR by determining the lowest value for dollars per gram of ^{232}U.

7.3. Proposed Production Pathway Steps and Associated Costs

For this study, the following production steps are considered, along with the assumed aggregate cost for performing each step of ^{232}U production. These steps are: raw material extraction, target fabrication, irradiation, and final product recovery. Enrichment of ^{230}Th will also be considered. Each of these steps and their associated costs are discussed below. The proposed thorium cycle is shown in Figure 7.1, and a protactinium cycle is shown in Figure 7.2

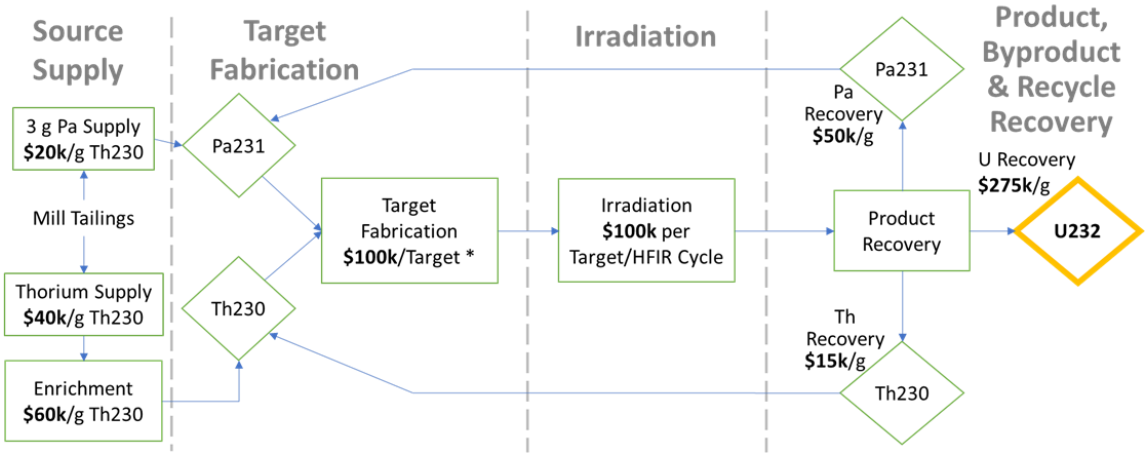

Figure 7.1. Proposed ^{230}Th Target cycle

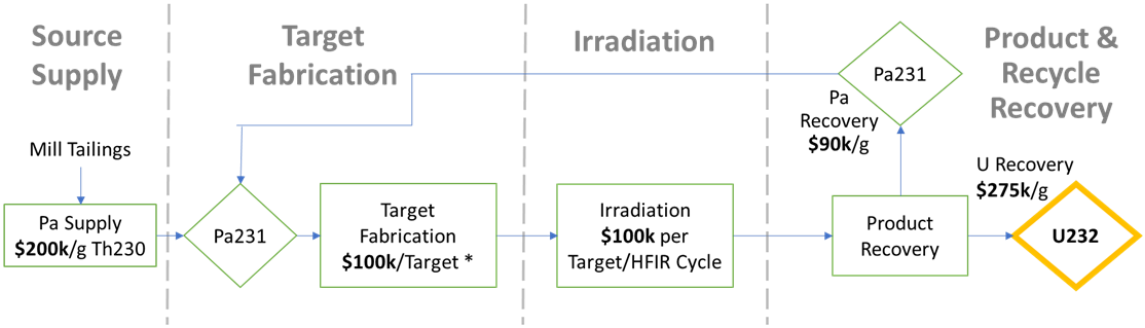

Figure 7.2. Proposed ^{231}Pa Target cycle.

7.3.1. Raw Material Extraction.

This is the initial step where protactinium and thorium are extracted from mined ores. As ^{231}Pa and ^{230}Th are decay daughters of the natural uranium isotopes ^{235}U and ^{234}U respectively, this raises the possibility for extracting from uranium ores. Significant studies for extraction of protactinium from uranium effluents have been conducted in the United Kingdom [31]. One such study recovered 100 grams of protactinium from five tons of uranium effluent [32]. Recovery of ^{230}Th has been less studied. Thorium-230 is more abundant than protactinium, but is expected to have significant ^{232}Th contamination due to the significantly higher abundance of ^{232}Th in elemental thorium [33]. A Mound Laboratory study from 1982 found Cotter Concentrate had a typical thorium assay of 3.2 percent ^{230}Th to 96.8 percent ^{232}Th. For this study, a range of ^{230}Th purities or enrichments will be considered. The enrichments examined are same as in the previous chapter as shown in Table 6.1.

In regard to the costs associated with extraction of protactinium and ^{230}Th, several assumptions have to be made. Because of the low abundance of protactinium, the extraction of protactinium is expected to be the more expensive process. Since protactinium extraction is not currently performed, there is no modern value to compare to the previous UK studies. This is a significant cause of uncertainty that must be accounted for when considering the use of protactinium as a target. This study predicts, with significant uncertainty, an extraction cost of $200,000 per gram of ^{231}Pa [34]. To account for this uncertainty, this study will assume a range of possible protactinium extraction costs from $100,000 to $650,000 per gram Pa in $50,000 increments to determine the sensitivity of the final ^{232}U production cost from protactinium to changes in the price of protactinium. For ^{230}Th, this study does not study the sensitivity to raw material price, and assumes a flat value of $40,000 per gram ^{230}Th [34].

7.3.2. Thorium-230 Enrichment

Because of the expected contamination of ^{230}Th with significant quantities of ^{232}Th, this study considers the enrichment of ^{230}Th using electromagnetic isotope separation (EMIS).

EMIS has been used in the past for pioneering uranium enrichment, and for the previous separation of other isotopes including ^{230}Th. This previous work has included enrichment studies for ^{230}Th, indicating what the resulting enrichment is from feeds with different initial ^{230}Th enrichments. These enrichment results are examined as possible contributions to the final cost per gram of ^{232}U, and are shown in Table 7.1 [35]. This would allow for examining the difference between the use of a target manufactured from enriched material versus a target manufactured in the case that the equivalent enrichment was found naturally in ore. An example would be the cost of using material enriched to 100 percent ^{230}Th versus finding 100 percent ^{230}Th naturally in ore. For this study, the cost of enrichment is assumed to be $60,000 per gram of enriched product across the modeled feed materials [34]. This project predicts that the most likely process for ^{230}Th sourcing is enriching to 80 percent ^{230}Th from 3 percent ^{230}Th extracted from ore [34].

7.3.3. Target Fabrication

Once the protactinium or thorium have been milled from ore, and any ^{230}Th enrichment has been performed, the materials must be fabricated into HFIR targets. This involves converting the protactinium or thorium into oxide-aluminum pellets and stacking them in aluminum claddings. For this process, the costs assumed are about $100,000 per target [34]. If a target is assumed to contain 18 grams of actinide, this gives a target fabrication cost of $5,555.56 per gram of target actinide.

7.3.4. Irradiation

The use of a nuclear reactor such as HFIR has associated costs with irradiating a target. Irradiation costs increase with a longer irradiation time. For this study, irradiation costs are assumed to be $100,000 per target per HFIR cycle [34]. As the ^{232}U mass changes with irradiation time, the ORIGEN data for each HFIR cycle from Chapter 6 will be used to relate ^{232}U yield with irradiation cost. The ORIGEN results in Chapter 6 indicated that the peak ^{232}U yield was reached in cycle two for protactinium irradiations, and in cycle five for ^{230}Th irradiations.

Table 7.1. EMIS Enrichment Feeds, Products, and Costs.

Feed Enrichment	Product Enrichment	Cost per Gram Product
3% Th-230	80% Th-230	$60,000.00
10% Th-230	90% Th-230	$60,000.00
≤ 20% Th-230	100% Th-230	$60,000.00
≥ 40% Th-230	100% Th-230	$60,000.00

It should be noted that as the ^{232}U yield approaches its maximum, the rate of production decreases, causing diminishing returns as the irradiation time increases until the maximum yield is reached. These diminishing returns may present a scenario where ending irradiation before the maximum yield is reached may be more cost effective per gram of ^{232}U.

7.3.5. Product Recovery

This is the final step under consideration for this analysis. After a target has been removed from HFIR and allowed to cool, chemical processing is performed to recover uranium from the target material. At this stage, any protactinium that has either been bred in a thorium target or unutilized in a protactinium target, can also be chemically recovered in a separate process. While the proposed process above includes recycling, ^{230}Th, the depletion of ^{230}Th complicates and this, so recycling ^{230}Th is not examined. The costs assumed for this study are $275,000 per gram uranium recovered [34].

As the recovery of uranium and protactinium are assumed to require separate processes, the recovery of protactinium will have separate cost values. Studied protactinium extraction processes have achieved recovery in excess of 85 percent, so this study assumes that almost the entirety of the ^{231}Pa can be recovered after a few extraction processes [36] [37]. These protactinium recovery costs are expected to differ between the protactinium targets and protactinium recovery from thorium. Recycling unutilized protactinium from a protactinium target is assumed to cost $90,000 per gram, while protactinium recovery from thorium is expected to cost $50,000 per gram [34].

7.3.6. Procedure for Analysis

With the above cost values, the costs per gram of ^{232}U can be calculated by simply summing the costs for each individual step together. Some of the production steps have their costs given on a per target basis, it is more convenient to determine the cost of determining the costs per target, and converting to a per-gram-^{232}U basis by dividing by the 18 grams of target material per target, and by dividing by the mass of ^{232}U produced per gram of target material.

Several scenarios for ^{232}U will be examined in order to examine the utilization of target material and determine the most cost-effective procedure for producing ^{232}U. Both protactinium could be used in once-through cycles. Unutilized protactinium from an irradiated protactinium target can be recovered and recycled. Because protactinium is an intermediate byproduct of irradiating ^{230}Th, recovering and recycling this protactinium bred from thorium irradiations will be considered for recovered from each ^{230}Th enrichment

7.4. Cost Analysis Results for Once-Through Production Cycles

The simplest means of producing ^{232}U is a once-through irradiation cycle, where a target is irradiated, and the products are chemically separated. Any unutilized target material is not recycled. This section examines once-through cycles for protactinium, and cycles that use varying enrichments of ^{230}Th.

7.4.1. Protactinium Once-Through

As stated earlier, the cost of extracting protactinium from uranium tailings is uncertain, so the sensitivity of ^{232}U costs to the price of protactinium extraction is examined. As the ^{231}Pa extraction costs examined increase linearly, the increase in the dollars per gram of ^{232}U increases linearly. These results are for two cycles of irradiation.

7.4.2. Thorium-230 Once-Through

For the ^{230}Th irradiation processes, extraction costs are assumed to be constant across the various enrichments. The sensitivity the of ^{232}U cost to the ^{230}Th enrichment is examined, as the enrichment of ^{230}Th that can be extracted from uranium effluent has some uncertainty. For this study, some of the higher ^{230}Th enrichments are examined with and without enrichment processes, as some of the higher enrichments may require enrichment.

As ^{230}Th targets require several HFIR cycles of irradiation to reach peak ^{232}U yield, the cost of ^{232}U based on irradiation time is also examined. As stated earlier in the examination of self-shielding and ^{230}Th depletion, the peak ^{232}U yield is reached in cycle five, but it may be preferred to end irradiation at cycle four or earlier due to the depletion of ^{230}Th and the buildup of ^{228}Th. When the dependence on irradiation time was examined, it was observed that the lowest cost per gram of ^{232}U is achieved in cycle four. This holds true for the higher enrichments.

7.5. Protactinium Recycling Costs Results

As protactinium is the more efficient target material, recovery of unutilized or built-up ^{231}Pa is important from a cost standpoint. This section examines recovery and recycling of ^{231}Pa from protactinium and thorium targets.

7.5.1. Unutilized Protactinium from a Protactinium Target

Based on the ORIGEN results for a protactinium target, about six grams of ^{231}Pa remain after irradiation. This material could be combined with fresh material to construct a new protactinium target. Alternatively, after a few targets of fresh ^{231}Pa have been irradiated and processed, enough unutilized ^{231}Pa will remain to construct a target entirely of recycled ^{231}Pa. As this target has no fresh ^{231}Pa, the extraction cost is listed as zero.
Protactinium Recovered from Thorium Targets

As stated before, the protactinium built up in a thorium target can be recovered and used for targets. As the cost of recovery of ^{231}Pa is on a per gram of ^{231}Pa basis, the cost per gram of ^{232}U is flat across the ^{230}Th enrichments. This assumes that the ^{231}Pa recovery costs will add up the same even though the lower enrichments require more targets to reach a gram of ^{231}Pa. Therefore, recycling ^{231}Pa from ^{230}Th should be examined not in isolation, but in conjunction with the costs of ^{230}Th utilization.

7.5.2. Weighted Average Cost of Once-through Thorium with Protactinium Recovery

To examine the cost of ^{232}U form ^{230}Th combined with recycled ^{231}Pa, a weighted average is performed. The ^{232}U yield for a given target type is multiplied by the cost per gram of ^{232}U from that target and divided by the yields multiplied together. The ^{232}U yield from a thorium target is multiplied by the number of thorium targets of a given enrichment needed to produce one protactinium target. This formula is given in Equation 7.1 below.

$$\bar{x} = \frac{\sum_{i=1}^{n} w_i X_i}{\sum_{i=1}^{n} w_i} \tag{7.1}$$

Where $\bar{x}$ is the weighted average, X_i is the ^{232}U cost, w_i is the ^{232}U yield to weight to the cost by, and n is the number of costs to be averaged. As stated earlier, for the thorium costs, this weight includes multiplying by the number of ^{230}Th targets to make one ^{231}Pa target. Notice that based on least to most expensive ^{232}U costs, the average cost is arranged in the same order as the once-through costs. From both of these results, it is clear that finding higher enriched ^{230}Th from ore is preferred. However, notice that the ^{230}Th fractions that required enrichment processes are among the more expensive thorium processes for ^{232}U production in both once-through and ^{231}Pa recovery from thorium.

7.6. Discussion of Analyses

So far, the costs of producing ^{232}U have been examined for the cases of once-through protactinium, once-through thorium, protactinium target recycling, and protactinium recovered from thorium combined with thorium irradiation. The ^{232}U costs from the varying protactinium extraction costs have been compared with each other. The various ^{230}Th enrichments have also been compared with each other. Now all of the various costs must be examined together. Figure 7.3 examines each of the above production processes examined.

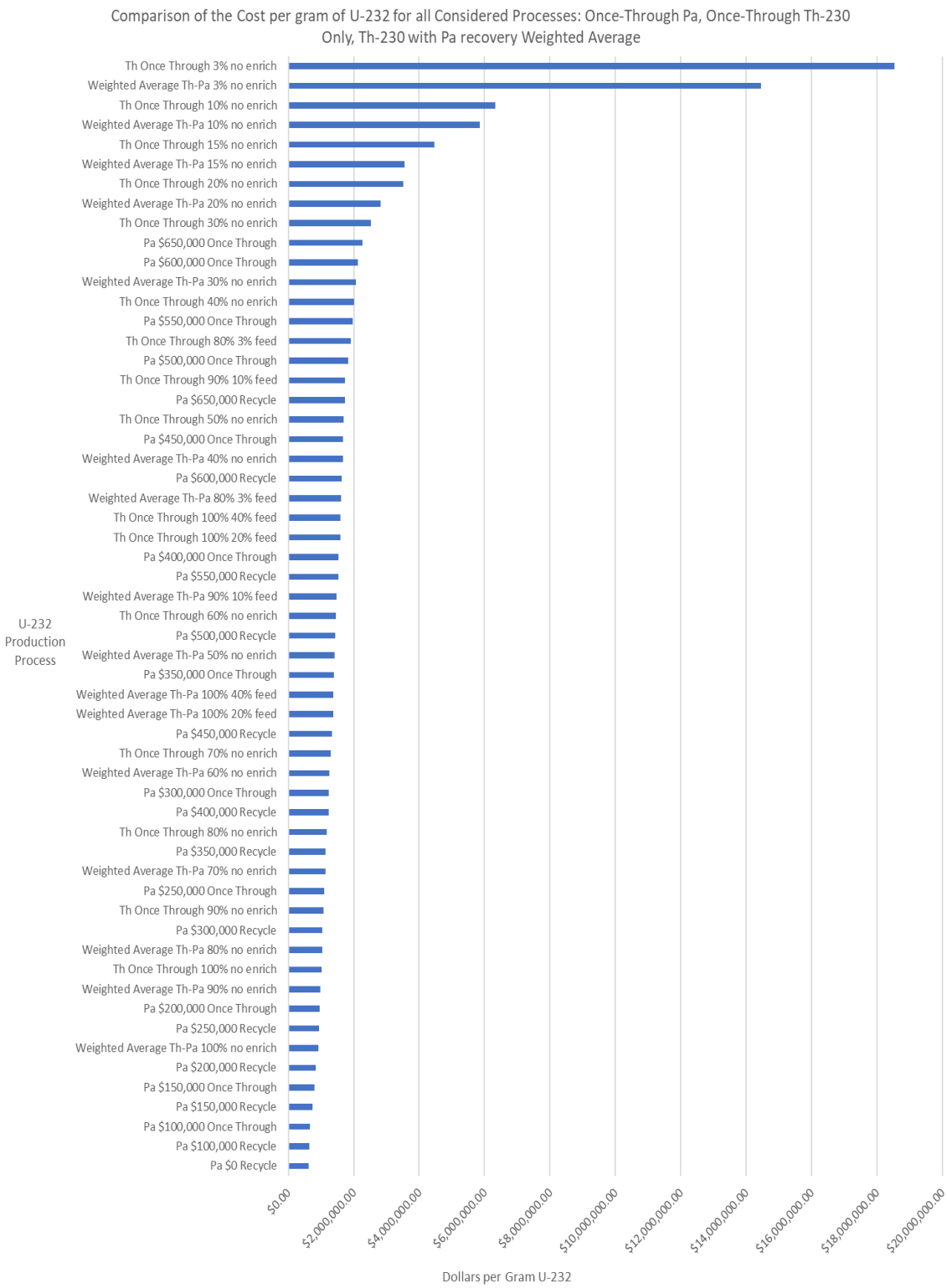

Figure 7.3. Costs per gram of ^{232}U for Each Production Process Examined.

The results as shown in Figure 7.3 allow for a direct comparison of thorium cases and protactinium cases, and determine under what conditions, based on the above costs at each process step, which production cases are more cost effective. The processes with the absolute lowest costs are protactinium processes, as shown in Figure 7.4. The first process involving thorium irradiation to appear at these lower costs is averaged thorium with protactinium recovery, where the thorium is 100 percent ^{230}Th straight from ore without any enrichment. This process falls in between recycled protactinium targets with extraction costs of $200,000 and $250,000. The once-through protactinium target is more costly than $250,000 extraction with protactinium recycling. The most like scenario is that the initial target in a production campaign, the initial target would have the once through costs due to all of the target material being fresh from ore, but would then feed into protactinium target recycling. Therefore, the expected costs are less.

The next region of interest is around the case where the weighted average cost of thorium irradiation with protactinium recovery for 80 percent ^{230}Th enriched from 3 percent is plotted in Figure 7.3. Figure 7.5 provides a closer examination of this region. This case is more expensive than Pa recycling at $550,000 for Pa extraction, and $400,000 Pa extraction for once-through irradiations. This thorium process is more cost-effective than Pa recycling with $600,000 Pa extraction from ore. This indicates that the most probable thorium process would only be more cost effective than Pa if the cost of extracting Pa is in excess of $600,000. Pa targets remain cost effective in comparison to this 80 percent ^{230}Th based process up to $550,000 for extracting Pa.

7.7. Cost Analysis Conclusions

Based on the above results, the most cost effective ^{232}U production process is protactinium irradiation, depending on the ^{231}Pa extraction cost from ore. If the ^{231}Pa extraction cost is around $200,000 per gram, a value predicted in this project, then ^{231}Pa is one of the most cost-effective options. As stated earlier, the only thorium process that is better is 100 percent ^{230}Th with ^{231}Pa recovery, an unlikely scenario as it is highly improbable to find pure ^{230}Th in nature, and enrichment processes to reach close to 100 percent require feed material that is already partially enriched, increasing costs.

Figure 7.4. Costs per gram of ^{232}U focused on the region of lowest cost per gram of ^{232}U. The Pa recycling case with $200,000 extraction costs is indicated.

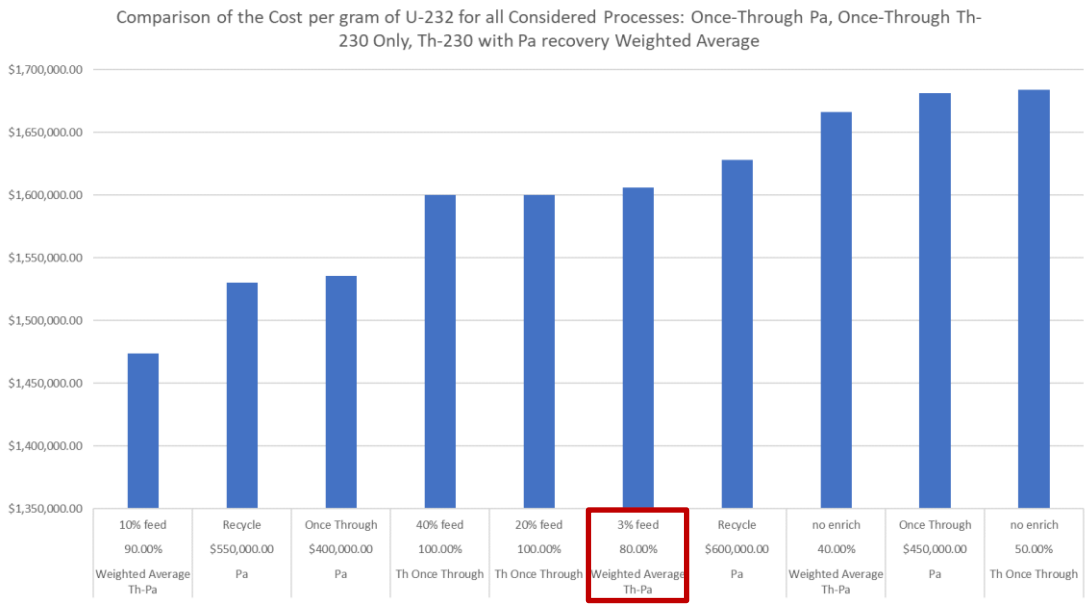

Figure 7.5. Costs per gram of ^{232}U centered on the weighted average of thorium irradiation with protactinium recovery. The case of averaged 80 percent enriched thorium from 3 percent feed with Pa recovery is indicated.

With the most probable thorium process being ^{230}Th enriched to 80 percent from 3 percent, the $200,000 protactinium extraction cost is significantly more cost-effective. For this thorium process to be the better option, ^{231}Pa extraction costs would have to be in excess of $550,000 per gram for an established Pa recycling process, at which point the average cost of using 80 percent ^{230}Th enriched from 3 percent with ^{231}Pa recycling is the better option.

It is clear that while protactinium is significantly more expensive to source, protactinium has significant advantages in cost savings in other steps of the production process. Protactinium does not require enrichment, and requires only half of the irradiation time. Along with the higher ^{232}U yield, more protactinium can be recycled from a ^{231}Pa target than a ^{230}Th target. Thorium-230 recycling was also ruled out due to the preferential depletion of ^{230}Th and buildup of ^{229}Th and ^{228}Th, as discussed in 6.5.3.

It should be reminded that the cost values above are based on rough assumptions of the cost of sourcing of target materials and the operations of the isotope production infrastructure of ORNL. Any changes in the cost values for each step of ^{232}U production for either Pa or ^{230}Th targets may impact the costs of each examined production case, which may change which processes are more cost effective than others. As such, the results of this study, and the conclusions drawn from them, may be subject to change depending on how the operating values for each step are changed.

CHAPTER 8.
MITIGATION OF PLUTONIUM-236 CONTAMINATION IN PLUTONIUM-238 PRODUCED IN IN THE ADVANCED TEST REACTOR VIA RECOVERY OF URANIUM-232

A version of this work was submitted as a conference proceeding to the Nuclear and Emerging Technologies for Space 2021 conference by Joshua Rhodes, Emory Colvin, Teyen Widdicombe, and Brad Kirkwood.

J. H. Rhodes, E. Colvin, T. Widdicombe and B. Kirkwood, "Mitigation of Tl-208 Gamma Dose from Pu-236 Decay Chain via Chemical Removal of U-232," in Nuclear and Emerging Technologies for Space, Oak Ridge, Tennessee, 2021.

This work was done as a part of the Center for Space Nuclear Research summer fellowship program at Idaho National Laboratory. Coauthors Emory Colvin, Teyen Widdicombe, Brad Kirkwood added insight into the background information, with Brad Kirkwood providing institutional input from INL.

8.1. Chapter Abstract

This chapter examines a possible ^{232}U source as a byproduct of ^{238}Pu production. Several space exploration missions have used radioisotope thermoelectric generators fueled by ^{238}Pu to generate electricity to power onboard systems and scientific instruments. Since the end of the cold war, several reactors used to produce ^{238}Pu have been shut down, and while some material was purchased from Russia, stockpiles have dwindled. The Department of Energy has recently restarted production of ^{238}Pu in 2015 using the High Flux Isotope Reactor. However, to meet NASA demands, the Advanced Test Reactor (ATR) at Idaho National Laboratory is also being considered. However, ^{208}Tl gamma emissions from ^{236}Pu contamination are a potential concern from ^{238}Pu produced in the ATR. SCALE 6.2 ORIGEN was used to examine ^{236}Pu decay and ^{208}Tl activity in order to develop strategies for mitigating against ^{208}Tl gammas using chemical processing removal features in ORIGEN to examine the possibility of removing ^{232}U.

8.2. Chapter Introduction

NASA has used radioisotope thermoelectric generators (RTGs) fueled with ^{238}Pu on several missions. These include several missions to the outer solar system, such as the Voyager probes, and the New Horizons mission, where the distance from the sun makes solar panels impractical. Other missions include Multi-Mission RTGs (MMRTG) used on the Mars Curiosity and Perseverance rovers, where the dust in the martial environment can limit solar energy collection. RTGs offer electric power in extreme environments in space that make other power sources impractical. However, when the RTG is being fueled and assembled, workers are exposed to gamma emissions from the ^{238}Pu. Plutonium-236, the decay parent of ^{232}U is a potential contaminant.

8.2.1. Problems with Using ^{237}Np for ^{232}U Production

As noted earlier in the initial production scoping study in Chapter 5, ^{232}U is a byproduct of ^{238}Pu production due to fast neutrons causing (n,2n) reactions in ^{237}Np targets. These (n,2n) reactions produce ^{236}Pu, which is the parent isotope of ^{232}U. As shown in Table 5.2, the amount of ^{232}U produced is low compared to ^{231}Pa and ^{230}Th irradiations. This make ^{237}Np irradiation impractical for ^{232}U production alone. However, ^{208}Tl may also contribute to doses during the handling of ^{238}Pu and an RTG, which opens the possibility for removing ^{232}U from ^{238}Pu as a means of mitigating against this additional dose rate.

8.2.2. History of ^{238}Pu Production.

Plutonium-238 was initially produced initially as a part of the weapons program using the K-Reactor at the Savannah River Site [38]. This material had typical ^{236}Pu concentrations ranging from 0.8-1.2 ppm, with efforts to reduce this to 0.3 ppm [39]. When the weapons material reactors were shut down at the end of the cold war, ^{238}Pu was no longer produced in the United States for many years. [38]. After the cold war, some ^{238}Pu was acquired from Russia, which was used for several missions. However, this stockpile was finite, and there was no domestic ^{238}Pu production for several years.

In 2015, HFIR produced the first ^{238}Pu in the United States since the shutdown of the K-reactor, with material being used for the Perseverance Rover [40]. However, to produce more material, the Advanced Test Reactor (ATR) at Idaho National Laboratory is being considered to increase production. NASA requirements call for 1.5 kilograms of ^{238}Pu to be produced annually, and ATR is being considered to help meet NASA demands [40]. The core of the Advanced Test Reactor is shown in Figure 8.1 [41].

8.2.3. Study Motivations.

As a part of the Center for Space Nuclear Research, previous studies examined several positions of the ATR to determine ^{238}Pu production from a ^{237}Np target irradiated in each position, as well as the resulting ^{236}Pu contamination from ^{238}Pu production in the ATR [42]. Each position has differing neutron fluxes, and the higher fluxes towards the center of the reactor may result in unacceptably high ^{236}Pu contamination. This higher ^{236}Pu contaminations may result in excessive ^{208}Tl contamination when the ^{238}Pu is being inserted into an RTG years after production. Therefore, this study will examine strategies for mitigate the ^{208}Tl dose via the chemical removal of ^{232}U and ^{228}Tl.

This study focuses on the removal of ^{232}U as a means of decreasing ^{208}Tl dose from the ^{238}Pu for years after production. Several variables will be studied, such as the initial ^{236}Pu concentration, material aging, and chemical removal factors. The results mainly focus on the usability of the plutonium by tracking ^{208}Tl contamination, but since that this study involves the removal of ^{232}U, the amount of ^{232}U removed can also be tracked. While the amount of ^{232}U is expected to be low, this may allow for the combining of ^{238}Pu and ^{232}U production anyways to provide quantities that may be sufficient for small-scale testing.

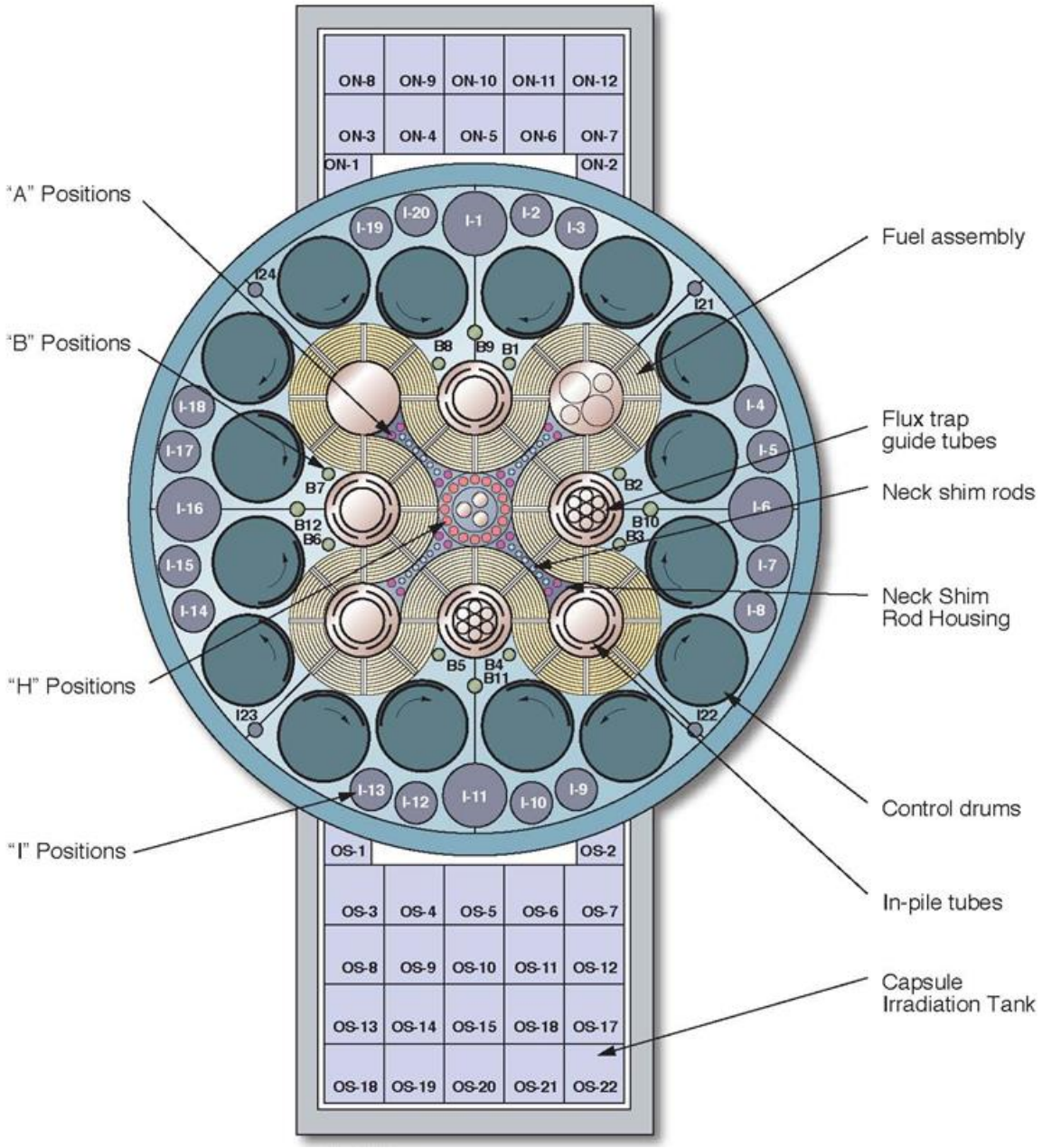

Figure 8.1. Cross-section of the Advanced Test Reactor

8.3. Simulated Processing Procedure, Methodology, and Variables.

For the simulation of the removal of ^{232}U from the plutonium product, a processing procedure within the ^{238}Pu production infrastructure must be determined that minimizes the ^{208}Tl dose from plutonium of varying ^{236}Pu contaminations. Each aspect of this processing procedure must be examined to determine what processes in the procedure are variables to examine. Computational methods must also be determined for simulating both radioactive decay and chemical removal.

8.3.1. Processing Procedure Steps

The neptunium target process considered is expected to have the following procedural steps. As the neptunium targets are irradiated, ^{236}Pu is expected to accumulate to different concentrations based on the incident neutron flux. After the targets are irradiated and removed from the ATR, the targets are allowed to decay for 150 days. After these 150 days, the targets undergo a chemical processing for removing fission products that will remove ^{232}U. After this first chemical process, the material will then be allowed to age for another variable amount of time. After this second aging, the target material will undergo a second chemical process of identical efficacy to the first.

8.3.2. Computational Methodology

As in previous chapters of this dissertation, the study discussed in this chapter involves the use of SCALE 6.2 ORIGEN. As previously discussed, ORIGEN is capable for calculating radioactive decay for multiple isotopes for varying material aging times. One feature of ORIGEN that has not been discussed so far is the ability to model chemical processing. Users can specify both batch chemical removal processes as well as continuous feed processes [16]. This study will consider batch chemical removal to simulate the chemical processes for removing ^{232}U from an irradiated solid target. Specifying the amount of removal of material is discussed later.

8.3.3. Parameters Examined

Since the ^{236}Pu concentration is expected to differ based on reactor irradiation position, this study examines a range of ^{236}Pu concentrations. Based on the previous findings by the CSNR when studying ^{238}Pu yield, ^{236}Pu concentrations are expected to range from 1 ppm in the outer "I" positions to upwards of 12 ppm briefly seen in the B positions, with 6-8 ppm maintained over time [42]. For this study, the ^{236}Pu concentration is varied from 1 ppm to 12 ppm in increments of 1 ppm.

As the irradiated target material ages, more ^{236}Pu decays to ^{232}U, which can then be removed. With a half-life of 2.85 years, ^{236}Pu decays to ^{232}U, where the bulk of these nuclides remain for several years. Allowing the ^{238}Pu to age for longer will allow for more ^{232}U to be removed. However, the material cannot be stored indefinitely due to mission needs. For this study, an aging time range of one to eight years in one-year increments will be considered. In terms of producing ^{232}U, the plutonium could be considered a cow for ^{232}U in a similar manner that ^{99}Mo decay is used to generate ^{99m}Tc.

As stated earlier in the procedure, the ^{238}Pu will undergo two chemical processing steps. While the first step will separate the ^{238}Pu from the ^{237}Np as well as remove fission products, ^{232}U will also be removed from this process. As this study focuses on minimizing the in-growth of ^{208}Tl, this study will focus on the ability of chemical processing to remove ^{232}U and ^{228}Th [43].

Chemical processing capabilities often use the term decontamination factor to describe how well a process is able to remove material. Anion exchange processes for removing plutonium are capable of decontamination factors upwards of $2*10^4$ in one removal cycle, and upwards of $4*10^7$ in two removal cycles [44]. For this study, it is more convenient to discuss the abilities of a chemical process in the fraction of an element in a compound that is removed or retained. When specifying batch chemical processing in ORIGEN, the fraction retained is specified for each retained element [16]. Elements that do not have a specified retained fraction are set to zero at the next time-step [16]. This study assumes that both ^{232}U and ^{228}Th have the same removal fractions. The ^{232}Th and ^{228}Th removal fractions examined are 0.97, 0.99, and 0.9999.

It should be noted that this study makes some assumptions about the capabilities of the relevant facilities that would perform such chemical processing procedures. The purpose of examining multiple removal fractions is to determine the importance of ^{232}U and ^{228}Th removal in what the final ^{208}Tl activity is. The specifics of the chemical processes and infrastructure required is beyond the project scope. In this study, it is assumed that a relevant facility such as REDC at ORNL is capable of achieving a ^{232}U removal fraction up to 0.9999. Based on the decontamination factors noted earlier, multiple treatments in an anion exchange column are possible. However, whether multiple anion exchange treatments are necessary, or by what means a removal fraction of 0.9999 are achievable, are beyond the scope of this study.

8.4. Modeling Objectives

With the above procedure and parameters, this study aims to determine what combinations of initial ^{236}Pu concentration, material aging, and chemical removal fraction suitably reduce ^{208}Tl activity. As workers handling an RTG may be doing so years after target irradiation, enough ^{208}Tl may have grown in to cause significant doses to workers. To limit these doses, this study aims to limit the ^{208}Tl activity to 1.7 µCi for at least two years after final chemical processing. Above this activity, dose rate will be deemed excessive. Keeping the ^{208}Tl activity below this activity provides a working window of two years for workers to assemble the RTG and mount it to the specified spacecraft. It is this later stage of handling the RTG when workers will be exposed to the highest dose when ^{208}Tl has had time to grown in.

One preliminary observation of this study is that at a concentration 2 ppm of ^{236}Pu, this objective is met with only the initial chemical processing after 150 days with a removal fraction of 0.97. For the purposes of this study, this observed case will be considered a baseline for comparing results for what each permutation of variables achieves in this processing procedure. This baseline case is shown in Figure 8.2.

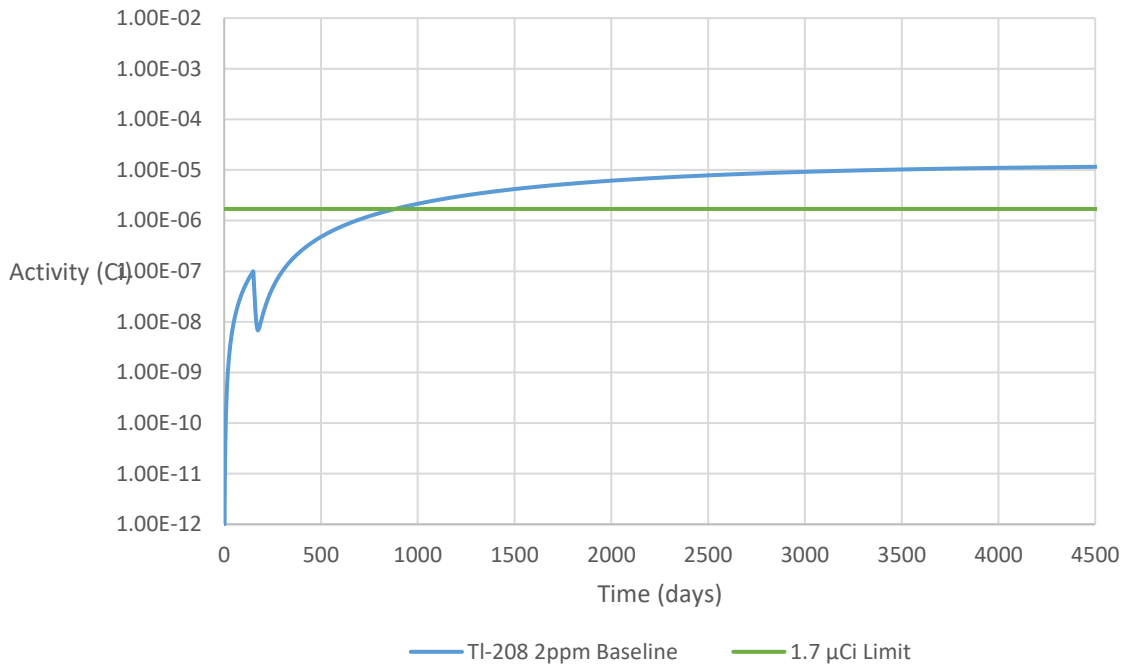

Figure 8.2. Baseline case with 2 ppm of ^{236}Pu with a single 0.97 removal reprocessing after 150 days.

8.5. ORIGEN Results and Observations on ^{208}Tl Mitigation

Each of the factors, ^{236}Pu concentration, material age, and chemical removal, affect material usability. After all of the ORIGEN calculations are run, each of the variables are examined for their individual effects. The results are also examined to determine what combination of these parameters have a ^{208}Tl activity that remains below 1.7 μCi for at least two years after processing. Examples of these ORIGEN calculations are provided in Appendix D:.

8.5.1. Effects of ^{236}Pu Concentration

As ^{236}Pu contamination is the primary concern, it is important to examine what effect the ^{236}Pu concentration has on final ^{208}Tl activity. This effect can be seen for a given aging time and removal fraction. Greater ^{236}Pu contamination may require longer aging, higher chemical removal, or a combination of both to stay below the 1.7 μCi ^{208}Tl activity limit. for at least two years. An example of the effects of different ^{236}Pu concentrations can be seen in Figure 8.3 and Figure 8.4. Notice that the overall shape of the activity curves is the same but the values are shifted higher or lower based on the initial ^{236}Pu concentration. In Figure 8.5, the ^{208}Tl activity for each ^{236}Pu concentration examined for five years of aging and a removal fraction of 0.99.

8.5.2. Effects of Material Aging and Decay Time Before Second Processing

As the plutonium ages between the first and second processing, the daughter isotopes grow in. As ^{232}U is the longest-lived isotope in this decay chain, each of the lower daughter isotopes approach secular equilibrium with respect to ^{232}U. Uranium-232 will approach equilibrium as ^{236}Pu decays away. Allowing the plutonium to decay for more time will eventually result in an effectively stable quantity of ^{232}U. Performing the second processing after this point when the activity of ^{236}Pu has sufficiently decreased will limit the regrowth of ^{232}U, and slowing the regrowth of ^{208}Tl. This results in a longer working duration for a given material. This can be observed by contrasting between the one-year aging in Figure 8.6, and the eight-year aging time in Figure 8.7.

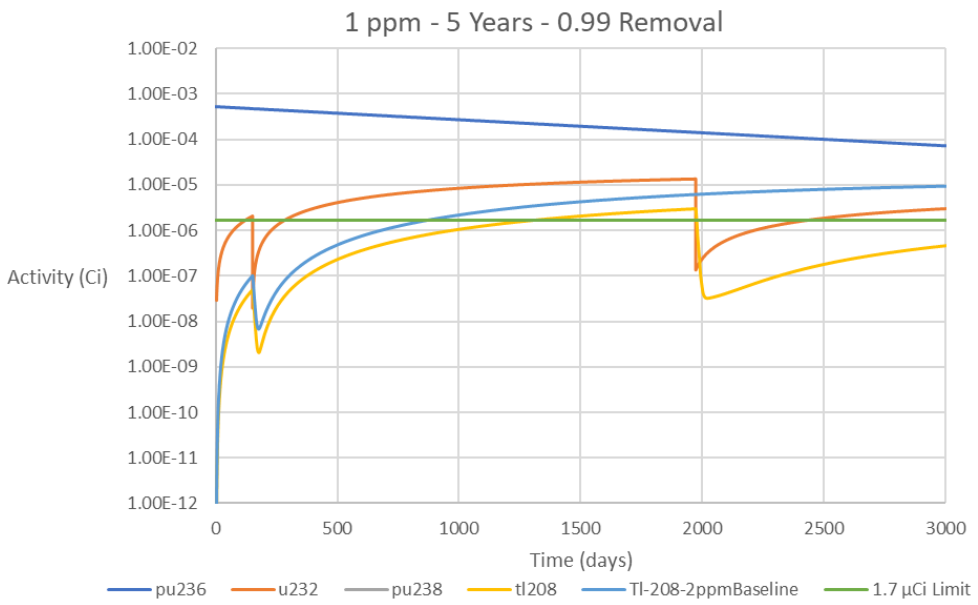

Figure 8.3. Activity vs. Time for relevant isotopes for 1 ppm ^{236}Pu for an aging time of 5 years and a removal fraction of 0.99.

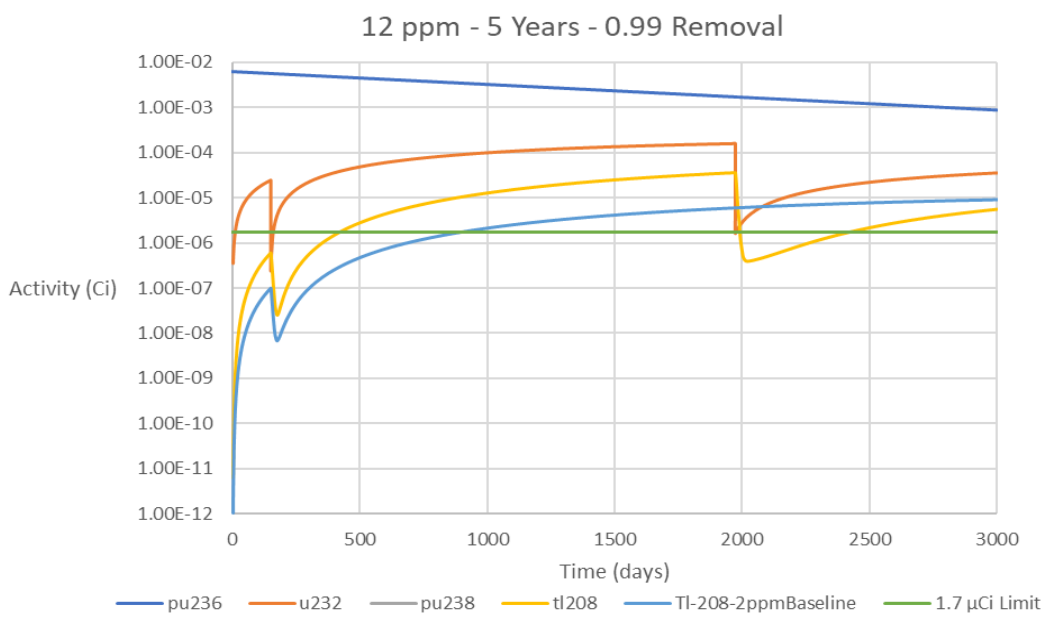

Figure 8.4. Activity vs. Time for relevant isotopes for 12 ppm ^{236}Pu for an aging time of 5 years and a removal fraction of 0.99.

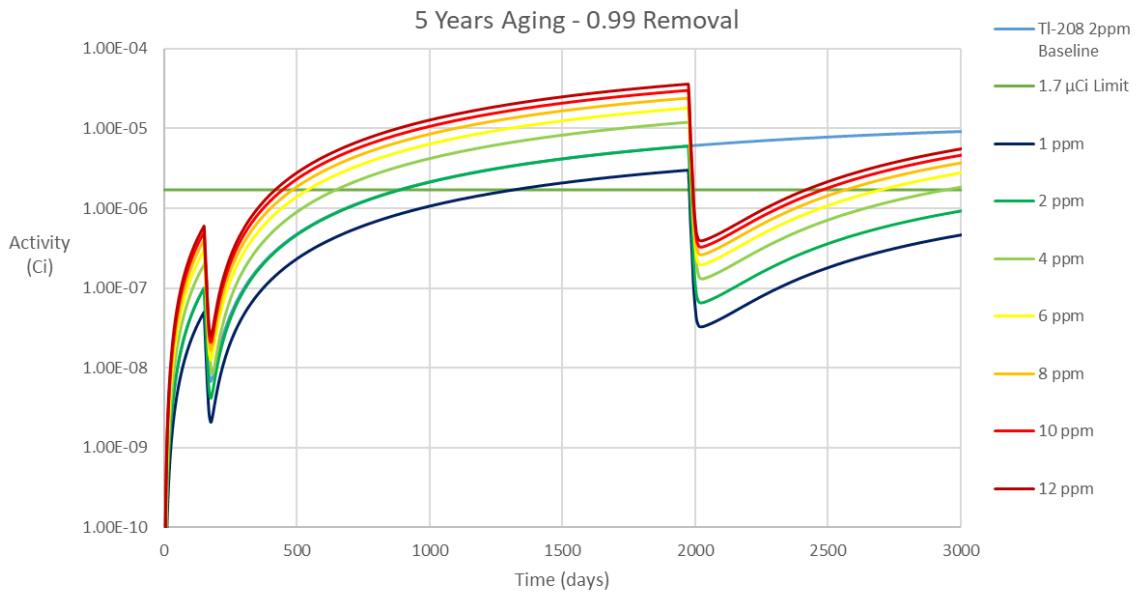

Figure 8.5. Thallium-208 Activity for each tested ^{236}Pu concentration for 5 years of decay and a removal fraction of 0.99

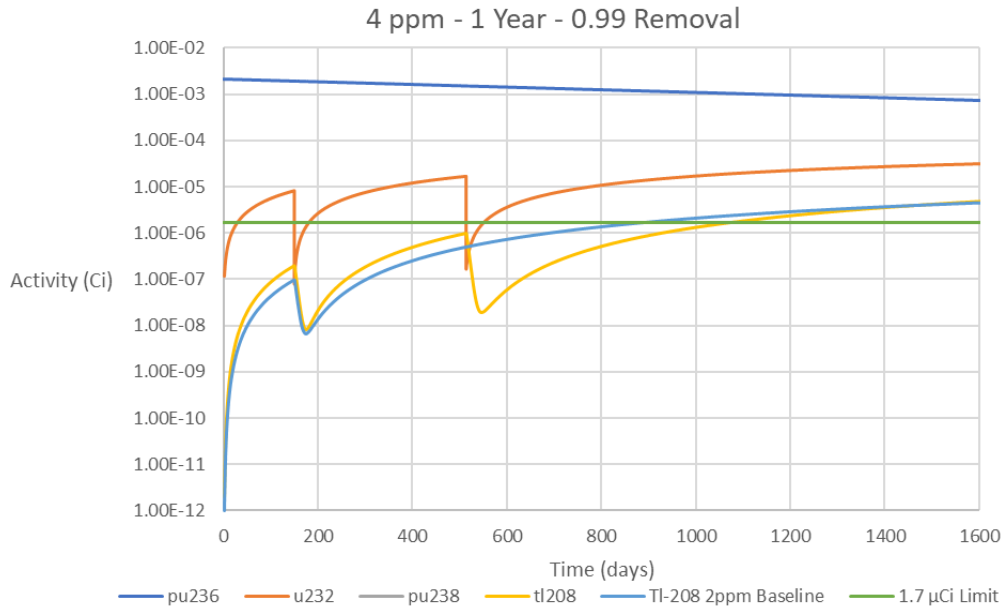

Figure 8.6. Activity vs. Time for relevant isotopes for 4 ppm ^{236}Pu for an aging time of 1 year a removal fraction of 0.99.

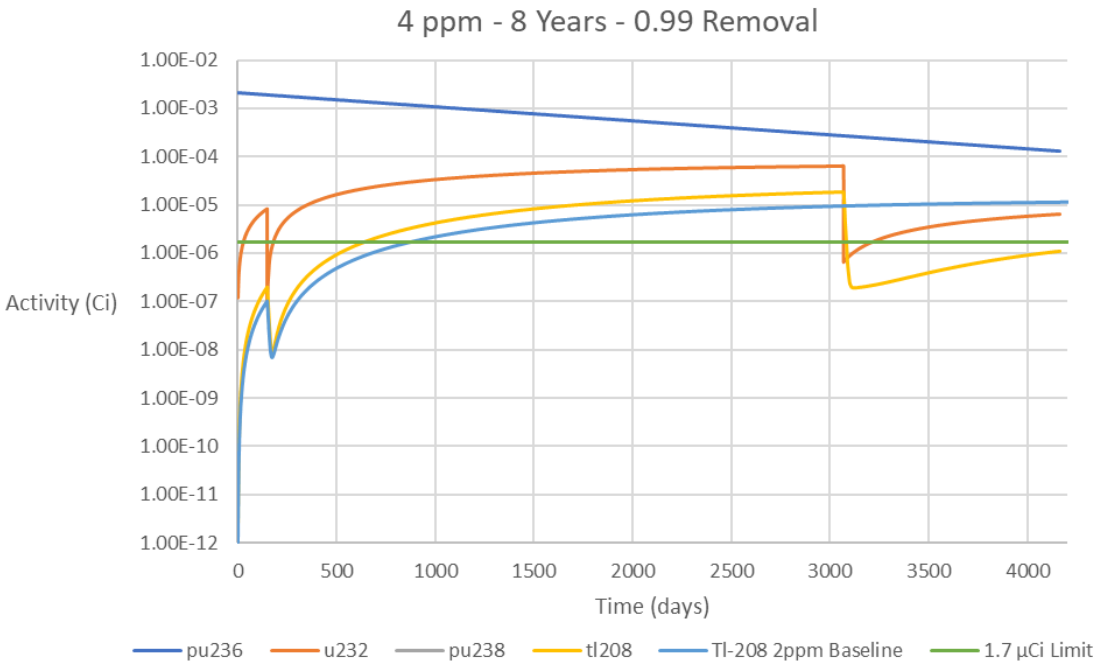

Figure 8.7. Activity vs. Time for relevant isotopes for 4 ppm ^{236}Pu for an aging time of 8 years and a removal fraction of 0.99.

8.5.3. Effects of Increased Removal of Uranium and Thorium

When the chemical processes are changed to increase the removal of ^{232}U and ^{228}Th, the result is a corresponding decrease in the ^{208}Tl activity to stay in equilibrium with the new ^{232}U activity. Removing more ^{232}U leads to a more significant decrease in the ^{208}Tl. The resulting ^{208}Tl activity must then increase more to stay in equilibrium, which requires more time. This may lead to more time below 1.7 μCi. This is observed when contrasting the 0.97 removal in Figure 8.8 and the 0.9999 removal in Figure 8.9. This is most visible when comparing the activities after the second removal.

The differences in ^{208}Tl activity when the removal fraction is changed for a given ^{236}Pu concentration and aging are apparent when the ^{208}Tl activities for each removal fraction are plotted together. Figure 8.10 contains the ^{208}Tl activity for each removal fraction for an initial ^{236}Pu concentration of 12 ppm with an aging time of five years. Note that the 0.9999 removal fraction causes the ^{208}Tl activity to stay below the 1.7 μCi limit for a longer time period. Also notice that the removal fractions had a greater effect on the second processing than the first. It may be possible to use a less effective process for the first removal while saving a more effective process for the second removal. If the lower removal fraction has less associated costs, this could result in cost savings for processing the plutonium.

8.5.4. Analysis of Parameters for ^{208}Tl Mitigation

Each of the parameters for processing the plutonium have so far been discussed individually. However, the processing regimen to be determined by this study is dependent on these parameters together. Not every ^{236}Pu combination can be allowed to age for a minimal amount of time and have the minimum ^{232}U removal process. Based on the results above, each combination of ^{236}Pu concentration, aging time, and ^{232}U removal fraction was examined to determine which combinations meet the requirement of having less than 1.7 μCi of ^{208}Tl for at least two years after processing, and are therefore most likely to be used. The results are shown in Figure 8.11, which shows the aging time versus ^{236}Pu concentration for each removal fraction.

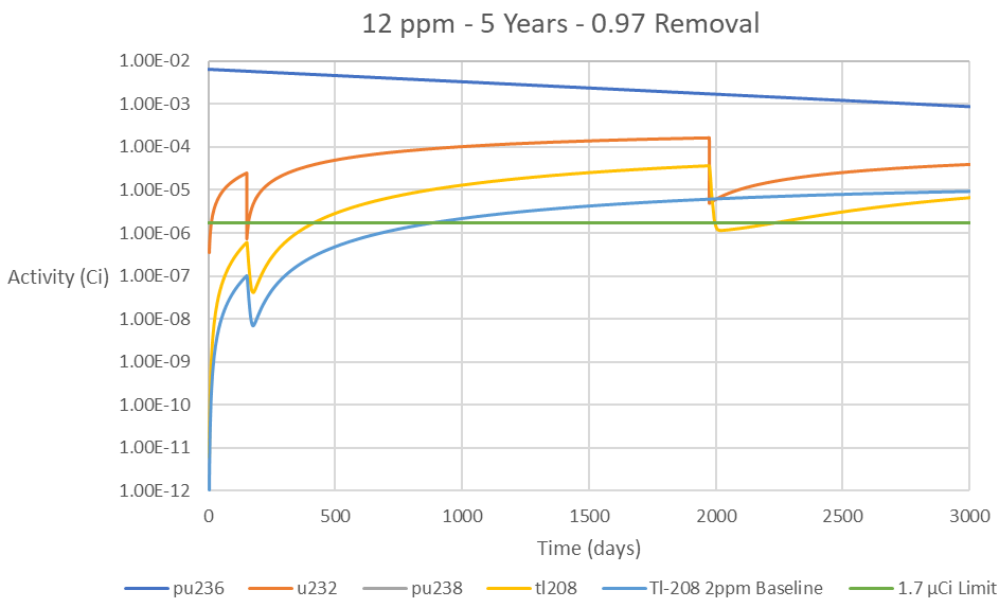

Figure 8.8. Activity vs. Time for relevant isotopes for 12 ppm ^{236}Pu for an aging time of 5 years and removal fraction of 0.97.

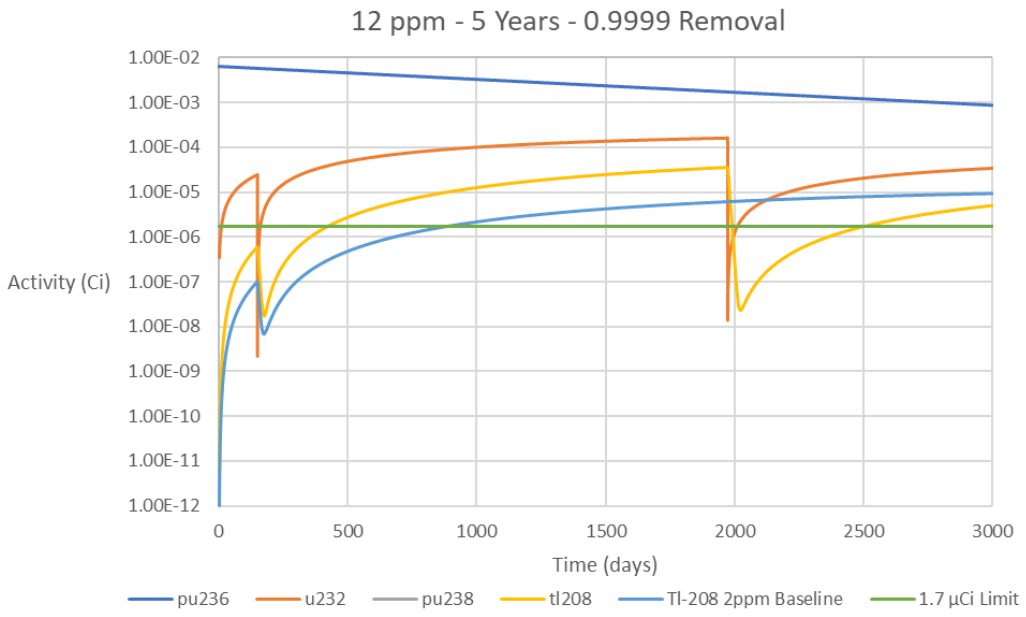

Figure 8.9. Activity vs. Time for relevant isotopes for 12 ppm ^{236}Pu for an aging time of 5 years and removal fraction of 0.9999.

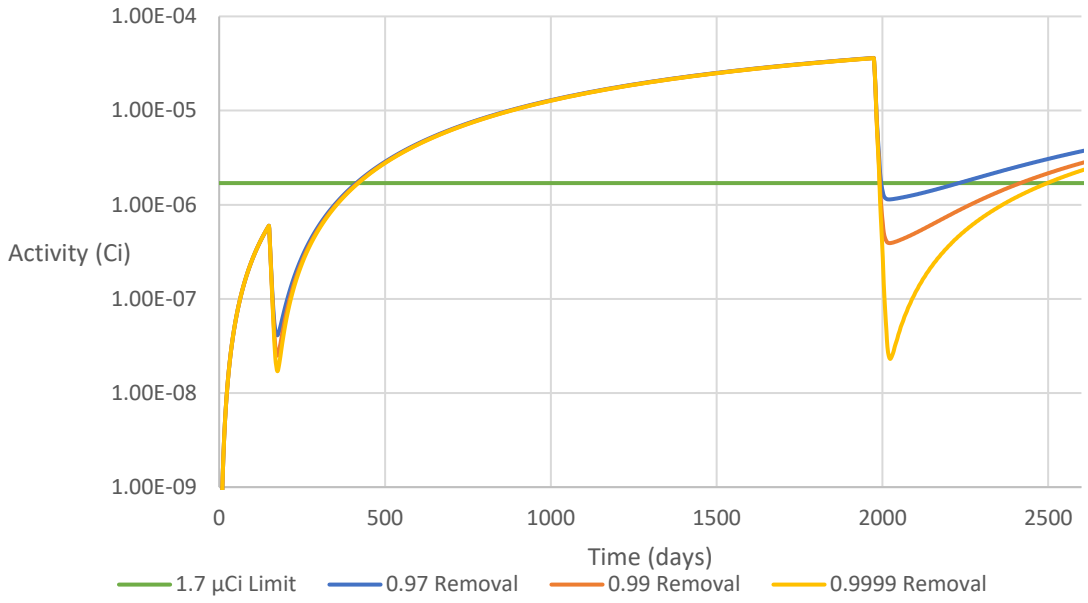

Figure 8.10. Comparison of ^{208}Tl activity from a ^{236}Pu concentration of 12 ppm with 5 years of aging for each removal fraction.

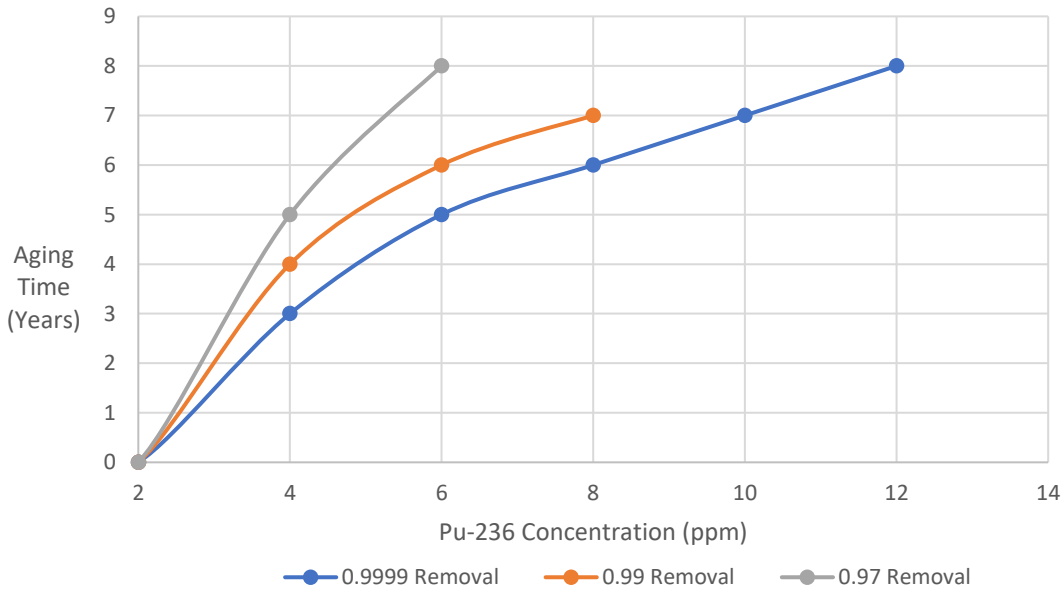

Figure 8.11. Aging time vs. ^{23}Pu concentration for each ^{232}U removal fraction.

Notice that for a given ^{236}Pu concentration, improving ^{232}U removal reduces the required material aging. It is also observed that increasing removal of ^{232}U allows for higher ^{236}Pu containing material to age for the same time as material processed with lower ^{232}U removal. For the requirements of this study, only the 0.9999 removal allowed for 10 ppm and 12 ppm ^{236}Pu material to stay below the 1.7 μCi limit on ^{208}Tl activity for two years, as this was the only removal fraction that resulted in a sufficiently low ^{208}Tl activity.

8.5.5. Analysis of ^{232}U Growth and Recovery in ^{238}Pu

The previously discussed results examined the effects of chemical processing on the ^{208}Tl concentration, but not so much on the ^{232}U removed to achieve those results. What the above results on what sets of parameters meet the 1.7 μCi limit on ^{208}Tl activity give is processing cases most likely to be used based on initial ^{236}Pu concentration. From these cases, the amount of ^{232}U extracted can be analyzed. The ^{232}U masses per gram of plutonium for the 4 ppm ^{236}Pu processes that sufficiently stayed below the ^{208}Tl limit are shown in Figure 8.12.

When analyzing these results in terms of the usability of the ^{238}Pu, all three results in Figure 8.12 meet the ^{208}Tl activity criteria. Counterintuitively, the processes that meet the ^{208}Tl activity limits are not necessarily the same processes that produce the most ^{232}U. The preferred process might be the three-year aging with 0.9999 removal, as the plutonium is ready to use earlier. However, the five-year aging time with 0.97 removal builds up more ^{232}U, making that process preferred for ^{232}U production.

Based on this, for a given ^{236}Pu concentration, material age has greater impact on ^{232}U recovered than removal fraction from the perspective of ^{232}U production. From a ^{232}U production perspective, the difference in the ^{232}U mass due to years of increased aging is more significant than the difference in the ^{232}U mass recovered by increasing removal fraction. The removal fractions are sufficiently similar that there is little difference in the ^{232}U recovered. The asymptoticly increased removal of 0.9999 is more important for limiting the ^{208}Tl activity. These observations are observed again when looking at the 6 ppm results that meet the ^{208}Tl activity criteria in Figure 8.13.

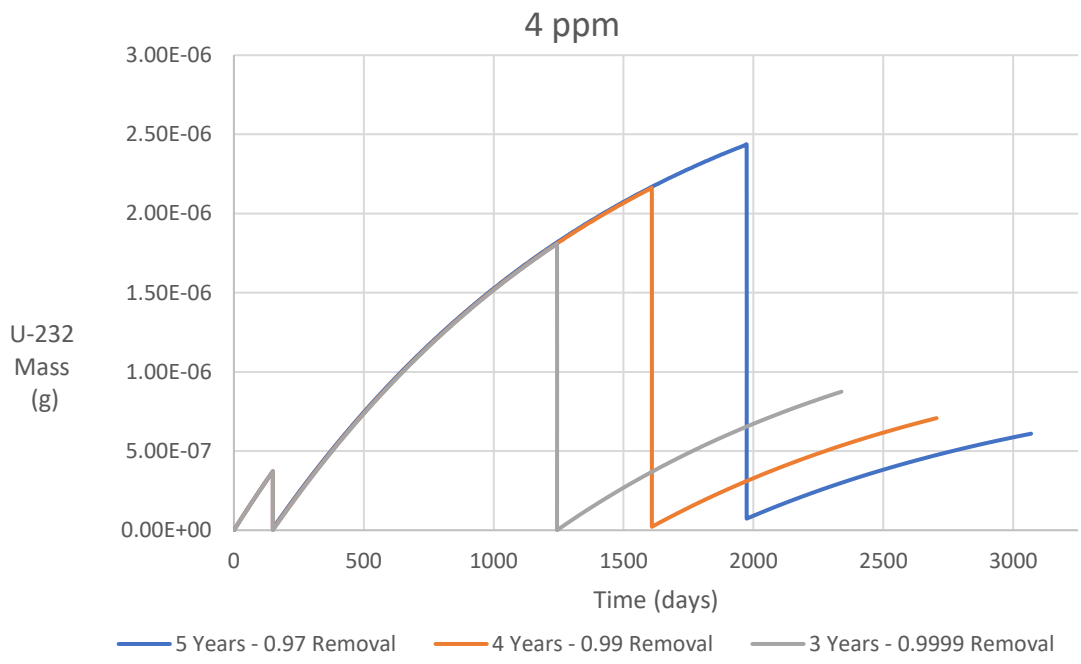

Figure 8.12. Uranium-232 Mass vs. time for 4 ppm ^{236}Pu for 5 Years – 0.97 Removal, 4 Years – 0.99 Removal, and 3 Years – 0.9999 Removal

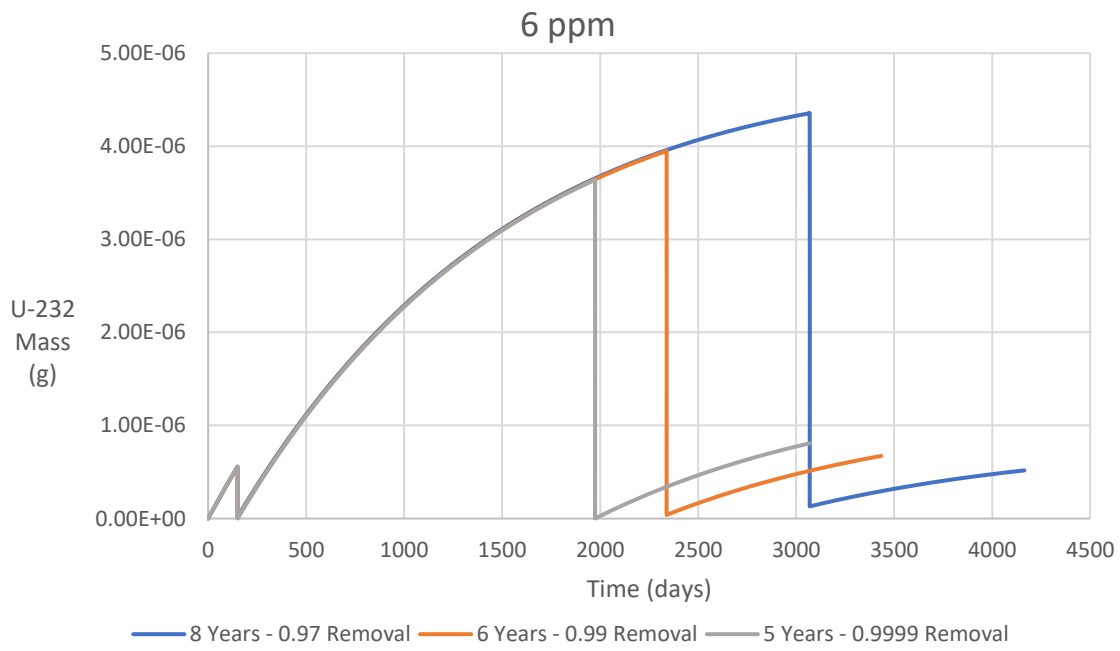

Figure 8.13. Uranium-232 Mass vs. time for 6 ppm ^{236}Pu for 8 Years – 0.97 Removal, 6 Years – 0.99 Removal, and 5 Years – 0.9999 Removal

As seen in both Figure 8.12 and Figure 8.13, all three removal fractions remove almost the entire quantity of ^{232}U, but differences between the maximum ^{232}U mass for each aging is greater than the differences in the masses recovered.

Based on the above observations, for a given ^{236}Pu concentration, the processes with the greater aging time will yield more ^{232}U. This is no surprise, but the significance of the of chemical removal fractions needed to be determined. For the processes that met the ^{208}Tl activity limit as shown in Figure 8.11, the mass of ^{232}U recovered per gram of plutonium is shown in Table 8.1

It should be noted that, as stated in 8.2.3, higher fluxes towards of the center of the ATR may result in the higher ^{236}Pu contaminations. However, as the center of the core is in higher demand, and the outer I positions have more space, it is more probable that the bulk of the plutonium produced at ATR will be from the I positions. This may result in less ^{236}Pu contamination to mitigate overall. As 2 ppm of ^{236}Pu does not require the second processing, only targets irradiated in the B positions or closer in would require the second processing. Based on the above ^{232}U masses, the expected ^{232}U mass recovered is expected to be in the range of 2-6 micrograms. Based on the 100 ppt concentration to use as additive as calculated in Chapter 4, this would be enough for one microgram per 10 kilograms, protecting 2-6 kg of uranium from a single B position target. While this is far from the 6.75 grams needed to protect the annual demand for fresh uranium, these small quantities may still have utility in protecting smaller, more critical stockpiles, or for testing purposes to verify this additive concept.

8.6. Chapter Conclusions

From the perspective of limiting ^{208}Tl contamination to ensure the usability of ^{238}Pu, both material aging and higher ^{232}U removal are significant parameters for limiting ^{208}Tl gamma emissions and minimizing dose. With the possibility of higher concentrations of ^{236}Pu if the ^{238}Pu is produced in the higher flux positions of ATR, this extra aging and chemical processing may be necessary. Increasing aging may allow for less capable chemical processing, but increasing ^{232}U removal will allow for material use with less

aging. While the need for such aging and extra processing is less than ideal, producing ^{238}Pu in higher flux positions may be required to produce all of the needed ^{238}Pu. Given the limited capacity of both HFIR and ATR, these processing procedures for mitigating ^{236}Pu contamination may be necessary to meet NASA demands.

In terms of producing ^{232}U, this is far from ideal, with quantities produced in the microgram range. However, with the potential need to mitigate against ^{236}Pu contamination, this small quantity of material may be available for testing purposes or for protecting smaller material stockpiles. Experimental testing is important to verify the detectability of the ^{232}U at 100 ppt quantities, but that is beyond the scope of this dissertation.

Table 8.1. Uranium-232 Recovered from processes that met the ^{208}Tl criteria

Pu-236 Removal Process	1st Removal (g)	2nd Removal (g)	Total U-232 Removed (g)
4ppm - 5 Years - 0.97 Removal	3.61E-07	2.36E-06	2.72E-06
4ppm - 4 Years - 0.99 Removal	3.68E-07	2.14E-06	2.51E-06
4ppm - 3 Years - 0.9999 Removal	3.72E-07	1.81E-06	2.18E-06
6ppm - 8 Years - 0.97 Removal	5.41E-07	4.22E-06	4.76E-06
6ppm - 6 Years - 0.99 Removal	5.52E-07	3.91E-06	4.46E-06
6ppm - 5 Years - 0.9999 Removal	5.58E-07	3.64E-06	4.20E-06
8ppm - 7 Years - 0.99 Removal	7.37E-07	5.51E-06	6.25E-06
8ppm - 6 Years - 0.9999 Removal	7.44E-07	5.26E-06	6.00E-06
10 ppm - 7 Years - 0.9999 Removal	9.30E-07	6.95E-06	7.88E-06
12 ppm - 8 Years - 0.9999 Removal	1.12E-06	8.68E-06	9.79E-06

CHAPTER 9.
CONCLUSIONS AND FUTURE WORK

As the results presented throughout the previous chapters show, the effects of ^{232}U concentration on dose rate indicate that the amount of ^{232}U that should be added to nuclear fuel is about 10-100 parts per trillion to minimize the increase in dose rates above baseline. Production studies indicate that ^{231}Pa is the ideal target material for neutron irradiation, producing 0.34 grams per gram of Pa. Thorium-230 is not as ideal due to its lower conversion, but is also a suitable for ^{232}U production, producing 0.15 grams of ^{232}U per gram of pure ^{230}Th. However, ^{230}Th yields are sensitive to neutron self-shielding. In a typical oxide HFIR target design, this yield decreased to 0.106 grams per gram of ^{230}Th due to self-shielding. While ^{237}Np is not suitable as a ^{232}U source, some ^{232}U may be available due to the need to mitigate against ^{236}Pu contamination. The presented cost analyses indicate that protactinium is the more cost-effective material for use as targets. Thorium, while less costly to source, is less cost effective due to requiring enrichment and the lower ^{232}U yields, but future studies could evaluate innovative target designs that may help address the self-shielding drawbacks.

For future work, experiments need to be conducted to verify the dose rate simulations with different concentrations of ^{232}U. This study also did not consider dose due to neutron emissions. Studies must also be conducted to determine that neutrons from ^{232}U do not excessively affect in-pile performance of fuel with ^{232}U additive. This could possibly be performed from any ^{232}U recovered from ^{238}Pu. Irradiation experiments also need to be performed in order to verify the production models and determine the ^{232}U production in the High Flux Isotope Reactor.

REFERENCES

[1] National Nuclear Data Center, "Interactive Chart of Nuclides," Brookhaven National Laboratory, [Online]. Available: https://www.nndc.bnl.gov/nudat2/.

[2] "ENDF/B-VIII.0: The 8th Major Release of the Nuclear Reaction Data Library with CIELO-project Cross Sections, New Standards and Thermal Scattering Data," *Nuclear Data Sheets,* vol. 148, pp. 1-142, 2018.

[3] J. Kang and F. N. von Hippel, "U-232 and the Proliferation-Resistance of U-233 in Spent Fuel," *Science and Global Security,* vol. 9, pp. 1-32, 2001.

[4] R. Moir, "U232 Nonproliferation Features," Lawrence Livermore National Laboratory, 2010.

[5] U. Gat and J. R. Engel, "Non-proliferation attributes of molten salt reactors," *Nuclear Engineering and Design,* vol. 201, pp. 327-334, 2000.

[6] C. Lloyd and B. Goddard, "Proliferation Resistant Uranium by way of U-232," in *Proceedings of ICONE-27,* Ibaraki, Japan, 2019.

[7] C. Lloyd, B. Goddard and R. Witherspoon, "The effects of U-232 on enrichment and material attractiveness over time," *Nuclear Engineering and Design,* vol. 352, 2019.

[8] C. Lloyd and B. Goddard, "Figure of Merit Analysis of Proliferation Resistant Plutonium and Uranium," in *INMM 60th Annual Meeting,* Palm Desert, 2019.

[9] V. Gusev, A. Smirnov, V. Nevinitsa and Y. Volkov, "Proliferation Resistance Analysis of LWR Fuel in Terms of IAEA Safeguards Implementation," in *AIP Conference Proceedings,* 2019.

[10] W. B. Arthur, "Uranium-232 Production in Current Design LWRs," Oak Ridge Gaseous Diffusion Plant, Oak Ridge, Tennessee, 1977.

[11] W. B. Arthur, "Uranium Production in Thorium/Denatured Uranium Fueled PWRS," Oak Ridge Gaseous Diffusion Plant, Oak Ridge, Tennessee, 1977.

[12] G. D. Rodriguez, L. G. Jodra and M. R. Gonzalez, "Study of the uranium-232 production by neutron irradiation of thorium-230 and thorium-232. Optimization of the process," *Energia Nuclear,* vol. 12, no. 22, pp. 14-21, 1981.

[13] M. Sakanoue and K. Komura, "The Preparation of Carrier-Free U-232 and the Estimation of Various Nuclides Produced by the Neutron Irradiation of Pa-231," *Journal of Nuclear Science and Technology,* vol. 3, no. 6, pp. 249-255, 1966.

[14] R. B. Firestone, "Table of Isotopes," Wiley-Interscience, Berkeley, California, 1996.

[15] H. Bateman, "The Solution of a System of Differential Equations Occuring in the Theory of Radioactive Transformations," *Proceedings of the Cambridge Philosophical Society, Mathematical and Physical Sciences,* vol. 15, pp. 423-427, 1908.

[16] B. T. Rearden and M. A. Jessee, Eds., *SCALE Code System,* Oak Ridge National Laboratory, 2018.

[17] "10 CFR Part 20, Subpart C, 20.1201 Occupatonal Dose Limits for Adults," 1991.

[18] MCNP6 Development Team, "MCNP6 User's Manual Code Version 6.2," Los Alamos National Laboratory, Los Alamos, NM, 2017.

[19] S.-d. Su, "Environmental Radiation Dose Assessment and Validation for Uranium Hexafluoride Storage Management (Ph.D. Dissertation)," University of New Mexico, Albuquerque, New Mexico, 2015.

[20] A. Meyering, "Investigations of the effective dose rate from UF6-cylinders by Monte-Carlo simulations in respect of radiation protection (Masters Thesis)," University of Muenster, Muenster, Germany, 2012.

[21] American National Standards Institute Inc, "American National Standard for Nuclear Materials — Uranium Hexafluoride – Packagings for Transport," American National Standards Institute, Inc., 2012.

[22] International Standards Organization, "Nuclear energy — Packaging of uranium hexafluoride (UF6) for transport," ISO, Geneva, Switzerland, 2005.

[23] W. B. Weihermiller and G. S. Allison, "LWR Nuclear Fuel Bundle Data for use in Fuel Bundle Handling," Pacific Northwest Laboratory, Richland, WA, 1979.

[24] ICRP, "ICRP Publication 116 Conversion Coefficients for Radiological Protection Quantities for External Radiation Exposures," The International Commission on Radiological Protection, 2010.

[25] "Uranium Markets," World Nuclear Association, June 2020. [Online]. Available: https://www.world-nuclear.org/information-library/nuclear-fuel-cycle/uranium-resources/uranium-markets.aspx.

[26] E. A. Coppinger and C. A. Rohrmann, "Ionium (Thorium-230) for Radioisotope Preparation (Status Report)," Hanford Laboratories, Hanford, WA, 1959.

[27] "High Flux Isotope Reactor (HFIR) User Guide," Oak Ridge National Laboratory, Oak Ridge, TN, 2011.

[28] J. R. Lamarsh and A. J. Baratta, Introduction to Nuclear Engineering Third Edition, Upper Saddle River, New Jersey: Prentice Hall, 2001.

[29] J. J. Duderstadt and L. J. Hamilton, Nuclear Reactor Analysis, John Wiley and & Sons, 1976.

[30] N. Xoubi and R. T. Rrimm III, "Modeling of the High Flux Isotope Reactor Cycle 400," Oak Ridge National Laboratory, Oak Ridge, Tennessee, 2005.

[31] "Britain Declassifies Protactinium Extraction," *C & E N*, pp. 48-49, 7 August 1961.

[32] D. A. Collins, J. J. Hillary, J. S. Nairn and G. M. Phillips, "The Development and Application of a Process for the Recovery of Over 100g fo Protactinium-231 from a Uranium Refinery Waste Material," *Journal of Inorganic and Nuclear Chemistry,* vol. 24, pp. 441-459, 1961.

[33] M. R. Hertz, P. E. Figgins and W. R. Deal, "The Recovery of Protactinium-231 and Thorium-230 from Cotter Concentrate: Pilot-Plant Operations and Process Development," Mound Laboratory, Miamisburg, Ohio, 1983.

[34] B. Grogan, A. Krichinsky, B. Patton and L. Sadergasky, *Personal Communications,* 2021.

[35] Oak Ridge National Laboratory, "Electromagnetic Isotope Separtations," Oak Ridge National Laboratory, Oak Ridge, Tennessee, 1963.

[36] S. M. Jerome, S. M. Collins, S. Happel, P. Ivanov and B. C. Russell, "Isolation and Purification of Protactinium-231," *Applied Radiation and Isotopes,* vol. 134, pp. 18-22, 2017.

[37] M. Solache-Rios, "Separation and Purification fo Protactinium-231," *Journal of Radioanalytical and Nuclear Chemistry,* vol. 125, no. 1, pp. 221-224, 1988.

[38] Idaho National Laboratory, Atomic Power in Space II: A History of Space Nuclear Power and Propulsion in the United States, Idaho Falls: Idaho National Laboratory, 2015.

[39] W. J. Lindsey, P. J. Roggenkamp and W. K. Woods, "Production of Plutonium-238 with Minimum Plutonium-236 Contamination," *Nuclear Technology,* vol. 13, no. 1, pp. 78-82, 1972.

[40] "ORNL-produced plutonium-238 to help power Perseverance on Mars," Oak Ridge National Laboratory, 29 July 2020. [Online]. Available: https://www.ornl.gov/news/ornl-produced-plutonium-238-help-power-perseverance-mars.

[41] Idaho National Laboratory, "Advanced Test Reactor National Scientific User Facility Users' Guide, INL/EXT-08-14709," Idaho National Laboratory, Idaho Falls, Idaho, 2009.

[42] B. Burt, L. Carpenter, E. Colvin, S. Ercanbrack, J. Freilich, R. Herner, T. Kajihara and J. Magnusson, "Optimization of Pu-238 Production in the Advanced Test Reactor," in *Nuclear and Emerging Technologies for Space*, Oak Ridge, Tennessee, 2020.

[43] B. Nath, S. A. Khot, D. Banerjee, C. Srinivas, D. S. Setty, G. Kalyanakrishnan and N. Saibaba, "Treatment fo Uranium and Thorium Bearing Nitrate Effluent," in *International Thorium Energy Conference*, Mumbai, India, 2015.

[44] J. D. Navratil and Y. Wei, "Actinide Ion Exchange Technology in the Back End of the Nuclear Fuel Cycle," *Nukleonika*, vol. 46, no. 2, pp. 75-80, 2001.

APPENDICES

Appendix A: Models and Data for ^{232}U Dosimetry

A.1. Example ORIGEN Input File: NU-100ppt.inp

```
=origen
solver{type=cram}
options{print_xs=no}
bounds{
       gamma=[348I 3.5e6 1.0e4]
      }
case(U232_Decay){
     title="Decay of U-232 for up to 10 Years"
     lib{file="end7dec"}
     time{
          t=[0.0  0.0833  0.25  1.0  3.0  10.0]
          units="years"
          start=0.0}
     flux=[6R 0]
     mat{
         iso=[U232 = 1.000000E-07
              U234 = 0.054999999994500
              U235 = 7.109999999290000
              U238 = 992.834999900716980]
         units=grams
        }
     print{
           gamma{
                 summary = yes
                 spectra = yes
                }
          }
     gamma{
           sublib = ALL
          }
     save{file="NU-100ppt.f71"
          steps=all
          time_units=years}
}
end
```

A.2. Example ORIGEN Input File: LEU5-100ppt.inp

```
=origen
solver{type=cram}
options{print_xs=no}
bounds{
       gamma=[348I 3.5e6 1.0e4]
      }
case(U232_Decay){
     title="Decay of U-232 for up to 10 Years"
     lib{file="end7dec"}
     time{
          t=[0.0  0.0833  0.25  1.0  3.0  10.0]
          units="years"
          start=0.0}
     flux=[6R 0]
     mat{
         iso=[U232 = 1.000000E-07
                 U234 = 0.449999999955000
                 U235 = 49.999999995000003
                 U238 = 949.549999905044956]
         units=grams
        }
     print{
           gamma{
                 summary = yes
                 spectra = yes
                }
          }
     gamma{
           sublib = ALL
          }
     save{file="LEU5-100ppt.f71"
          steps=all
          time_units=years}
}
end
```

A.3. Example MCNP Input File: U3O8SteelDrum-NU-100ppt-1Year.inp

```
Steel Drum (55 Gallon) Filled with U-232 doped U3O8
c
c ********* Cell Cards
*********************************************************
1   1    -1.5       -1  4  -5             imp:n=1 imp:p=1       $
U3O8 Powder Filling
2   2    -8.03      -2  3  -6  (1:-4:5)   imp:n=1 imp:p=1       $
Steel Drum Material
3   3    -0.001124  -7  (2:-3:6)          imp:n=1 imp:p=1       $
Surrounding Air
4   0                7                    imp:n=0 imp:p=0       $
Outside of the System

c ********* Surface Cards
*****************************************************
1  cz     28.6         $ Drum Inner Radius
2  cz     29.2         $ Drum Outer Radius
3  pz    -43.8         $ Drum Bottom Outer Surface
4  pz    -42.55        $ Drum Bottom Inner Surface
5  pz     42.55        $ Drum Top Inner Surface
6  pz     43.8         $ Drum Top Outer Surface
7  so    500           $ Outer Surface of System

c ********* Data Cards
*********************************************************
c
mode p
c
m1    92232    3.077467e-10                   $ Stand-in U3O8
Material, rho = 1.5 g/cm^3
      92234    1.678115e-04
      92235    2.160088e-02
      92238    2.978231e+00
       8016    8
        plib = 84p
c
m2    26000   -64.995       $ Assume Drum is composed of 304
Stainless Steel, rho = 8.03 g/cm^3
      28000   -12
      24000   -20
       6000    -0.08
      25000    -2
      15000    -0.045
      16000    -0.03
      14000    -0.75
       7000    -0.1
```

```
        plib = 84p
c
m3      6012     0.000125    $ Air, rho = 0.001124 g/cm^3
        7014     0.6869
        8016     0.301248
       18040     0.011717
        plib = 84p
c
sdef    par = p
        pos = 0 0 0
        axs = 0 0 1
        erg = d1
        wgt = 4.078427e+09         rad = d2
        ext = d3
c
c
si1     1.00E-02
        2.00E-02
        3.00E-02
        4.00E-02
        5.00E-02
        6.00E-02
        7.00E-02
        8.00E-02
        9.00E-02
        1.00E-01
        1.10E-01
        1.20E-01
        1.30E-01
        1.40E-01
        1.50E-01
        1.60E-01
        1.70E-01
        1.80E-01
        1.90E-01
        2.00E-01
        2.10E-01
        2.20E-01
        2.30E-01
        2.40E-01
        2.50E-01
        2.60E-01
        2.70E-01
        2.80E-01
        2.90E-01
        3.00E-01
        3.10E-01
        3.20E-01
        3.30E-01
```

3.40E-01
3.50E-01
3.60E-01
3.70E-01
3.80E-01
3.90E-01
4.00E-01
4.10E-01
4.20E-01
4.30E-01
4.40E-01
4.50E-01
4.60E-01
4.70E-01
4.80E-01
4.90E-01
5.00E-01
5.10E-01
5.20E-01
5.30E-01
5.40E-01
5.50E-01
5.60E-01
5.70E-01
5.80E-01
5.90E-01
6.00E-01
6.10E-01
6.20E-01
6.30E-01
6.40E-01
6.50E-01
6.60E-01
6.70E-01
6.80E-01
6.90E-01
7.00E-01
7.10E-01
7.20E-01
7.30E-01
7.40E-01
7.50E-01
7.60E-01
7.70E-01
7.80E-01
7.90E-01
8.00E-01
8.10E-01
8.20E-01

8.30E-01
8.40E-01
8.50E-01
8.60E-01
8.70E-01
8.80E-01
8.90E-01
9.00E-01
9.10E-01
9.20E-01
9.30E-01
9.40E-01
9.50E-01
9.60E-01
9.70E-01
9.80E-01
9.90E-01
1.00E+00
1.01E+00
1.02E+00
1.03E+00
1.04E+00
1.05E+00
1.06E+00
1.07E+00
1.08E+00
1.09E+00
1.10E+00
1.11E+00
1.12E+00
1.13E+00
1.14E+00
1.15E+00
1.16E+00
1.17E+00
1.18E+00
1.19E+00
1.20E+00
1.21E+00
1.22E+00
1.23E+00
1.24E+00
1.25E+00
1.26E+00
1.27E+00
1.28E+00
1.29E+00
1.30E+00
1.31E+00

1.32E+00
1.33E+00
1.34E+00
1.35E+00
1.36E+00
1.37E+00
1.38E+00
1.39E+00
1.40E+00
1.41E+00
1.42E+00
1.43E+00
1.44E+00
1.45E+00
1.46E+00
1.47E+00
1.48E+00
1.49E+00
1.50E+00
1.51E+00
1.52E+00
1.53E+00
1.54E+00
1.55E+00
1.56E+00
1.57E+00
1.58E+00
1.59E+00
1.60E+00
1.61E+00
1.62E+00
1.63E+00
1.64E+00
1.65E+00
1.66E+00
1.67E+00
1.68E+00
1.69E+00
1.70E+00
1.71E+00
1.72E+00
1.73E+00
1.74E+00
1.75E+00
1.76E+00
1.77E+00
1.78E+00
1.79E+00
1.80E+00

1.81E+00
1.82E+00
1.83E+00
1.84E+00
1.85E+00
1.86E+00
1.87E+00
1.88E+00
1.89E+00
1.90E+00
1.91E+00
1.92E+00
1.93E+00
1.94E+00
1.95E+00
1.96E+00
1.97E+00
1.98E+00
1.99E+00
2.00E+00
2.01E+00
2.02E+00
2.03E+00
2.04E+00
2.05E+00
2.06E+00
2.07E+00
2.08E+00
2.09E+00
2.10E+00
2.11E+00
2.12E+00
2.13E+00
2.14E+00
2.15E+00
2.16E+00
2.17E+00
2.18E+00
2.19E+00
2.20E+00
2.21E+00
2.22E+00
2.23E+00
2.24E+00
2.25E+00
2.26E+00
2.27E+00
2.28E+00
2.29E+00

2.30E+00
2.31E+00
2.32E+00
2.33E+00
2.34E+00
2.35E+00
2.36E+00
2.37E+00
2.38E+00
2.39E+00
2.40E+00
2.41E+00
2.42E+00
2.43E+00
2.44E+00
2.45E+00
2.46E+00
2.47E+00
2.48E+00
2.49E+00
2.50E+00
2.51E+00
2.52E+00
2.53E+00
2.54E+00
2.55E+00
2.56E+00
2.57E+00
2.58E+00
2.59E+00
2.60E+00
2.61E+00
2.62E+00
2.63E+00
2.64E+00
2.65E+00
2.66E+00
2.67E+00
2.68E+00
2.69E+00
2.70E+00
2.71E+00
2.72E+00
2.73E+00
2.74E+00
2.75E+00
2.76E+00
2.77E+00
2.78E+00

2.79E+00
2.80E+00
2.81E+00
2.82E+00
2.83E+00
2.84E+00
2.85E+00
2.86E+00
2.87E+00
2.88E+00
2.89E+00
2.90E+00
2.91E+00
2.92E+00
2.93E+00
2.94E+00
2.95E+00
2.96E+00
2.97E+00
2.98E+00
2.99E+00
3.00E+00
3.01E+00
3.02E+00
3.03E+00
3.04E+00
3.05E+00
3.06E+00
3.07E+00
3.08E+00
3.09E+00
3.10E+00
3.11E+00
3.12E+00
3.13E+00
3.14E+00
3.15E+00
3.16E+00
3.17E+00
3.18E+00
3.19E+00
3.20E+00
3.21E+00
3.22E+00
3.23E+00
3.24E+00
3.25E+00
3.26E+00
3.27E+00

```
        3.28E+00
        3.29E+00
        3.30E+00
        3.31E+00
        3.32E+00
        3.33E+00
        3.34E+00
        3.35E+00
        3.36E+00
        3.37E+00
        3.38E+00
        3.39E+00
        3.40E+00
        3.41E+00
        3.42E+00
        3.43E+00
        3.44E+00
        3.45E+00
        3.46E+00
        3.47E+00
        3.48E+00
        3.49E+00
        3.50E+00
c
sp1     0.000000
        4.372391e-01
        9.039012e-02
        5.239599e-02
        4.214773e-02
        2.430910e-02
        5.813600e-02
        2.206520e-02
        2.145751e-02
        5.492975e-02
        1.110899e-02
        1.115946e-02
        9.980903e-03
        9.886100e-03
        1.170441e-02
        7.447824e-03
        7.809985e-03
        5.795117e-03
        2.710817e-02
        4.946460e-03
        4.969786e-03
        2.587096e-03
        2.742600e-03
        3.308757e-03
        2.720093e-03
```

3.202360e-03
2.698199e-03
2.775406e-03
2.705975e-03
2.757605e-03
2.750921e-03
2.700655e-03
1.708771e-03
1.726708e-03
1.724049e-03
1.720638e-03
1.746283e-03
1.723162e-03
1.172077e-03
1.145956e-03
1.149025e-03
1.146160e-03
1.151139e-03
1.145819e-03
8.003683e-04
8.708225e-04
8.213750e-04
8.263538e-04
8.028918e-04
7.990042e-04
5.073319e-04
6.160142e-04
4.750716e-04
4.602851e-04
4.926818e-04
4.609671e-04
6.370277e-04
4.656663e-04
9.769472e-04
4.624949e-04
3.872528e-04
3.856091e-04
3.931183e-04
3.814691e-04
3.896262e-04
4.047470e-04
4.163893e-04
3.890806e-04
3.880712e-04
5.832424e-04
3.802346e-04
2.369049e-04
3.495635e-04
3.655709e-04

1.258355e-03
2.546856e-04
2.924431e-03
2.352544e-04
8.095758e-04
2.799482e-04
2.657073e-04
1.888214e-04
2.348520e-04
2.057427e-04
1.636202e-04
2.078025e-04
2.371095e-04
1.836721e-04
4.885282e-04
1.999045e-04
9.962488e-05
9.661029e-05
4.465489e-04
1.050402e-04
4.099441e-04
1.069431e-04
1.014800e-04
9.652162e-05
1.914132e-04
1.438821e-04
7.149775e-03
6.139544e-05
7.087710e-05
6.151003e-05
7.231619e-05
8.133270e-05
7.939572e-05
7.221389e-05
8.306507e-05
6.362638e-05
4.025986e-05
3.997408e-05
9.452326e-05
3.911745e-05
3.911745e-05
4.018824e-05
3.918360e-05
5.728959e-05
3.934866e-05
1.537989e-04
2.480767e-05
2.780657e-05
2.480767e-05

6.909699e-05
2.824922e-05
2.584027e-05
2.478311e-05
2.539694e-05
2.509753e-05
3.120993e-05
1.543514e-05
1.543514e-05
1.543514e-05
1.543514e-05
1.560633e-05
3.543036e-05
1.543514e-05
1.543514e-05
1.647729e-05
7.427363e-05
1.241168e-05
2.845314e-05
1.165462e-05
9.130405e-05
1.422521e-05
3.738712e-05
9.369117e-06
9.483699e-06
9.969308e-06
1.145410e-05
1.328877e-05
1.212727e-04
2.243146e-05
5.492498e-06
1.506070e-05
8.161915e-05
5.649570e-06
1.563497e-05
7.492157e-06
2.572432e-05
7.039967e-06
3.199222e-06
2.881462e-05
5.927159e-06
3.368435e-06
3.106397e-06
2.335016e-05
5.569636e-06
7.355068e-06
2.018074e-05
3.041604e-06
1.856227e-06

2.099032e-06
1.819602e-04
3.182308e-06
1.603942e-06
7.558996e-05
3.460647e-06
1.946733e-06
8.432683e-06
3.382008e-05
8.397217e-06
8.980357e-07
1.480562e-04
7.695403e-07
7.695403e-07
8.893739e-05
7.014732e-05
9.837676e-07
2.022985e-05
3.268108e-07
5.311758e-05
8.296276e-06
1.854658e-05
3.268108e-07
4.639203e-07
3.799754e-06
5.924635e-07
4.267903e-07
3.268108e-07
7.659937e-08
7.659937e-08
7.659937e-08
7.659937e-08
7.659937e-08
7.659937e-08
7.659937e-08
1.337266e-07
7.659937e-08
7.659937e-08
7.659937e-08
7.661983e-08
7.659937e-08
7.659937e-08
7.659937e-08
7.659937e-08
7.659937e-08
7.659937e-08
7.659937e-08
7.659937e-08
7.668122e-08

7.659937e-08
7.659937e-08
7.659937e-08
7.659937e-08
7.293002e-08
7.293002e-08
7.293002e-08
7.293002e-08
7.293684e-08
7.293002e-08
7.293002e-08
7.293002e-08
7.293002e-08
7.293002e-08
7.293002e-08
7.293002e-08
7.293002e-08
7.293002e-08
7.293002e-08
5.151344e-09
5.151344e-09
5.151480e-09
5.151344e-09
5.177329e-09
5.151344e-09
5.151344e-09
5.151412e-09
5.151412e-09
5.151344e-09
5.151412e-09
5.151344e-09
5.151344e-09
5.151344e-09
5.151344e-09
5.151344e-09
5.151344e-09
5.151344e-09
5.151344e-09
5.151344e-09
5.151344e-09
6.036693e-04
5.151344e-09
5.151344e-09
5.151344e-09
5.151344e-09
5.151344e-09
5.151344e-09
5.151344e-09
5.151344e-09
5.151889e-09

5.151344e-09
5.151412e-09
5.151344e-09
5.151344e-09
5.151344e-09
3.025167e-09
3.025576e-09
3.025167e-09
3.025235e-09
3.025167e-09
2.930842e-09
2.930842e-09
2.930910e-09
2.930842e-09
2.930842e-09
2.930842e-09
2.930842e-09
2.930842e-09
2.931046e-09
2.930978e-09
2.930842e-09
2.930842e-09
2.931114e-09
2.930842e-09
2.930842e-09
2.930842e-09
2.930842e-09
2.931114e-09
2.930842e-09
2.930978e-09
2.930842e-09
2.930842e-09
2.930842e-09
2.930842e-09
2.930842e-09
2.931183e-09
2.930842e-09
2.930842e-09
2.930910e-09
2.930842e-09
2.930842e-09
2.930842e-09
2.930842e-09
2.930842e-09
2.930842e-09
2.930842e-09
2.930842e-09
2.930842e-09
2.930842e-09

```
       2.411131e-08
       2.930842e-09
       2.930842e-09
       2.930842e-09
       2.930842e-09
       2.930842e-09
       1.698881e-09
       1.698881e-09
       1.698881e-09
       1.698881e-09
       1.698881e-09
       1.698881e-09
       1.698881e-09
       1.698881e-09
       1.698881e-09
       1.698881e-09
       1.698881e-09
       1.698881e-09
       1.698881e-09
       1.698881e-09
       1.698881e-09
       1.698881e-09
       1.698881e-09
       1.698881e-09
       1.698881e-09
       1.698881e-09
       1.698881e-09
       1.698881e-09
       1.698881e-09
       1.077616e-08
       1.698881e-09
       1.698881e-09
c
c
si2   0  28.6
sp2   -21 1
si3   -42.55  42.55
sp3   0  1
c
c
nps    1E9
c
c
c
c  Detector Tallies. Combined with Source weight, give units of
p/(cm^2*s).
c  Radial Point Detectors at Midplane Surface of Drum, Exclusion
Sphere of 0.5 cm radius
f5:p    0  29.7 0  0.5      $ Surface of drum
        0  39.7 0  0.5      $ 10cm. from drum
```

```
        0  49.7 0  0.5      $ 20cm. from drum
        0  59.7 0  0.5      $ 1 ft. from drum
        0  89.7 0  0.5      $ 2 ft. from drum
        0 119.7 0  0.5      $ 3 ft. from drum
c
c  Ring Detector at Midplane Surface of Drum, Exclusion Sphere of
0.5 cm radius
f15z:p  0   29.7    0.5      $ Surface of drum
        0   39.7    0.5      $ 10cm. from drum
        0   49.7    0.5      $ 20cm. from drum
        0   59.7    0.5      $ 1 ft. from drum
        0   89.7    0.5      $ 2 ft. from drum
        0  119.7    0.5      $ 3 ft. from drum
c
c Axial Point Detectors from Top of Drum , Exclusion Sphere of
0.5 cm radius
f25:p   0  0  44.3  0.5     $ Surface of drum
        0  0  54.3  0.5     $ 10cm. from drum
        0  0  64.3  0.5     $ 20cm. from drum
        0  0  74.3  0.5     $ 1 ft. from drum
        0  0 104.3  0.5     $ 2 ft. from drum
        0  0 134.3  0.5     $ 3 ft. from drum
c
c
c     Photon Dose Tables for from ICRP-116 (pSv)/(p/(cm^2))
c     Converts final tally result to pSv/s
DE0   0.01
      0.015
      0.02
      0.03
      0.04
      0.05
      0.06
      0.07
      0.08
      0.1
      0.15
      0.2
      0.3
      0.4
      0.5
      0.511
      0.6
      0.662
      0.8
      1
      1.117
      1.33
      1.5
```

```
        2
        3
        4
        5
        6
        6.129
        8
        10
        15
        20
        30
        40
        50
        60
        80
        100
        150
        200
        300
        400
        500
        600
        800
        1000
        1500
        2000
        3000
        4000
        5000
        6000
        8000
        10000
C
DF0     0.0337
        0.0664
        0.0986
        0.158
        0.199
        0.226
        0.248
        0.273
        0.297
        0.355
        0.528
        0.721
        1.12
        1.52
        1.92
        1.96
```

2.3
2.54
3.04
3.72
4.1
4.75
5.24
6.55
8.84
10.8
12.7
14.4
14.6
17.6
20.6
27.7
34.4
46.1
56
64.4
71.2
82
89.7
102
111
121
128
133
136
142
145
152
156
161
165
168
170
172
175

c

A.4. Tabular Results for Each Dosimetry Model

Table A.1. Radial Dose Rate (rem/hour) at 30 cm vs ^{232}U Concentration for a 55-gallon Drum of U_3O_8

U-232 Concentration	0 Years	1 Month	3 Months	1 Year	3 Years	10 Years
zero	5.13E-06	0.000385	0.00061	0.000657	0.000657	0.000657
ppq	5.13E-06	0.000385	0.00061	0.000657	0.000657	0.000657
3ppq	5.13E-06	0.000385	0.00061	0.000657	0.000657	0.000657
10ppq	5.13E-06	0.000385	0.00061	0.000657	0.000657	0.000657
30ppq	5.13E-06	0.000385	0.00061	0.000657	0.000657	0.000657
100ppq	5.13E-06	0.000385	0.00061	0.000657	0.000657	0.000657
300ppq	5.13E-06	0.000385	0.00061	0.000657	0.000657	0.000658
ppt	5.13E-06	0.000385	0.00061	0.000658	0.000658	0.000659
3ppt	5.13E-06	0.000385	0.00061	0.000659	0.000661	0.000663
10ppt	5.13E-06	0.000385	0.000612	0.000664	0.000671	0.000677
30ppt	5.13E-06	0.000387	0.000615	0.000677	0.0007	0.000717
100ppt	5.13E-06	0.00039	0.000628	0.000723	0.000801	0.000858
300ppt	5.13E-06	0.000401	0.000664	0.000856	0.001091	0.001259
ppb	5.13E-06	0.000438	0.00079	0.00132	0.002101	0.002664
3ppb	5.14E-06	0.000545	0.001151	0.002648	0.004987	0.006678
10ppb	5.18E-06	0.000918	0.002413	0.00729	0.01508	0.020703
30ppb	5.28E-06	0.001985	0.00602	0.020535	0.043938	0.06082
100ppb	5.62E-06	0.00571	0.01862	0.066947	0.14493	0.201194
300ppb	6.64E-06	0.016354	0.054668	0.199522	0.433451	0.602262
ppm	1.02E-05	0.053634	0.180788	0.663523	1.443337	2.005913
3ppm	2.03E-05	0.160129	0.541134	1.98922	4.328784	6.016608
10ppm	5.57E-05	0.532876	1.802308	6.629364	14.42848	20.05409
30ppm	0.000157	1.597748	5.40576	19.88665	43.28352	60.16032
100ppm	0.00051	5.325012	18.01793	66.28644	144.2689	200.5358
300ppm	0.001521	15.97424	54.05292	198.86	432.8244	601.5888
ppth	0.005059	53.24508	180.1681	662.85	1442.657	2005.2

Table A.2. Radial Dose Rate (rem/hour) at 30 cm vs ^{232}U Concentration for a UF_6 30B Cylinder with Natural Uranium

U-232 Concentration	0 Years	1 Month	3 Months	1 Year	3 Years	10 Years
zero	2.58E-06	0.000325	0.000517	0.000557	0.000557	0.000557
ppq	2.58E-06	0.000325	0.000517	0.000557	0.000557	0.000557
3ppq	2.58E-06	0.000325	0.000517	0.000557	0.000557	0.000557
10ppq	2.58E-06	0.000325	0.000517	0.000557	0.000557	0.000557
30ppq	2.58E-06	0.000325	0.000517	0.000557	0.000557	0.000557
100ppq	2.58E-06	0.000325	0.000517	0.000557	0.000557	0.000557
300ppq	2.58E-06	0.000325	0.000517	0.000557	0.000557	0.000557
ppt	2.58E-06	0.000325	0.000517	0.000557	0.000558	0.000559
3ppt	2.58E-06	0.000325	0.000517	0.000559	0.000561	0.000563
10ppt	2.58E-06	0.000326	0.000519	0.000564	0.000571	0.000576
30ppt	2.58E-06	0.000327	0.000522	0.000576	0.0006	0.000617
100ppt	2.58E-06	0.000331	0.000534	0.000622	0.000701	0.000759
300ppt	2.59E-06	0.000342	0.000571	0.000757	0.001	0.001164
ppb	2.59E-06	0.000379	0.000698	0.001226	0.002027	0.002601
3ppb	2.59E-06	0.000486	0.001062	0.002583	0.004944	0.006642
10ppb	2.62E-06	0.000863	0.002354	0.00728	0.01518	0.020878
30ppb	2.67E-06	0.001943	0.005987	0.020706	0.044312	0.061413
100ppb	2.87E-06	0.005726	0.018768	0.067615	0.146551	0.203502
300ppb	3.44E-06	0.016479	0.055173	0.201811	0.438574	0.609289
ppm	5.51E-06	0.05422	0.182856	0.671468	1.459901	2.028827
3ppm	1.13E-05	0.161951	0.547556	2.011792	4.377852	6.084756
10ppm	3.16E-05	0.539219	1.822752	6.704496	14.59109	20.2801
30ppm	8.94E-05	1.615957	5.466996	20.11194	43.77456	60.84108
100ppm	0.000292	5.385672	18.22039	67.03632	145.8994	202.8118
300ppm	0.000871	16.15745	54.66348	201.114	437.7204	608.3892
ppth	0.002898	53.85168	182.2097	670.3452	1459.019	2027.963

Table A.3. Radial Dose Rate (rem/hour) at 30 cm vs ^{232}U Concentration for a UF_6 30B Cylinder with 5 percent Enriched Uranium

U-232 Concentration	0 Years	1 Month	3 Months	1 Year	3 Years	10 Years
zero	1.71E-05	0.000325	0.000508	0.000546	0.000546	0.000546
ppq	1.71E-05	0.000325	0.000508	0.000546	0.000546	0.000546
3ppq	1.71E-05	0.000325	0.000508	0.000546	0.000546	0.000546
10ppq	1.71E-05	0.000325	0.000508	0.000546	0.000546	0.000546
30ppq	1.71E-05	0.000325	0.000508	0.000546	0.000546	0.000546
100ppq	1.71E-05	0.000325	0.000508	0.000546	0.000546	0.000546
300ppq	1.71E-05	0.000325	0.000508	0.000546	0.000546	0.000547
ppt	1.71E-05	0.000325	0.000508	0.000547	0.000547	0.000548
3ppt	1.71E-05	0.000326	0.000508	0.000548	0.00055	0.000552
10ppt	1.71E-05	0.000326	0.00051	0.000553	0.000561	0.000566
30ppt	1.71E-05	0.000327	0.000513	0.000566	0.000589	0.000607
100ppt	1.71E-05	0.000331	0.000526	0.000613	0.00069	0.000748
300ppt	1.71E-05	0.000341	0.000562	0.000746	0.00099	0.001155
ppb	1.71E-05	0.000379	0.000689	0.001216	0.002015	0.00259
3ppb	1.71E-05	0.000486	0.001054	0.002573	0.004933	0.006633
10ppb	1.72E-05	0.000863	0.002342	0.00725	0.015161	0.02086
30ppb	1.72E-05	0.001951	0.005978	0.020687	0.044285	0.061368
100ppb	1.74E-05	0.005724	0.018761	0.067547	0.146535	0.203391
300ppb	1.8E-05	0.016508	0.055142	0.20174	0.438264	0.60903
ppm	2E-05	0.054162	0.182777	0.671011	1.459487	2.028416
3ppm	2.58E-05	0.161978	0.547214	2.011342	4.378248	6.084396
10ppm	4.66E-05	0.538772	1.8225	6.70464	14.5922	20.28053
30ppm	0.000104	1.615759	5.467356	20.11172	43.7724	60.84468
100ppm	0.000307	5.385708	18.22104	67.0374	145.913	202.801
300ppm	0.000885	16.15594	54.66132	201.1046	437.7024	608.4144
ppth	0.002909	53.84808	182.1942	670.3524	1459.001	2028.049

Table A.4. Radial Dose Rate (rem/hour) at 30 cm vs ^{232}U Concentration for a UF_6 48Y Cylinder with Natural Uranium

U-232 Concentration	0 Years	1 Month	3 Months	1 Year	3 Years	10 Years
zero	2.45E-06	0.000367	0.000583	0.000628	0.000628	0.000628
ppq	2.45E-06	0.000367	0.000583	0.000628	0.000628	0.000628
3ppq	2.45E-06	0.000367	0.000583	0.000628	0.000628	0.000628
10ppq	2.45E-06	0.000367	0.000583	0.000628	0.000628	0.000628
30ppq	2.45E-06	0.000367	0.000583	0.000628	0.000628	0.000628
100ppq	2.45E-06	0.000367	0.000583	0.000628	0.000628	0.000628
300ppq	2.45E-06	0.000367	0.000583	0.000628	0.000629	0.000629
ppt	2.45E-06	0.000367	0.000583	0.000629	0.00063	0.000631
3ppt	2.45E-06	0.000367	0.000583	0.00063	0.000633	0.000635
10ppt	2.45E-06	0.000368	0.000585	0.000636	0.000646	0.000652
30ppt	2.45E-06	0.000369	0.000589	0.000652	0.00068	0.0007
100ppt	2.45E-06	0.000374	0.000605	0.000707	0.000801	0.000869
300ppt	2.45E-06	0.000386	0.000647	0.000867	0.001149	0.001345
ppb	2.45E-06	0.000431	0.000798	0.001424	0.002364	0.003054
3ppb	2.46E-06	0.00056	0.001227	0.003033	0.005875	0.007908
10ppb	2.47E-06	0.001008	0.002763	0.008664	0.018087	0.024885
30ppb	2.53E-06	0.002306	0.007127	0.024682	0.053007	0.073431
100ppb	2.73E-06	0.00681	0.02238	0.08086	0.175248	0.243236
300ppb	3.25E-06	0.019688	0.065992	0.241216	0.524138	0.728237
ppm	5.22E-06	0.064818	0.218578	0.802303	1.745428	2.427509
3ppm	1.08E-05	0.193576	0.654214	2.40736	5.23476	7.278804
10ppm	3E-05	0.644314	2.179588	8.015832	17.44657	24.24956
30ppm	8.55E-05	1.93225	6.536736	24.04717	52.33896	72.74592
100ppm	0.000279	6.440148	21.78785	80.15616	174.4517	242.4902
300ppm	0.000833	19.31861	65.35764	240.4598	523.3644	727.4232
ppth	0.002769	64.39932	217.8871	801.6768	1744.754	2425.1

Table A.5. Side Dose Rate (rem/hour) at 30 cm vs ^{232}U Concentration for a UO_2 17x17 PWR Fuel Assembly with 5 percent Enriched Uranium

U-232 Concentration	0 Years	1 Month	3 Months	1 Year	3 Years	10 Years
zero	5.2E-05	0.000427	0.000649	0.000696	0.000696	0.000696
ppq	5.2E-05	0.000427	0.000649	0.000696	0.000696	0.000696
3ppq	5.2E-05	0.000427	0.000649	0.000696	0.000696	0.000696
10ppq	5.2E-05	0.000427	0.000649	0.000696	0.000696	0.000696
30ppq	5.2E-05	0.000427	0.000649	0.000696	0.000696	0.000696
100ppq	5.2E-05	0.000427	0.000649	0.000696	0.000696	0.000696
300ppq	5.2E-05	0.000427	0.000649	0.000696	0.000697	0.000697
ppt	5.2E-05	0.000427	0.00065	0.000697	0.000698	0.000698
3ppt	5.2E-05	0.000427	0.00065	0.000698	0.0007	0.000702
10ppt	5.2E-05	0.000427	0.000651	0.000702	0.00071	0.000715
30ppt	5.2E-05	0.000429	0.000655	0.000715	0.000738	0.000754
100ppt	5.2E-05	0.000432	0.000667	0.000759	0.000835	0.000889
300ppt	5.2E-05	0.000442	0.000701	0.000887	0.001113	0.001275
ppb	5.2E-05	0.000479	0.000823	0.001334	0.002088	0.002631
3ppb	5.2E-05	0.000582	0.001169	0.002616	0.004864	0.006482
10ppb	5.21E-05	0.000941	0.002389	0.007073	0.014547	0.01994
30ppb	5.22E-05	0.001967	0.005848	0.019777	0.042299	0.058524
100ppb	5.27E-05	0.005545	0.017936	0.064419	0.139318	0.19336
300ppb	5.43E-05	0.015763	0.052593	0.191764	0.416361	0.578581
ppm	5.99E-05	0.051616	0.173753	0.637468	1.386577	1.926993
3ppm	7.6E-05	0.153863	0.519857	1.910817	4.158304	5.780067
10ppm	0.000133	0.511885	1.73142	6.369087	13.85968	19.26594
30ppm	0.000293	1.534963	5.193024	19.10589	41.58247	57.7962
100ppm	0.000854	5.116108	17.31049	63.68469	138.6025	192.6508
300ppm	0.002455	15.3462	51.93081	191.0485	415.7914	577.9487
ppth	0.008057	51.153	173.0773	636.769	1385.902	1926.385

Appendix B: Example ORIGEN Models for Chapter 5 HFIR HT and VXF

B.1. Example of ^{231}Pa irradiation, using HT neutron spectrum:

Pa231-HFIR-HT-24Days-6Cycles.inp

```
=couple
*****************************************************************
***************
*                 cross sections from 238-group JEFF-3.0/A
*

0$$ a3 80 a6 33 e
1$$ a18 238 e t
9**
7.20E+08
5.71E+09
1.28E+10
1.86E+10
3.76E+10
5.72E+11
1.87E+12
6.49E+12
2.04E+13
1.21E+13
5.77E+13
4.68E+13
1.70E+13
6.62E+13
5.97E+13
1.98E+13
9.60E+12
8.06E+12
1.43E+13
1.17E+13
2.29E+13
2.21E+13
2.16E+13
5.81E+12
6.71E+12
4.01E+12
1.24E+13
2.40E+13
3.00E+13
3.65E+12
```

2.74E+13
1.09E+13
9.08E+12
2.16E+13
1.28E+13
1.11E+13
6.68E+12
8.59E+12
3.68E+13
3.39E+13
4.47E+13
3.56E+13
2.17E+13
2.92E+13
1.08E+13
3.04E+12
1.21E+13
3.83E+12
2.17E+13
1.34E+13
3.55E+12
9.02E+12
3.08E+13
1.87E+13
3.15E+13
2.10E+13
2.43E+13
1.28E+13
2.22E+13
3.22E+13
3.03E+12
1.68E+13
1.15E+13
8.77E+12
3.12E+12
1.54E+13
1.12E+13
2.40E+12
2.02E+13
1.45E+13
2.53E+13
1.47E+12
1.50E+13
4.49E+13
5.25E+12
1.31E+13
1.03E+13
9.31E+11
5.80E+12

2.68E+12
3.26E+13
1.86E+12
2.68E+12
4.88E+12
6.00E+12
8.16E+12
7.19E+12
1.97E+12
3.90E+12
4.15E+12
5.06E+12
2.89E+12
5.04E+12
2.65E+12
7.57E+12
2.10E+12
2.13E+12
2.15E+12
1.46E+12
2.18E+12
3.15E+12
2.13E+12
2.78E+12
2.63E+12
2.75E+12
1.01E+12
2.22E+12
2.11E+12
3.07E+12
2.00E+12
1.93E+12
1.19E+12
3.60E+12
1.29E+12
3.10E+12
6.84E+12
7.18E+12
8.28E+12
5.26E+12
3.81E+12
4.04E+12
2.06E+12
6.57E+12
4.81E+12
4.37E+12
3.74E+12
3.62E+12
5.13E+12

6.29E+12
2.72E+12
1.10E+13
7.15E+12
9.02E+12
9.75E+12
1.57E+12
2.78E+12
2.83E+12
3.04E+12
3.21E+12
8.14E+12
6.06E+12
4.00E+12
1.35E+13
5.54E+12
4.95E+12
8.35E+12
2.58E+12
1.30E+12
7.88E+11
2.79E+12
2.85E+12
3.03E+12
3.01E+12
3.31E+12
2.91E+12
2.74E+12
3.20E+12
3.35E+12
4.63E+12
2.30E+12
3.38E+12
3.97E+12
4.24E+12
4.55E+12
4.71E+12
2.82E+12
2.74E+12
2.99E+12
3.12E+12
3.21E+12
1.67E+12
1.71E+12
1.78E+12
1.70E+12
7.32E+11
7.41E+11
7.18E+11

7.52E+11
7.66E+11
7.20E+11
7.70E+11
7.93E+11
7.58E+11
8.07E+11
8.17E+11
7.83E+11
7.79E+11
8.13E+11
8.68E+11
2.21E+12
2.15E+12
2.12E+12
2.32E+12
4.76E+12
5.09E+12
5.52E+12
5.94E+12
6.54E+12
3.38E+12
3.48E+12
7.93E+12
8.59E+12
9.76E+12
1.11E+13
6.07E+12
6.39E+12
7.08E+12
7.64E+12
8.37E+12
1.00E+13
1.17E+13
1.51E+13
2.13E+13
3.20E+13
5.52E+13
9.92E+13
6.16E+13
7.77E+13
9.84E+13
1.22E+14
1.50E+14
1.81E+14
2.03E+14
9.97E+13
2.94E+14
3.38E+13

```
2.67E+13
7.80E+12
6.84E+12
2.88E+12
1.80E+12
1.44E+12
8.48E+11
4.68E+11
5.27E+11
2.32E+11
1.70E+11
6.17E+09
e t
done
end



=origen
solver{type=cram}
options{print_xs=no}
case(Irradiation){
    title="Pa231 Irradiation 1 in HFIR-HT for 24 Days"
    lib{file="ft33f001"}
    time{
         t=[22I 1  24]
         units="days"
         start= 0}
    flux=[24r 3.461407E+15]
    mat{
        iso=[Pa231 = 1]
        units=grams
       }
    save{
         file="Pa231-HFIR-HT-24Days-6Cycles.f71"
         steps=all
         time_units=days
        }
}
case(Decay){
    title="Intermediate Decay Step 1"
    lib{file="end7dec"}
    time{
         t=[16I  26  42]
         units="days"
         start=25
         }
    flux=[18r 0]
    save{
```

```
         file="Pa231-HFIR-HT-24Days-6Cycles.f71"
         steps=all
         time_units=days
        }
}
case(Irradiation){
    title="Pa231 Irradiation 2 in HFIR-HT for 24 Days"
    lib{file="ft33f001"}
    time{
         t=[22I 44  67]
         units="days"
         start= 43}
    flux=[24r 3.461407E+15]
    save{
         file="Pa231-HFIR-HT-24Days-6Cycles.f71"
         steps=all
         time_units=days
        }
}
case(Decay){
    title="Intermediate Decay Step 2"
    lib{file="end7dec"}
    time{
         t=[16I  69  85]
         units="days"
         start=68
         }
    flux=[18r 0]
    save{
         file="Pa231-HFIR-HT-24Days-6Cycles.f71"
         steps=all
         time_units=days
        }
}
case(Irradiation){
    title="Pa231 Irradiation 3 in HFIR-HT for 24 Days"
    lib{file="ft33f001"}
    time{
         t=[22I 87  110]
         units="days"
         start= 86}
    flux=[24r 3.461407E+15]
    save{
         file="Pa231-HFIR-HT-24Days-6Cycles.f71"
         steps=all
         time_units=days
        }
}
case(Decay){
```

```
    title="Intermediate Decay Step 3"
    lib{file="end7dec"}
    time{
         t=[16I  112  128]
         units="days"
         start=111
         }
    flux=[18r 0]
    save{
         file="Pa231-HFIR-HT-24Days-6Cycles.f71"
         steps=all
         time_units=days
        }
}
case(Irradiation){
    title="Pa231 Irradiation 4 in HFIR-HT for 24 Days"
    lib{file="ft33f001"}
    time{
         t=[22I 130  153]
         units="days"
         start= 129}
    flux=[24r 3.461407E+15]
    save{
         file="Pa231-HFIR-HT-24Days-6Cycles.f71"
         steps=all
         time_units=days
        }
}
case(Decay){
    title="Intermediate Decay Step 4"
    lib{file="end7dec"}
    time{
         t=[16I  155  171]
         units="days"
         start=154
         }
    flux=[18r 0]
    save{
         file="Pa231-HFIR-HT-24Days-6Cycles.f71"
         steps=all
         time_units=days
        }
}
case(Irradiation){
    title="Pa231 Irradiation 5 in HFIR-HT for 24 Days"
    lib{file="ft33f001"}
    time{
         t=[22I 173  196]
         units="days"
```

```
         start= 172}
    flux=[24r 3.461407E+15]
    save{
         file="Pa231-HFIR-HT-24Days-6Cycles.f71"
         steps=all
         time_units=days
        }
}
case(Decay){
    title="Intermediate Decay Step 5"
    lib{file="end7dec"}
    time{
         t=[16I  198  214]
         units="days"
         start=197
         }
    flux=[18r 0]
    save{
         file="Pa231-HFIR-HT-24Days-6Cycles.f71"
         steps=all
         time_units=days
        }
}
case(Irradiation){
    title="Pa231 Irradiation 6 in HFIR-HT for 24 Days"
    lib{file="ft33f001"}
    time{
         t=[22I 216  240]
         units="days"
         start= 215}
    flux=[24r 3.461407E+15]
    save{
         file="Pa231-HFIR-HT-24Days-6Cycles.f71"
         steps=all
         time_units=days
        }
}
case(Decay){
    title="Intermediate Decay Step 6"
    lib{file="end7dec"}
    time{
         t=[88I  242  330]
         units="days"
         start=241
         }
    flux=[90r 0]
    save{
         file="Pa231-HFIR-HT-24Days-6Cycles.f71"
         steps=all
```

```
         time_units=days
        }
}
end
=opus
    data="Pa231-HFIR-HT-24Days-6Cycles.f71"
    typa=nucl
    units=grams
    symn=th-228
         th-229
         th-230
         th-231
         th-232
         th-233
         pa-231
         pa-232
         pa-233
         pa-234
         u-232
         u-233
         u-234
         u-235
         u-236
         u-237
         u-238
         np-237
         pu-238
          pu-239
          i-131
          end

end
```

B.2. Example of 100 percent ^{230}Th irradiation, using ISVXF neutron spectrum:

Th230-HFIR-ISVXF -24Days-8Cycles.inp

```
=couple
*****************************************************************
***************
*                cross sections from 238-group JEFF-3.0/A
*

0$$ a3 80 a6 33 e
1$$ a18 238 e t
9**
6.94E+07
3.58E+08
4.48E+08
4.04E+08
1.17E+09
1.59E+10
4.57E+10
1.54E+11
4.18E+11
2.31E+11
8.29E+11
4.64E+11
2.08E+11
1.38E+12
1.72E+12
5.72E+11
2.57E+11
2.17E+11
3.88E+11
3.14E+11
6.25E+11
5.50E+11
5.99E+11
1.51E+11
1.96E+11
1.12E+11
3.52E+11
6.40E+11
7.12E+11
9.00E+10
5.98E+11
2.75E+11
2.62E+11
6.30E+11
```

3.94E+11
3.81E+11
2.48E+11
3.01E+11
1.26E+12
1.28E+12
1.75E+12
1.53E+12
7.94E+11
1.21E+12
7.36E+11
1.60E+11
4.20E+11
1.19E+11
8.79E+11
6.24E+11
1.67E+11
4.51E+11
1.66E+12
7.42E+11
1.58E+12
1.10E+12
1.29E+12
6.86E+11
1.21E+12
1.82E+12
1.79E+11
9.51E+11
6.53E+11
5.18E+11
1.77E+11
8.96E+11
6.70E+11
1.48E+11
1.21E+12
8.73E+11
1.55E+12
9.07E+10
9.44E+11
2.84E+12
3.40E+11
8.55E+11
6.71E+11
5.99E+10
3.80E+11
1.75E+11
2.17E+12
1.29E+11
1.79E+11

3.28E+11
4.02E+11
5.58E+11
4.91E+11
1.33E+11
2.75E+11
2.90E+11
3.45E+11
2.05E+11
3.42E+11
1.81E+11
5.42E+11
1.45E+11
1.51E+11
1.54E+11
1.02E+11
1.50E+11
2.14E+11
1.48E+11
2.06E+11
1.86E+11
1.91E+11
7.03E+10
1.58E+11
1.49E+11
2.32E+11
1.45E+11
1.39E+11
8.33E+10
2.60E+11
8.89E+10
2.32E+11
4.91E+11
5.42E+11
6.04E+11
3.97E+11
2.81E+11
2.97E+11
1.55E+11
4.92E+11
3.55E+11
3.41E+11
2.79E+11
2.72E+11
3.74E+11
4.79E+11
2.03E+11
8.33E+11
5.68E+11

7.08E+11
7.60E+11
1.30E+11
2.21E+11
2.31E+11
2.42E+11
2.52E+11
6.50E+11
4.79E+11
3.20E+11
1.09E+12
4.45E+11
4.05E+11
6.76E+11
2.09E+11
1.06E+11
6.56E+10
2.21E+11
2.29E+11
2.40E+11
2.49E+11
2.59E+11
2.44E+11
2.26E+11
2.64E+11
2.79E+11
3.88E+11
2.04E+11
2.83E+11
3.34E+11
3.54E+11
3.75E+11
3.98E+11
2.35E+11
2.42E+11
2.53E+11
2.63E+11
2.73E+11
1.43E+11
1.46E+11
1.47E+11
1.52E+11
6.18E+10
6.16E+10
6.32E+10
6.40E+10
6.45E+10
6.48E+10
6.62E+10

6.61E+10
6.64E+10
6.72E+10
6.92E+10
6.82E+10
6.91E+10
7.10E+10
7.15E+10
1.83E+11
1.87E+11
1.93E+11
1.98E+11
4.19E+11
4.47E+11
4.80E+11
5.19E+11
5.63E+11
3.01E+11
3.19E+11
6.84E+11
7.58E+11
8.49E+11
9.67E+11
5.42E+11
5.84E+11
6.38E+11
7.06E+11
8.10E+11
9.69E+11
1.25E+12
1.80E+12
2.95E+12
5.15E+12
9.96E+12
1.97E+13
1.27E+13
1.63E+13
2.11E+13
2.64E+13
3.26E+13
3.95E+13
4.48E+13
2.19E+13
6.53E+13
7.50E+12
5.98E+12
1.75E+12
1.55E+12
6.60E+11

```
4.07E+11
3.15E+11
1.98E+11
1.14E+11
1.34E+11
5.51E+10
3.95E+10
1.31E+09
e t
done
end



=origen
solver{type=cram}
options{print_xs=no}
case(Irradiation){
    title="Th230-100% Irradiation 1 in HFIR-InnerSmallVXF for 24
Days"
    lib{file="ft33f001"}
    time{
         t=[21I 1  23]
         units="days"
         start= 0}
    flux=[23r 4.324893E+14]
    mat{
        iso=[Th230=1]
        units=grams
       }
    save{
         file="Th230-100%-HFIR-InnerSmallVXF-24Days-8Cycles.f71"
         steps=all
         time_units=days
        }
}
case(Decay){
    title="Intermediate Decay Step 1"
    lib{file="end7dec"}
    time{
         t=[15I  25  41]
         units="days"
         start=24
         }
    flux=[17r 0]
    save{
         file="Th230-100%-HFIR-InnerSmallVXF-24Days-8Cycles.f71"
         steps=all
         time_units=days
```

```
        }
}
case(Irradiation){
    title="Th230-100% Irradiation 2 in HFIR-InnerSmallVXF for 24
Days"
    lib{file="ft33f001"}
    time{
         t=[21I 43  65]
         units="days"
         start= 42}
    flux=[23r 4.324893E+14]
    save{
         file="Th230-100%-HFIR-InnerSmallVXF-24Days-8Cycles.f71"
         steps=all
         time_units=days
        }
}
case(Decay){
    title="Intermediate Decay Step 2"
    lib{file="end7dec"}
    time{
         t=[15I  67  83]
         units="days"
         start=66
         }
    flux=[17r 0]
    save{
         file="Th230-100%-HFIR-InnerSmallVXF-24Days-8Cycles.f71"
         steps=all
         time_units=days
        }
}
case(Irradiation){
    title="Th230-100% Irradiation 3 in HFIR-InnerSmallVXF for 24
Days"
    lib{file="ft33f001"}
    time{
         t=[21I 85  107]
         units="days"
         start= 84}
    flux=[23r 4.324893E+14]
    save{
         file="Th230-100%-HFIR-InnerSmallVXF-24Days-8Cycles.f71"
         steps=all
         time_units=days
        }
}
case(Decay){
    title="Intermediate Decay Step 3"
```

```
    lib{file="end7dec"}
    time{
         t=[15I  109  125]
         units="days"
         start=108
         }
    flux=[17r 0]
    save{
         file="Th230-100%-HFIR-InnerSmallVXF-24Days-8Cycles.f71"
         steps=all
         time_units=days
        }
}
case(Irradiation){
    title="Th230-100% Irradiation 4 in HFIR-InnerSmallVXF for 24
Days"
    lib{file="ft33f001"}
    time{
         t=[21I 127  149]
         units="days"
         start= 126}
    flux=[23r 4.324893E+14]
    save{
         file="Th230-100%-HFIR-InnerSmallVXF-24Days-8Cycles.f71"
         steps=all
         time_units=days
        }
}
case(Decay){
    title="Intermediate Decay Step 4"
    lib{file="end7dec"}
    time{
         t=[15I  151  167]
         units="days"
         start=150
         }
    flux=[17r 0]
    save{
         file="Th230-100%-HFIR-InnerSmallVXF-24Days-8Cycles.f71"
         steps=all
         time_units=days
        }
}
case(Irradiation){
    title="Th230-100% Irradiation 5 in HFIR-InnerSmallVXF for 24
Days"
    lib{file="ft33f001"}
    time{
         t=[21I 169  191]
```

```
         units="days"
         start= 168}
    flux=[23r 4.324893E+14]
    save{
         file="Th230-100%-HFIR-InnerSmallVXF-24Days-8Cycles.f71"
         steps=all
         time_units=days
        }
}
case(Decay){
    title="Intermediate Decay Step 5"
    lib{file="end7dec"}
    time{
         t=[15I  193  209]
         units="days"
         start=192
         }
    flux=[17r 0]
    save{
         file="Th230-100%-HFIR-InnerSmallVXF-24Days-8Cycles.f71"
         steps=all
         time_units=days
        }
}
case(Irradiation){
    title="Th230-100% Irradiation 6 in HFIR-InnerSmallVXF for 24
Days"
    lib{file="ft33f001"}
    time{
         t=[21I 211  233]
         units="days"
         start= 210}
    flux=[23r 4.324893E+14]
    save{
         file="Th230-100%-HFIR-InnerSmallVXF-24Days-8Cycles.f71"
         steps=all
         time_units=days
        }
}
case(Decay){
    title="Intermediate Decay Step 6"
    lib{file="end7dec"}
    time{
         t=[15I  235  251]
         units="days"
         start=234
         }
    flux=[17r 0]
    save{
```

```
         file="Th230-100%-HFIR-InnerSmallVXF-24Days-8Cycles.f71"
         steps=all
         time_units=days
        }
}
case(Irradiation){
    title="Th230-100% Irradiation 7 in HFIR-InnerSmallVXF for 24
Days"
    lib{file="ft33f001"}
    time{
         t=[21I 253  275]
         units="days"
         start= 252}
    flux=[23r 4.324893E+14]
    save{
         file="Th230-100%-HFIR-InnerSmallVXF-24Days-8Cycles.f71"
         steps=all
         time_units=days
        }
}
case(Decay){
    title="Intermediate Decay Step 7"
    lib{file="end7dec"}
    time{
         t=[15I  277  293]
         units="days"
         start=276
         }
    flux=[17r 0]
    save{
         file="Th230-100%-HFIR-InnerSmallVXF-24Days-8Cycles.f71"
         steps=all
         time_units=days
        }
}
case(Irradiation){
    title="Th230-100% Irradiation 8 in HFIR-InnerSmallVXF for 24
Days"
    lib{file="ft33f001"}
    time{
         t=[21I 295  317]
         units="days"
         start= 294}
    flux=[23r 4.324893E+14]
    save{
         file="Th230-100%-HFIR-InnerSmallVXF-24Days-8Cycles.f71"
         steps=all
         time_units=days
        }
```

```
}
case(Decay){
    title="Intermediate Decay Step 8"
    lib{file="end7dec"}
    time{
         t=[87I  319  406]
         units="days"
         start=318
         }
    flux=[89r 0]
    save{
         file="Th230-100%-HFIR-InnerSmallVXF-24Days-8Cycles.f71"
         steps=all
         time_units=days
        }
}
end
=opus
    data="Th230-100%-HFIR-InnerSmallVXF-24Days-8Cycles.f71"
    typa=nucl
    units=grams
    symn=th-228
         th-229
         th-230
         th-231
         th-232
         th-233
         pa-231
         pa-232
         pa-233
         pa-234
         u-232
         u-233
         u-234
         u-235
         u-236
         u-237
         u-238
         np-237
         pu-238
         pu-239
         i-131
         end

end
```

Appendix C: ORIGEN Models for Chapter 6 Self-Shielded Production Results

C.1. Example of ^{231}Pa irradiation, using Self-Shielded MCNP Target neutron spectrum: Pa231-HFIR-FluxTrap-24Days-6Cycles.inp

```
=couple
*****************************************************************
***************
*                cross sections from 238-group JEFF-3.0/A
*

0$$ a3 80 a6 33 e
1$$ a18 238 e t
9**
2.22E+09
5.10E+09
1.07E+10
1.90E+10
4.40E+10
6.44E+11
1.94E+12
6.85E+12
2.16E+13
1.28E+13
6.12E+13
4.88E+13
1.87E+13
6.92E+13
6.43E+13
2.15E+13
9.19E+12
9.14E+12
1.57E+13
1.27E+13
2.44E+13
2.36E+13
2.34E+13
6.18E+12
7.25E+12
4.11E+12
1.32E+13
2.60E+13
3.21E+13
3.95E+12
2.98E+13
1.17E+13
```

1.01E+13
2.28E+13
1.42E+13
1.22E+13
7.23E+12
9.30E+12
4.00E+13
3.73E+13
4.98E+13
3.94E+13
2.32E+13
3.21E+13
1.25E+13
3.18E+12
1.25E+13
4.09E+12
2.40E+13
1.47E+13
3.79E+12
1.00E+13
3.34E+13
2.02E+13
3.43E+13
2.30E+13
2.64E+13
1.40E+13
2.42E+13
3.55E+13
3.42E+12
1.82E+13
1.24E+13
9.81E+12
3.31E+12
1.65E+13
1.23E+13
2.70E+12
2.19E+13
1.56E+13
2.71E+13
1.57E+12
1.62E+13
4.82E+13
5.59E+12
1.41E+13
1.09E+13
7.70E+11
6.08E+12
3.02E+12
3.43E+13

2.02E+12
2.69E+12
5.14E+12
6.20E+12
8.72E+12
7.59E+12
2.03E+12
4.21E+12
4.41E+12
5.20E+12
2.99E+12
5.08E+12
2.77E+12
7.62E+12
2.01E+12
2.12E+12
2.35E+12
1.54E+12
2.19E+12
3.13E+12
2.25E+12
2.93E+12
2.70E+12
2.79E+12
1.05E+12
2.36E+12
2.06E+12
3.17E+12
2.10E+12
1.98E+12
1.25E+12
3.64E+12
1.02E+12
3.51E+12
6.75E+12
7.40E+12
8.80E+12
5.09E+12
3.66E+12
4.10E+12
1.86E+12
6.37E+12
4.63E+12
4.52E+12
3.91E+12
3.04E+12
4.42E+12
6.69E+12
2.11E+12

9.40E+12
7.14E+12
8.33E+12
9.46E+12
1.72E+12
2.22E+12
2.94E+12
3.20E+12
3.41E+12
7.94E+12
3.90E+12
3.82E+12
1.25E+13
5.92E+12
5.19E+12
8.61E+12
2.80E+12
1.45E+12
8.78E+11
2.97E+12
2.80E+12
3.06E+12
3.35E+12
3.45E+12
3.27E+12
2.99E+12
3.53E+12
3.66E+12
5.01E+12
2.36E+12
3.55E+12
4.39E+12
4.64E+12
4.86E+12
5.18E+12
2.99E+12
3.09E+12
3.18E+12
3.16E+12
2.54E+12
7.88E+11
1.38E+12
1.18E+12
2.10E+12
7.42E+11
7.57E+11
7.64E+11
7.75E+11
7.92E+11

8.01E+11
7.98E+11
8.09E+11
8.33E+11
8.37E+11
8.49E+11
8.56E+11
8.76E+11
8.99E+11
9.09E+11
2.29E+12
2.34E+12
2.43E+12
2.47E+12
5.12E+12
5.33E+12
4.83E+12
4.73E+12
6.26E+12
3.38E+12
3.49E+12
6.90E+12
5.07E+12
3.86E+12
2.09E+12
7.24E+11
1.63E+12
3.25E+12
4.85E+12
6.36E+12
8.14E+12
1.02E+13
1.36E+13
1.99E+13
3.05E+13
5.08E+13
9.15E+13
5.39E+13
7.14E+13
8.25E+13
1.05E+14
1.24E+14
1.44E+14
1.56E+14
7.29E+13
1.97E+14
1.82E+13
1.28E+13
4.52E+12

```
2.55E+12
9.07E+11
7.29E+11
5.94E+11
3.16E+11
1.16E+11
1.00E+11
5.57E+10
3.28E+10
3.80E+08
e t
done
end



=origen
solver{type=cram}
options{print_xs=no}
case(Irradiation){
    title="Pa231 Irradiation 1 in HFIR-FluxTrap for 24 Days"
    lib{file="ft33f001"}
    time{
         t=[22I 1  24]
         units="days"
         start= 0}
    flux=[24r 3.187103E+15]
    mat{
        iso=[Pa231 = 1]
        units=grams
       }
    save{
         file="Pa231-HFIR-FluxTrap-24Days-6Cycles.f71"
         steps=all
         time_units=days
        }
}
case(Decay){
    title="Intermediate Decay Step 1"
    lib{file="end7dec"}
    time{
         t=[16I  26  42]
         units="days"
         start=25
         }
    flux=[18r 0]
    save{
         file="Pa231-HFIR-FluxTrap-24Days-6Cycles.f71"
         steps=all
```

```
         time_units=days
        }
}
case(Irradiation){
    title="Pa231 Irradiation 2 in HFIR-FluxTrap for 24 Days"
    lib{file="ft33f001"}
    time{
         t=[22I 44  67]
         units="days"
         start= 43}
    flux=[24r 3.187103E+15]
    save{
         file="Pa231-HFIR-FluxTrap-24Days-6Cycles.f71"
         steps=all
         time_units=days
        }
}
case(Decay){
    title="Intermediate Decay Step 2"
    lib{file="end7dec"}
    time{
         t=[16I  69  85]
         units="days"
         start=68
         }
    flux=[18r 0]
    save{
         file="Pa231-HFIR-FluxTrap-24Days-6Cycles.f71"
         steps=all
         time_units=days
        }
}
case(Irradiation){
    title="Pa231 Irradiation 3 in HFIR-FluxTrap for 24 Days"
    lib{file="ft33f001"}
    time{
         t=[22I 87  110]
         units="days"
         start= 86}
    flux=[24r 3.187103E+15]
    save{
         file="Pa231-HFIR-FluxTrap-24Days-6Cycles.f71"
         steps=all
         time_units=days
        }
}
case(Decay){
    title="Intermediate Decay Step 3"
    lib{file="end7dec"}
```

```
    time{
         t=[16I  112  128]
         units="days"
         start=111
         }
    flux=[18r 0]
    save{
         file="Pa231-HFIR-FluxTrap-24Days-6Cycles.f71"
         steps=all
         time_units=days
        }
}
case(Irradiation){
    title="Pa231 Irradiation 4 in HFIR-FluxTrap for 24 Days"
    lib{file="ft33f001"}
    time{
         t=[22I 130  153]
         units="days"
         start= 129}
    flux=[24r 3.187103E+15]
    save{
         file="Pa231-HFIR-FluxTrap-24Days-6Cycles.f71"
         steps=all
         time_units=days
        }
}
case(Decay){
    title="Intermediate Decay Step 4"
    lib{file="end7dec"}
    time{
         t=[16I  155  171]
         units="days"
         start=154
         }
    flux=[18r 0]
    save{
         file="Pa231-HFIR-FluxTrap-24Days-6Cycles.f71"
         steps=all
         time_units=days
        }
}
case(Irradiation){
    title="Pa231 Irradiation 5 in HFIR-FluxTrap for 24 Days"
    lib{file="ft33f001"}
    time{
         t=[22I 173  196]
         units="days"
         start= 172}
    flux=[24r 3.187103E+15]
```

```
    save{
         file="Pa231-HFIR-FluxTrap-24Days-6Cycles.f71"
         steps=all
         time_units=days
        }
}
case(Decay){
    title="Intermediate Decay Step 5"
    lib{file="end7dec"}
    time{
         t=[16I  198  214]
         units="days"
         start=197
         }
    flux=[18r 0]
    save{
         file="Pa231-HFIR-FluxTrap-24Days-6Cycles.f71"
         steps=all
         time_units=days
        }
}
case(Irradiation){
    title="Pa231 Irradiation 6 in HFIR-FluxTrap for 24 Days"
    lib{file="ft33f001"}
    time{
         t=[22I 216  240]
         units="days"
         start= 215}
    flux=[24r 3.187103E+15]
    save{
         file="Pa231-HFIR-FluxTrap-24Days-6Cycles.f71"
         steps=all
         time_units=days
        }
}
case(Decay){
    title="Intermediate Decay Step 6"
    lib{file="end7dec"}
    time{
         t=[88I  242  330]
         units="days"
         start=241
         }
    flux=[90r 0]
    save{
         file="Pa231-HFIR-FluxTrap-24Days-6Cycles.f71"
         steps=all
         time_units=days
        }
```

```
}
end
=opus
    data="Pa231-HFIR-FluxTrap-24Days-6Cycles.f71"
    typa=nucl
    units=grams
    symn=th-228
         th-229
         th-230
         th-231
         th-232
         th-233
         pa-231
         pa-232
         pa-233
         pa-234
         u-232
         u-233
         u-234
         u-235
         u-236
         u-237
         u-238
         np-237
         pu-238
         pu-239
         i-131
         end

end
```

C.2. Example of 100 percent ^{230}Th irradiation, using Self-Shielded MCNP Target neutron spectrum: Th230-100%-HFIR-FluxTrap-24Days-6Cycles.inp

```
=couple
*****************************************************************
***************
*                cross sections from 238-group JEFF-3.0/A
*

0$$ a3 80 a6 33 e
1$$ a18 238 e t
9**
1.89E+09
7.31E+09
1.18E+10
1.92E+10
4.64E+10
6.00E+11
1.89E+12
6.65E+12
2.08E+13
1.25E+13
5.93E+13
4.75E+13
1.81E+13
6.70E+13
6.23E+13
2.09E+13
8.93E+12
8.86E+12
1.52E+13
1.23E+13
2.36E+13
2.30E+13
2.27E+13
6.01E+12
7.05E+12
4.00E+12
1.28E+13
2.52E+13
3.13E+13
3.87E+12
2.90E+13
1.14E+13
9.79E+12
2.23E+13
1.38E+13
1.19E+13
7.07E+12
```

9.03E+12
3.89E+13
3.61E+13
4.82E+13
3.83E+13
2.26E+13
3.11E+13
1.21E+13
3.08E+12
1.22E+13
4.00E+12
2.34E+13
1.42E+13
3.72E+12
9.67E+12
3.25E+13
1.96E+13
3.33E+13
2.23E+13
2.58E+13
1.37E+13
2.35E+13
3.45E+13
3.38E+12
1.78E+13
1.21E+13
9.53E+12
3.23E+12
1.62E+13
1.21E+13
2.64E+12
2.14E+13
1.53E+13
2.65E+13
1.56E+12
1.59E+13
4.77E+13
5.51E+12
1.38E+13
1.08E+13
7.03E+11
5.72E+12
3.21E+12
3.41E+13
2.05E+12
2.53E+12
5.13E+12
6.14E+12
8.70E+12

7.25E+12
2.04E+12
4.18E+12
4.26E+12
5.31E+12
3.07E+12
5.02E+12
2.74E+12
8.20E+12
2.20E+12
2.24E+12
2.31E+12
1.26E+12
1.90E+12
3.22E+12
2.19E+12
3.04E+12
2.75E+12
2.17E+12
1.07E+12
2.35E+12
2.17E+12
3.40E+12
2.11E+12
1.93E+12
1.22E+12
3.16E+12
1.31E+12
3.50E+12
7.21E+12
7.86E+12
7.27E+12
5.65E+12
3.98E+12
4.22E+12
2.14E+12
4.89E+12
4.79E+12
4.72E+12
3.89E+12
3.47E+12
5.56E+12
6.69E+12
2.81E+12
1.15E+13
7.81E+12
9.61E+12
1.02E+13
1.75E+12

3.01E+12
3.09E+12
3.26E+12
3.34E+12
8.72E+12
6.37E+12
4.26E+12
1.44E+13
5.90E+12
5.42E+12
8.99E+12
2.76E+12
1.41E+12
8.55E+11
2.92E+12
3.04E+12
3.14E+12
3.22E+12
3.37E+12
3.18E+12
2.93E+12
3.39E+12
3.54E+12
4.97E+12
2.58E+12
3.54E+12
4.10E+12
4.21E+12
4.13E+12
3.06E+12
4.24E+11
1.16E+11
6.75E+11
1.84E+12
2.56E+12
1.15E+12
1.84E+12
1.29E+12
2.03E+12
6.82E+11
7.20E+11
7.19E+11
7.23E+11
7.37E+11
7.52E+11
7.61E+11
7.83E+11
7.86E+11
7.86E+11

7.96E+11
8.11E+11
8.18E+11
8.42E+11
8.51E+11
2.19E+12
2.23E+12
2.31E+12
2.38E+12
5.03E+12
5.40E+12
5.82E+12
6.24E+12
6.81E+12
3.67E+12
3.80E+12
8.11E+12
9.04E+12
1.01E+13
1.14E+13
6.30E+12
6.75E+12
7.44E+12
8.15E+12
9.09E+12
1.05E+13
1.26E+13
1.63E+13
2.31E+13
3.50E+13
5.86E+13
1.07E+14
6.35E+13
8.44E+13
9.86E+13
1.27E+14
1.53E+14
1.83E+14
2.06E+14
9.97E+13
2.95E+14
3.18E+13
2.43E+13
9.26E+12
5.74E+12
2.20E+12
1.85E+12
1.63E+12
9.22E+11

```
3.62E+11
3.58E+11
2.19E+11
1.58E+11
3.71E+09
e t
done
end



=origen
solver{type=cram}
options{print_xs=no}
case(Irradiation){
    title="Th230-100% Irradiation 1 in HFIR-FluxTrap for 24 Days"
    lib{file="ft33f001"}
    time{
         t=[22I 1  24]
         units="days"
         start= 0}
    flux=[24r 3.571893E+15]
    mat{
        iso=[Th230=1]
        units=grams
       }
    save{
         file="Th230-100%-HFIR-FluxTrap-24Days-6Cycles.f71"
         steps=all
         time_units=days
        }
}
case(Decay){
    title="Intermediate Decay Step 1"
    lib{file="end7dec"}
    time{
         t=[16I  26  42]
         units="days"
         start=25
         }
    flux=[18r 0]
    save{
         file="Th230-100%-HFIR-FluxTrap-24Days-6Cycles.f71"
         steps=all
         time_units=days
        }
}
case(Irradiation){
    title="Th230-100% Irradiation 2 in HFIR-FluxTrap for 24 Days"
```

```
    lib{file="ft33f001"}
    time{
         t=[22I 44  67]
         units="days"
         start= 43}
    flux=[24r 3.571893E+15]
    save{
         file="Th230-100%-HFIR-FluxTrap-24Days-6Cycles.f71"
         steps=all
         time_units=days
        }
}
case(Decay){
    title="Intermediate Decay Step 2"
    lib{file="end7dec"}
    time{
         t=[16I  69  85]
         units="days"
         start=68
         }
    flux=[18r 0]
    save{
         file="Th230-100%-HFIR-FluxTrap-24Days-6Cycles.f71"
         steps=all
         time_units=days
        }
}
case(Irradiation){
    title="Th230-100% Irradiation 3 in HFIR-FluxTrap for 24 Days"
    lib{file="ft33f001"}
    time{
         t=[22I 87  110]
         units="days"
         start= 86}
    flux=[24r 3.571893E+15]
    save{
         file="Th230-100%-HFIR-FluxTrap-24Days-6Cycles.f71"
         steps=all
         time_units=days
        }
}
case(Decay){
    title="Intermediate Decay Step 3"
    lib{file="end7dec"}
    time{
         t=[16I  112  128]
         units="days"
         start=111
         }
```

```
    flux=[18r 0]
    save{
         file="Th230-100%-HFIR-FluxTrap-24Days-6Cycles.f71"
         steps=all
         time_units=days
        }
}
case(Irradiation){
    title="Th230-100% Irradiation 4 in HFIR-FluxTrap for 24 Days"
    lib{file="ft33f001"}
    time{
         t=[22I 130  153]
         units="days"
         start= 129}
    flux=[24r 3.571893E+15]
    save{
         file="Th230-100%-HFIR-FluxTrap-24Days-6Cycles.f71"
         steps=all
         time_units=days
        }
}
case(Decay){
    title="Intermediate Decay Step 4"
    lib{file="end7dec"}
    time{
         t=[16I  155  171]
         units="days"
         start=154
         }
    flux=[18r 0]
    save{
         file="Th230-100%-HFIR-FluxTrap-24Days-6Cycles.f71"
         steps=all
         time_units=days
        }
}
case(Irradiation){
    title="Th230-100% Irradiation 5 in HFIR-FluxTrap for 24 Days"
    lib{file="ft33f001"}
    time{
         t=[22I 173  196]
         units="days"
         start= 172}
    flux=[24r 3.571893E+15]
    save{
         file="Th230-100%-HFIR-FluxTrap-24Days-6Cycles.f71"
         steps=all
         time_units=days
        }
```

```
}
case(Decay){
    title="Intermediate Decay Step 5"
    lib{file="end7dec"}
    time{
         t=[16I  198  214]
         units="days"
         start=197
         }
    flux=[18r 0]
    save{
         file="Th230-100%-HFIR-FluxTrap-24Days-6Cycles.f71"
         steps=all
         time_units=days
        }
}
case(Irradiation){
    title="Th230-100% Irradiation 6 in HFIR-FluxTrap for 24 Days"
    lib{file="ft33f001"}
    time{
         t=[22I 216  240]
         units="days"
         start= 215}
    flux=[24r 3.571893E+15]
    save{
         file="Th230-100%-HFIR-FluxTrap-24Days-6Cycles.f71"
         steps=all
         time_units=days
        }
}
case(Decay){
    title="Intermediate Decay Step 6"
    lib{file="end7dec"}
    time{
         t=[88I  242  330]
         units="days"
         start=241
         }
    flux=[90r 0]
    save{
         file="Th230-100%-HFIR-FluxTrap-24Days-6Cycles.f71"
         steps=all
         time_units=days
        }
}
end
=opus
    data="Th230-100%-HFIR-FluxTrap-24Days-6Cycles.f71"
    typa=nucl
```

```
    units=grams
    symn=th-228
         th-229
         th-230
         th-231
         th-232
         th-233
         pa-231
         pa-232
         pa-233
         pa-234
         u-232
         u-233
         u-234
         u-235
         u-236
         u-237
         u-238
         np-237
         pu-238
         pu-239
         i-131
         end

end
```

Appendix D: Example ORIGEN Models for Chapter 8 ^{236}Pu Mitigation

D.1. Example of 99.99 percent Removal of ^{232}U: Pu236Decay-4ppm-5Years-Curies.inp

```
=origen
solver{type=cram}
options{print_xs=no}
bounds{
       gamma=[348I 3.5e6 1.0e4]
       neutron="scale.rev04.xn252v7.1"
      }
case(U232_Decay){
     title="Decay of Pu238 for up to 150 Days"
     lib{file="end7dec"}
     time{
          t=[148I 1 150]
          units="days"
          start=0.0}
     flux=[150R 0]
     mat{
         iso=[Pu236 = 4.0000e-06
              Pu238 = 8.5000e-01
              Pu239 = 1.2750e-01
              Pu240 = 2.0000e-02
              Pu241 = 1.5000e-03
              Pu242 = 1.0000e-03]
         units=grams
        }
     print{
           gamma{
                 summary = yes
                 spectra = yes
                }
           neutron{
                   summary = yes
                   spectra = yes
                   detailed = yes
                  }
           nuc{ total=yes units=GRAMS}
           cutoffs[ ALL=1e-15]
          }
```

```
     gamma{
           sublib = ALL
          }
     neutron{
             alphan_medium = case
             alphan_bins = 200
             alphan_cutoff = 0.0
             alphan_step = LAST
            }
     save{file="Pu236Decay-4ppm-5Years-Curies.f71"
          steps=all
          time_units=years}
}
case(SecondDecay){
     title="Second Decay of Pu238"
     lib{file="end7dec"}
     time{
          t=[298I 152 1975.000000]
          units="days"
          start=151}
     flux=[300R 0]
     processing{
           retained=[u=0.0001 th=0.0001 pu=1.0  Ra=1  Rn=1
Po=1  Pb=1  Bi=1 Tl=1]
                }
     save{file="Pu236Decay-4ppm-5Years-Curies.f71"
          steps=all
          time_units=years}
print{
      nuc{ total=yes units=GRAMS}
      cutoffs[ ALL=1e-15]
     }
}
case(ThirdDecay){
     title="Third Decay of Pu238"
     lib{file="end7dec"}
     time{
          t=[298I 1977.000000  3071.000000]
          units="days"
          start=1976.000000}
     flux=[300R 0]
     processing{
           retained=[u=0.0001 th=0.0001 pu=1.0  Ra=1  Rn=1
Po=1  Pb=1  Bi=1 Tl=1]
                }
```

```
     save{file="Pu236Decay-4ppm-5Years-Curies.f71"
          steps=all
          time_units=years}
print{
      nuc{ total=yes units=GRAMS}
      cutoffs[ ALL=1e-15]
     }
}
end

=opus
     data="Pu236Decay-4ppm-5Years-Curies.f71"
     typa=nucl
     units=curies
     symn=th-228
           th-229
           th-230
           th-231
           th-232
           th-233
           pa-231
           pa-232
           pa-233
           pa-234
            u-232
            u-233
            u-234
            u-235
            u-236
            u-237
            u-238
           np-237
           pu-236
           pu-238
           pu-239
           pu-240
           pu-241
           am-241
            i-131
           tl-208
          end

end
```

D.2. Example of 97 percent Removal of ^{232}U: Pu236Decay-6ppm-5Years-Curies.inp

```
=origen
solver{type=cram}
options{print_xs=no}
bounds{
       gamma=[348I 3.5e6 1.0e4]
       neutron="scale.rev04.xn252v7.1"
      }
case(U232_Decay){
     title="Decay of Pu238 for up to 150 Days"
     lib{file="end7dec"}
     time{
          t=[148I 1 150]
          units="days"
          start=0.0}
     flux=[150R 0]
     mat{
         iso=[Pu236 = 6.0000e-06
              Pu238 = 8.5000e-01
              Pu239 = 1.2750e-01
              Pu240 = 2.0000e-02
              Pu241 = 1.5000e-03
              Pu242 = 1.0000e-03]
         units=grams
        }
     print{
           gamma{
                 summary = yes
                 spectra = yes
                }
           neutron{
                   summary = yes
                   spectra = yes
                   detailed = yes
                  }
           nuc{ total=yes units=GRAMS}
           cutoffs[ ALL=1e-15]
          }
     gamma{
           sublib = ALL
          }
     neutron{
             alphan_medium = case
             alphan_bins = 200
             alphan_cutoff = 0.0
             alphan_step = LAST
            }
```

```
     save{file="Pu236Decay-6ppm-5Years-Curies.f71"
          steps=all
          time_units=years}
}
case(SecondDecay){
     title="Second Decay of Pu238"
     lib{file="end7dec"}
     time{
          t=[298I 152 1975.000000]
          units="days"
          start=151}
     flux=[300R 0]
     processing{
           retained=[u=0.03 th=0.03 pu=1.0  Ra=1  Rn=1  Po=1
Pb=1  Bi=1 Tl=1]
                }
     save{file="Pu236Decay-6ppm-5Years-Curies.f71"
          steps=all
          time_units=years}
print{
      nuc{ total=yes units=GRAMS}
      cutoffs[ ALL=1e-15]
     }
}
case(ThirdDecay){
     title="Third Decay of Pu238"
     lib{file="end7dec"}
     time{
          t=[298I 1977.000000  3071.000000]
          units="days"
          start=1976.000000}
     flux=[300R 0]
     processing{
           retained=[u=0.03 th=0.03 pu=1.0  Ra=1  Rn=1  Po=1
Pb=1  Bi=1 Tl=1]
                }
     save{file="Pu236Decay-6ppm-5Years-Curies.f71"
          steps=all
          time_units=years}
print{
      nuc{ total=yes units=GRAMS}
      cutoffs[ ALL=1e-15]
     }
}
end

=opus
      data="Pu236Decay-6ppm-5Years-Curies.f71"
      typa=nucl
```

```
      units=curies
      symn=th-228
            th-229
            th-230
            th-231
            th-232
            th-233
            pa-231
            pa-232
            pa-233
            pa-234
             u-232
             u-233
             u-234
             u-235
             u-236
             u-237
             u-238
            np-237
            pu-236
            pu-238
            pu-239
            pu-240
            pu-241
            am-241
             i-131
            tl-208
           end

end
```

VITA

Joshua H. Rhodes was born on October 12, 1992 in St. Louis, Missouri, to his parents Dwight and Triphosa Rhodes. He earned his B.S. degree in Nuclear Engineering from the Missouri University of Science and Technology in Rolla, Missouri (Missouri S&T) in 2016, and his Master's of Science in Nuclear Engineering from Missouri S&T in 2018. He joined the University of Tennessee's graduate program in nuclear engineering in 2019 to pursue a Ph.D. degree in Nuclear Engineering. He was awarded a US Nuclear Regulatory Commission Graduate Fellowship and also received project sponsorship from Oak Ridge National Laboratory (ORNL). He expects to complete all Ph.D. degree requirements and graduate in December of 2021.